QATAR UNIVERSITY

COLLEGE OF PHARMACY

PRODUCTION OF LETROZOLE-LOADED MONODISPERSE POLYMERIC-BASED MICROPARTICLES FOR BREAST CANCER THERAPY

BY

BAYAN ALEMRAYAT

A Thesis Submitted to the Faculty of

the College of Pharmacy

in Partial

Fulfillment of the

Requirements for

the Degree of

Masters of Science

in Pharmacy

January 2017

COMMITTEE PAGE

The members of the Committee approve the Thesis of Bayan Alemrayat

defended on 20/12/2016.

Dr. Husam Younes
Thesis/Dissertation Supervisor

Dr. Feras Alali
Committee Member

Dr. Abdelbary Elhissi
Committee Member

Dr. Mohammed El-Rayess
Committee Member

Approved:

Mohammad Diab, Dean, College of Pharmacy

ABSTRACT

Alemrayat, Bayan F. Masters: January: 2017, Pharmacy .

Title: Production of Letrozole-Loaded Monodisperse Polymeric-Based Microparticles for Breast Cancer Therapy.

Supervisor of Thesis: Dr. Husam M Younes.

Letrozole (LTZ) is effective for the treatment of hormone-receptor-positive breast cancer in postmenopausal women. However, due to its adverse effects this study was designed to investigate the feasibility of producing monodisperse LTZ microparticles using either Poly-ε-Caprolactone (PCL) or Poly (D,L-Lactide) (PDLLA) as polymeric carriers to improve its release and safety profiles. An amount of 1 g PCL or PDLLA was mixed with 5-30% w/w LTZ in 1-2 % w/v ml dichloromethane. Using Vibrating Orifice Aerosol Generator (VOAG) with a 300-µm orifice at a rate of 0.17-1.7 ml/min, and a frequency of 100-1000 KHz, a constant stream of monodisperse microdroplets was generated. These droplets were collected in a 0.04-1% Polyvinyl Alcohol (PVA) aqueous medium and stirred at 250-500 rpm for 24 hours. Solidified microparticles were collected through filtration and dried under vacuum over 48 hours. Optimized microparticles were characterized for yield, morphology, particle size, entrapment efficiency, thermal and structural properties, in vitro release profile, and in vitro cytotoxicity evaluation using

4′,6-Diamidino-2-phenylindole dihydrochloride (DAPI) staining. Monodisperse microparticles were prepared with a high yield that ranged from 88.2-96.1%. Particles appeared to be spherical with smooth surfaces in both carriers. The particle size varied from 15.6 µm to 91.6 µm and from 22.7 µm to 99.6 µm with a span ranging from 0.22 to 1.24 and from 0.29 to 1.48 in PCL- and PDLLA-based formulations, respectively. Liquid flow rate and PVA concentration were the main contributors to the variation in particle size. Upon optimizing the production parameters, span was reduced to 0.162-0.195. High entrapment efficiency was obtained reaching up to 96.8%. LTZ became completely amorphous at 5-10% w/w drug loading using PDLLA, and at all loadings using PCL. Drug release from PDLLA and PCL followed a biphasic zero-order release over 31 days using 5% and 30% w/w drug loadings. In vitro cytotoxicity results have shown that all LZT-PDLLA/PCL formulations significantly inhibited the growth of MCF-7 cell line at low concentrations reaching 10 nM, suggesting its potential clinical importance in suppressing breast tumor growth and invasiveness. This study indicated the potential of manufacturing new LTZ formulations for monthly administration as intramuscular injections (IM) which offer better release profiles that may result in minimal adverse effects.

DEDICATION

To my Exquisite Family,

My supportive parents,

Mr. Faleh Al-Mrayat and Mrs. Hanan Alajarmeh

My great, lovely and loyal fiancé,

Eng. Sufyan Al-Mrayat

And my wonderful brothers and sisters,

Eng. Ahmad, Dr. Mohammad, Dr. Hamza, Eng. Afnan, Eng. Razan, and Hamad

ACKNOWLEDGMENTS

I would like to thank my supervisor and mentor Dr. Husam Younes for his continuous guidance, assistance and unconditional support and motivation. Dr. Husam has done a tremendous effort in providing me with the needed knowledge; research skills and skepticism that made this dissertation come to light. I would have not achieved what I have so far without his great advices, recommendations, and inspiration. My research skills have been improved massively due to his valuable comments. I would also like to acknowledge the members of my supervisory committee; Dr. Abdelbary Elhissi, Dr. Mohamed El-Rayess, and the committee chair, Dr. Feras Alali, for their efforts, critical appraisal of this thesis work, constructive feedback to make it better and their acts of motivation along the way. You were all great teachers who were not only educating, but also inspiring. Many thanks to Dr. Abdelbary Elhissi who continued to support and provide me with the necessary advices throughout my work. Dr. Mohamed El-Rayess deserves great acknowledgements for his close supervision during my work at the ADLQ. I would like to appreciate the support of Dr. Fatima Mraiche for availing all the facilities in her lab when needed. I would like to thank Mr. Nabeel Abdulrahman for his help, Dr. Saeed Al Meer and his team at the central lab unit for their support with morphological analyses. I would like to thank Qatar University and College of Pharmacy for all their support. They helped me through the funding I got as a graduate teaching assistant and through funding my trip to Berlin, Germany to attend the 6^{th} International Colloids Conference.

I would like to express my warm appreciation to my colleagues at the Pharmaceutics and Polymeric Drug Delivery Research Lab. Big thanks to our lab professional, Loai Saifan who provided me with great support during UPLC analyses. I would like to also thank Shijimol Arakkal and Jensa Joseph for their support in the lab. Many thanks to my great sister, Youmna Hassouna for providing me with great advices along with sharing with me happy unforgettable times. A big thank you to my lab members and friends: Hesham Ismail, Khaled Al-Zahabi, Sandy Al-Deeb, Hend Allouch, Fatima Al-Suliti, Soumaya Allouch and Nada Khudair for their help and for making every moment in my journey as joyous as it gets.

Finally, yet more importantly, I would like to express my greatest gratitude to my supportive, lovely parents who never stopped supporting me at all levels. Thank you for all the years you dedicated to raise me and make me who I am today. Words can never ever describe your magnificent amount of efforts you spent to see me at this stage. My deepest greatest gratitude is directed towards my lovely, heartwarming, supportive, loyal and delightful fiancé (Eng. Sufyan Al-Mrayat) who showed all forms of support, love and motivation to the levels of infinity. Throughout my MSc journey, you dedicate yourself to stand by my side without hesitation. I'm really speechless to describe how amazing you were during all that times. Without your exceptional, enormous support, this work would have never been accomplished. Huge thanks to all my sisters and brothers, especially for my great, lovely sisters (Eng. Afnan and Eng. Razan) for their unconditional emotional and mental support. I would have never done this without you.

TABLE OF CONTENTS

LIST OF TABLES

LIST OF FIGURES

ABBREVIATIONS

PTEN, Phosphatase and Tensin Homolog

TP53, Tumor Protein p53

BRCA 1 and 2, Breast Cancer Genes 1 and 2

HER2, Human Epidermal Growth Factor Receptor 2

ER, Estrogen Receptor

LTZ, Letrozole

PCL, Poly-ε-Caprolactone

PDLLA, Poly (D,L-Lactide)

VOAG, Vibrating Orifice Aerosol Generator

PVA, Polyvinyl Alcohol

IM, Intramuscular

UPLC, Ultra-Performance Liquid Chromatography

ICH, International Council for Harmonization

EMEM, Eagle's Minimum Essential Medium

DAPI, 4′,6-Diamidino-2-Phenylindole Dihydrochloride

D-PBS, Dulbecco's Phosphate Buffered Saline

Chapter 1: Introduction

1.1 Breast Cancer

1.1.1 Epidemiology

Breast cancer is a life-threating disease that is highly common in women across the globe (1). It lies on top of the most prevalent types of cancer and it is considered the primary reason for cancer-related mortality (2), with nearly 1.68 million incidents and more than half a million deaths being documented worldwide in 2012 (3). Over 231,000 new cases of invasive breast cancer were diagnosed in USA in 2015 alone (4). In United Kingdom, more than 60,000 women are diagnosed with breast cancer annually (5). By itself, the disease makes up 25% of all cancers recorded and 15% of all human losses due to cancer among women universally (6). Although the disease prevalence is higher in developed countries, three quarters of the worldwide disease-associated deaths are arising from developing countries (7,8).

In the Middle East, breast cancer is identified as the most widely spread cancer among females (9). Alarming figures indicate that the disease continues to affect more and more women in the region starting from the early 1980s; the majority of which are sadly in their 30s and 40s, and a significant percentage presenting with late disease stages (10). From a local perspective, breast cancer constitutes to be the number one diagnosed cancer in Qatar among women and both genders as well. According to Bener et al., a dramatic

increase of roughly 52.8% in the total new cases of breast cancer have been recorded in just 15-year period; from early 1990s to 2006 (11). In 2007 alone, breast cancer has accounted for approximately 20% of all treated cancers in National Center for Cancer Care and Research (NCCR) hospital (11). Overall incidence rate of breast cancer has been estimated to be 38.1 per 100,000 women, placing the country third in terms of breast cancer prevalence in the Middle East region (12). Recent reports from the World Health Organization (WHO) have highlighted that breast cancer is not only residing on top of detected cancers in Qatar, but also holds the highest mortality rates as compared to all other types with 12.9 deaths per 100,000 patients (13,14). Such finding reflects an extremely poor disease prognosis to be drawn in Qatar.

1.1.2 Pathophysiology

Multiple complex pathological transformations at the cellular level underlie the emergence of cancer (15–18). These primarily involve the mutation of certain genes that are responsible for the commencement or suppression of cell cycle. Such events result in uncontrollable cell proliferation, leading to the formation of neoplastic clusters. In breast cancer, particularly, the mutation of certain tumor suppressor genes such as phosphatase and tensin homolog (PTEN), tumor protein p53 (TP53), and breast cancer genes 1 and 2 (BRCA1 and BRCA2) along with the overexpression of an oncogene called human epidermal growth factor receptor 2 (HER2) have been implicated in the predisposition of the disease (19–24). Mutations in BRCA1 and BRCA2 are thought to hold the highest

risk for developing cancerous manifestations within breast tissues (25–27). It has been estimated that women with this type of mutation carry a higher probability of developing breast cancer that reaches 40-60% as compared with those who do not have such mutation (28,29). Moreover, women who have been exposed to estrogen for prolonged period of time, whether endogenously or exogenously through hormonal supplements, are also more susceptible to develop breast cancers than others (30–33). Estrogen actually plays a significant role in triggering breast cancer as it binds to its receptor (ER) in the epithelial lining of breast tissues, prompting a cascade of cellular growth and proliferation. Progesterone binding to its receptor (PR) comes second to estrogen binding in terms of its importance in the development of breast cancer. In general, hormone receptor-positive breast cancers are widely common, accounting for roughly 50-70% of all breast cancer cases (34–36). Therefore, hormonal therapy is considered essential in the treatment of breast cancer most of the time.

Classification of breast cancer depends predominantly on the histological and biological characteristics of epithelial cells. Tumors that are localized to the site of origin are termed in-situ tumors. On the other hand, tumors invading the surrounding tissues, spreading to other regions of the body are termed invasive or metastatic tumors. In essence, invasive tumors/metastasis have poorer prognosis and more severe clinical presentation compared to in-situ tumors (37–40). However, pharmacological advancements have brought promising solutions to manage invasive breast cancer and prolong the expected lifetime span of patients suffering from such devastating disease (41).

1.1.3 Treatment Strategies

A number of pharmacological therapies are now available for the treatment and management of breast cancer. Based on the disease stage and other prognostic factors such as the activation of hormonal receptors, the therapeutic regimen is designed (42).

The accurate staging of the disease followed by a prompt initiation of the appropriate therapeutic intervention is crucial in controlling the deleterious symptoms associated with breast cancer, prolonging survival, and enhancing patients' quality of life (43,44). These therapeutic modalities include surgical interventions to remove the localized tumor or the entire breast, termed as lumpectomy and mastectomy, respectively, radiotherapy, chemotherapy, biologic (trastuzumab), and hormonal therapy (42,45–50). Figure 1 summarizes the different therapeutic modalities involved in the management of breast cancer with some examples for each category.

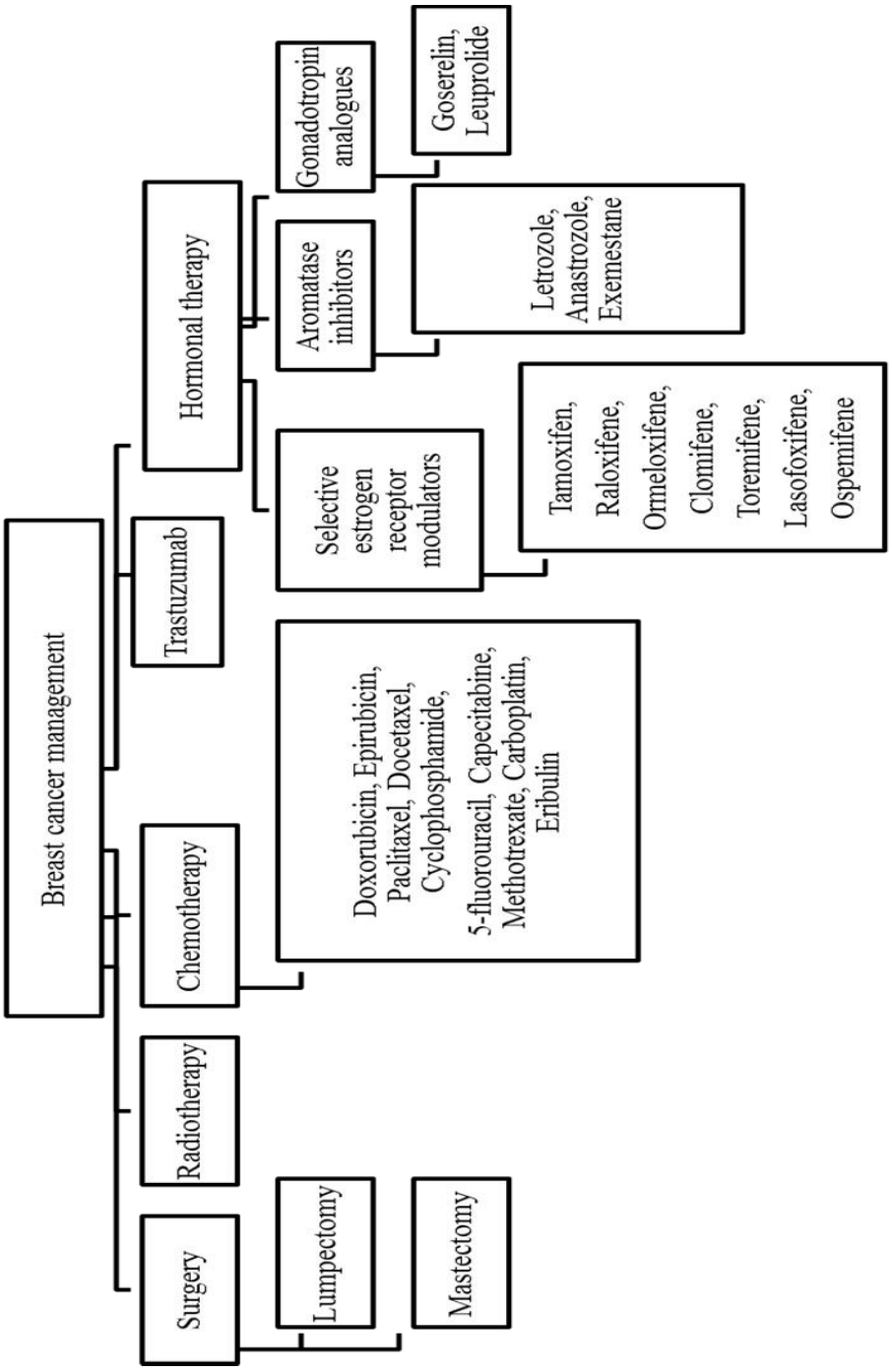

Figure 1. Therapeutic modalities involved in the management of breast cancer.

Since ER-positive breast cancer comprises the vast majority of breast cancer cases, hormonal therapy plays an important role in the management of these patients. Hormonal therapy includes 3 different categories; selective estrogen receptor modulators, aromatase inhibitors, and gonadotropin analogues (51–53). Among the different hormonal therapies currently used in practice, letrozole (LTZ) is considered one of the most promising aromatase inhibitors in the realm of breast cancer management. The drug has gained attention after demonstrating relatively high effectiveness and safety profile as compared with other alternatives, specifically tamoxifen (54,55). The US Food and Drug Administration (FDA) has approved the drug as an adjuvant for the treatment of hormonally positive local or metastatic breast cancers in postmenopausal women (56). The following sections will highlight the clinical benefits of LTZ, its place in therapy, the adverse effects associated with it, and the new formulations developed in order to overcome its limitations.

1.2 Letrozole

In 2004, LTZ was approved by the FDA as extended adjuvant therapy for the treatment of ER-positive breast cancer in postmenopausal women after the completion of a 5-year tamoxifen therapy (57). A year later, the drug was rapidly approved as an adjuvant monotherapy for the same condition without the need for prior administration of tamoxifen (58,59). This was due to its proven efficacy elicited from two large, multi-center trials where patients received LTZ for an average duration of 2-5 years, and followed up for about 2.3 and 2.17 years in extended adjuvant and adjuvant monotherapy trials, respectively (60–62).

1.2.1 Mechanism of Action

LTZ is a 3rd generation, irreversible aromatase inhibitor with steroids-free actions. Aromatase is a metabolic enzyme that presents in a number of various tissues such as the ovaries (prior to menopause), adipose, muscular, hepatic, and breast tissues. It acts as a catalyst for estrogen biosynthesis, promoting the conversion of testosterone and androstenedione into the freely circulating forms of estrogen; estradiol and estrone, respectively (63). In postmenopausal women, aromatase serves as the primary source of estrogen supply since the ovaries become inactive (64). Therefore, the inhibitory effects of LTZ suppresses the levels of estrogen to more than 99% in just 48-78 hours (65). At first, scientist have developed aromatase inhibitors that later were found to have anti-steroidal actions (1st generation), resulting in numerous adverse effects due to the suppression of steroids production. This led to the development of newer agents that are

of non-steroidal actions with higher potency, efficacy, and selectivity (3rd generation). These include LTZ, anastrozole, and exemestane (66). In vitro studies have revealed that LTZ has a potency that exceeds that of anastrozole and exemestane 2-5 times, whilst in-vivo models have shown that the potency of LTZ is even 10-20 times more than its competitors (67).

1.2.2 Dosing and Place in Therapy

LTZ is given orally, 2.5 mg daily, marketed as a tablet dosage form (Femara®) (59). Two large, multi-center, double-blind, randomized clinical trials have demonstrated its superiority over tamoxifen. In the first trial (n=8010), LTZ significantly improved disease-free survival (the duration at which the patient did not experience relapse, recurrence, metastasis, or death) as compared with tamoxifen (p= 0.002). Although, the two drugs did not significantly differ in the overall survival rates, nearly 70% of the patients receiving tamoxifen had to switch to LTZ after 2 years of treatment to complete another 3 years of LTZ therapy. Upon completion of therapy, those treated with LTZ had an overall disease-free survival of 87.4%, whist those who completed their tamoxifen therapy had an overall disease-free survival of 84.7% (P= 0.03). Hazards ratio was also lower in LTZ arm as compared with tamoxifen arm (95% CI, 0.75–1.02). In addition, there was no significant difference between those who received LTZ after initial tamoxifen therapy when compared to those who just received LTZ from the beginning in terms of disease-free survival (61,62).

In the second randomized clinical trial, tamoxifen was given for 5 years followed by LTZ for 2 years in one arm. In the other arm, LTZ monotherapy was given for 5 years. Results have shown that LTZ monotherapy had significantly higher disease-free survival rates over tamoxifen/LTZ therapy (60). Based on these findings, treatment guidelines that have long recommended tamoxifen as a first-line option to postmenopausal women with ER-positive breast cancer, switched to recommend LTZ as a first-line option for these patients, instead (42,68).

1.2.3 Chemical Structure and Pharmacokinetic Profile

LTZ is a drug that has a molecular formula of $C_{17}H_{11}N_5$ and a molecular weight of 285.3 g/mol. It has one major 1,2,4-Triazole group and two nitriles groups which explain the basic nature of the drug with a pKa of 1.6 (Figure 2). The drug is crystalline in nature, existing in a stable polymorphic form with a melting point of 184-186 °C, and it is readily soluble in organic solvents such as dichloromethane, acetone, and acetonitrile (57). The water solubility of the drug was reported to be 0.0799 mg/ml. According to the Biopharmaceutics Classification System (BSC), LTZ is classified as either class 1 (high permeability, high solubility) or class 3 (low permeability, high solubility). Since almost 20 mg of LTZ (8 times the dose strength; 2.5 mg) can be dissolved in less than 250 ml of water (pH 1-7.5), the drug is considered to be highly soluble (69). LTZ is rapidly absorbed from the gut as it has a partition coefficient (log P) value of 2.5, giving rise to a bioavailability of almost 99.9% (65), which indicates its high permeability. Therefore,

LTZ is more likely to be a class 1 drug rather than class 3. In addition, the absorption of the drug is not affected by the food which is an advantage over many other drugs. Protein binding is not common with LTZ, thus, the drug has a large volume of distribution, reaching various tissue types. The metabolism of the drug occurs very slowly via CYP3A4 and CYP2A6 hepatic enzymes which convert LTZ into an inactive metabolite that is a conjugate of glucuronide (70). Renal excretion represents the major clearance pathway where 90% of LTZ was found to be excreted in urine with 6% in an unchanged form. Approximately, the reported half-life of the drug is about 2 days, and its concentrations reach the steady state in the plasma in an average of 2-6 weeks (71). However, these concentrations are found to be 1.5-2 times higher than the estimated levels, indicating a non-linear pharmacokinetic release profile (72). Such non-linearity in release profile makes the drug exceed its therapeutic window, causing serious adverse effects (73). Therefore, it is of high importance to prevent the occurrence of this phenomenon through designing new delivery systems with accurately predictable pharmacokinetic profiles to keep LTZ within its therapeutic levels without reaching the toxic concentrations.

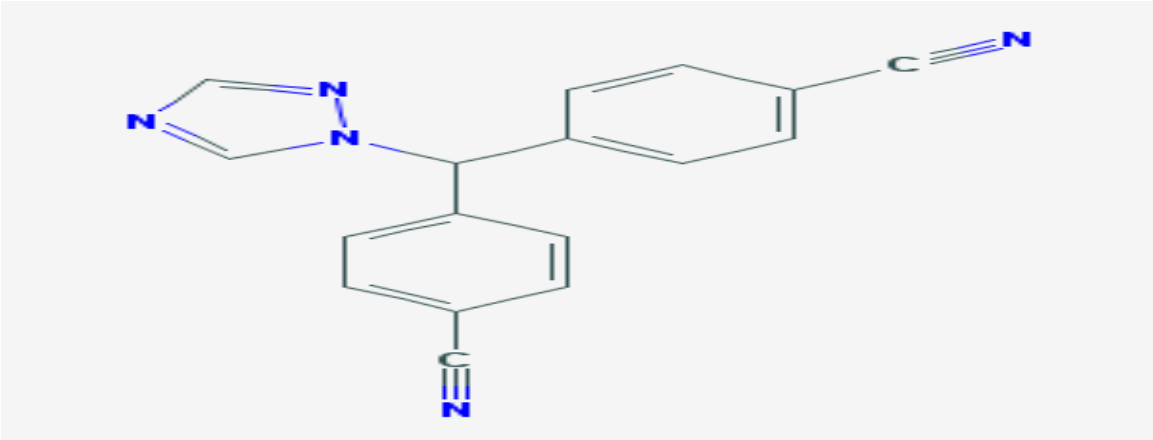

Figure 2. Chemical structure of LTZ.

1.2.4 Adverse Effects

According to the two clinical trial conducted on LTZ, the drug was found to associated with several adverse effects related to cardiovascular, musculoskeletal, respiratory, neurologic, and gastrointestinal systems (60–62). Table 1 summarizes the common adverse effects experienced with the administration of LTZ among patients.

Table 1. *Adverse Effects of LTZ*

Adverse effect	**Frequency (%)**
Hot flashes	49.7%
Night sweats	24.2%
Increased weight	10.7%
Nausea/ vomiting	7-17%
Diarrhea/ constipation	8-11.3%
Fatigue (lethargy, malaise, asthenia)	8.4%
Dizziness	14.2%
Myalgia/ arthralgia/ arthritis	22%
Bone pain/ fractures	5.6%
Headache	20.1%
Dyspnea	18%
Edema	18.5%
Thromboembolic events	1.1%
Pulmonary embolism	2%
Myocardial infarction	0.5%

1.2.5 Literature Review of Letrozole Formulations

a. Nanospheres Prepared by Nanoprecipitation

Nanoprecipitation is a simple, easy, and highly reproducible technique that allows rapid formation of nanoparticles. Ever since its development by Fessi et al. in the late nineties (74), the technique has gained considerable attention in preparing polymeric drug delivery carriers. In this technique, a polymer is basically dissolved in a volatile solvent that is miscible with water to form a polymeric solution. This formed solution is then poured slowly into surfactant-containing aqueous medium, causing the solvent to diffuse quickly to the aqueous phase, resulting in the precipitation of the polymer as nanoparticles. Therefore, the technique was termed "solvent displacement", and both expressions are used interchangeably nowadays (75).

Recently, Mondal and colleagues have utilized this technique in their attempt to prepare a new formulation of LTZ that would offer sustained-release actions of the drug (76). Formulations of varying polymer-to-drug ratios (5:1, 10:1, and 20:1) were prepared using acetone as a solvent and poly (D, L-lactide-co-glycolide) (PLGA) as a polymeric carrier. The authors were successful in generating spherical LTZ-PLGA nanoparticles with smooth surfaces, which held the potential of offering enhanced controlled-release actions. In addition, the produced particles were ranging from 140 nm to 167 nm. It was reported that particles with aerodynamic diameters less than 300 nm are easily transported across cell membranes (77). Therefore, the formulated particles in this study were expected to possess reasonable penetration through the cancerous tissues. However, the drug entrapment efficiency in these formulations was very low with 27% being the highest percentage obtained. This represents a critical limitation in their study which could be attributed to several factors such as the use of a high mixing speed (78), rapid addition of

the polymer solution to the aqueous phase (79), high concentration of the surfactant (80), and the use of a strong solvent such as acetone which resisted the precipitation of PLGA (81). The first three factors could be modified by simply decreasing the mixing speed and the concentration of the used surfactant with drop-wise addition of the polymer solution to the aqueous medium. Nevertheless, the last factor is not as simple. Although it is true that the use of less soluble solvents would facilitate polymer precipitation, and as such would improve drug entrapment efficiency, reduction in polymer solubility would diminish its elasticity, and hence, would result in less efficient drug release from the polymer (82). Thus, to overcome this issue, it is better to seek another technique that is not affected by the type of solvent used such as dispersion-solvent evaporation which conquers the limitations of the precipitation technique (83).

b. Nanospheres Prepared by Emulsification

This technique is very similar to the nanoprecipitation technique with the only exception being the use of two immiscible solvents. This implies that both the polymer and the drug are dissolved in a solvent that is not miscible with the external phase to which they are dispersed in (84). Different types of emulsions have been produced through altering the dispersed phase and the dispersion medium. These include oil in water (o/w), water in oil (w/o), water in oil in water (w/o/w), oil in water in oil (o/w/o), and many other complex systems (85). In usual emulsification procedures, micro-sized droplets are formed and dispersed in the continuous phase due to differences in surface tension between the two phases (86). The reduction in droplet size is enabled through diverse mechanisms such as

homogenization, ultra-sonication, and microfluidic filtration. Despite the variations in the three mechanisms, they all carry the same concept of applying external forces on the dispersed droplets, producing a shearing stress that breaks them down into smaller sizes (87,88).

In 2009, the group of Mandal et al. used the dispersion-solvent evaporation technique in preparing LTZ-PLGA nanoparticles. In general, LTZ and PLGA were dissolved in dichloromethane, and this solution was then added slowly to an aqueous phase to form a dispersion. The formed dispersion was subjected to ultra-sonication for particle size reduction, followed by mechanical stirring to evaporate the solvent, and finally lyophilization was carried out to eliminate the water from the formulation in order to obtain dried LTZ-PLGA nanoparticles (89). Generated particles from this technique were ranging from 64 nm to 255 nm in size with a poly-dispersity index range of 0.27 to 0.66. Although the particle size was within an acceptable range that would ensure tissue penetration, the wide size distribution as indicated by the poly-dispersity index may impact the homogeneity of particles uptake by the cells (90). In contrast to the previous trial that used solvent precipitation technique, the entrapment efficiency obtained with this technique was very high, ranging from 68% to 82%. On the other hand, in vitro release studies revealed that LTZ release from PLGA in these formulations followed zero-order kinetics which entails that concentration-independent drug release actions were achieved (91). However, there was an initial burst release of LTZ encountered. This could be related to the type of PLGA used which consisted of 75% lactic acid: 25% glycolic acid. The high content of lactic acid triggered the autocatalytic degradation of

the polymer chains which accelerated the release of the drug. Therefore, whenever PLGA is used, lower contents of lactic acid (≤ 50%) should be selected in order to avoid the burst effect (92).

c. Solid Lipid Nanoparticles

Solid lipid nanocarriers are recently emerging drug delivery systems evolved as alternatives to polymeric carrier systems. They consist of a single layer of physiologically-tolerated lipids that encloses inside its core the hydrophobic solid drug particles (93). The inclusion of a lipid bilayer would create an aqueous core for the encapsulation of water-soluble drugs, and such a system is called a liposome (94,95).

Basically, the lipid shell is formed when the lipid particles which are amphiphilic in nature (composed of hydrophilic heads and hydrophobic tails) are placed in an aqueous medium. The hydrophilic heads immerse themselves inside the aqueous phase, exposing their tails to the surface. Upon increasing the concentration of the lipid particles above their critical micelle concentration, they align themselves in a circle with polar heads exposed to the water phase and non-polar tails hidden towards the core. This phenomenon occurs since this alignment establishes a more favorable thermodynamic state for the lipid particles, providing them with lowest energy levels, and yet, highest physiochemical stability levels (96).

These lipid-based carriers hold the advantage of being less toxic to the biological systems as compared with polymeric carriers owing to their tolerable lipid composition. In addition, reports have shown that these systems have higher bioavailability than

polymeric systems which is again due to their lipid composition which is close to that of the physiologic membranes, making their cellular uptake easier and more favorable than the polymeric carriers (97).

Recently, Nerella et al. presented a new formulation of LTZ-solid lipid nanoparticles using trimyristin as a solid lipid core. Briefly, LTZ, trimyristin, and surface active agents were mixed with methanol and chloroform (50%:50%). The solvent was evaporated using rotary evaporator by heating at 62 °C. An aqueous phase was heated also at 62 °C, and then added to the drug-containing mixture. Particle size reduction was facilitated through homogenization followed by ultra-sonication (98). Of the eight different formulations prepared, one formulation carried promising results. In this formulation, the particles were 29 nm in size with very narrow size distribution as indicated by a poly-dispersity index of 0.162, and a very high entrapment efficiency of 85.6%. In vitro release studies showed that the drug followed first order kinetics over a 24-hours period. The formulation was stable for one month only where significant changes in the formulation characteristics were observed after one month. Such limitation is related to the lipid composition of the formulation which is thought to possess various degrees of polymorphism, resulting in drug leakage (97). Since this formulation seems very promising, optimizing its stability is worthwhile. Decreasing the water content and increasing the concentration of surfactants could be valid options to enhance the stability of this formulation. In-vivo studies are also needed to investigate the efficacy, safety, and pharmacokinetic profile of this formulation.

d. Niosomes

Niosomes are newly developed drug delivery systems that are very similar to liposomes in structure. The only difference between the two systems is that niosomes are composed of a single bilayer of non-ionic surfactants (which consist of one polar head and one non-polar tail) with cholesterol (99). On the other hand, liposomes are composed of a single bilayer of phospholipids (which consist of one polar head and two non-polar tails) with or without cholesterol. Similar to liposomes, niosomes are thought to have higher biocompatibility and bioavailability when compared to other polymeric drug delivery systems. Therefore, much attention is being paid on the utilization of these carriers for drug delivery purposes (100).

Norouzian and Azizi have recently reported a new formulation of LTZ incorporated into a PEGylated niosomal system. In summary, LTZ, polyethylene glycol (PEG), cholesterol, and surfactants (tween and span 60) were dissolved in alcohol under mechanical stirring for half an hour. Alcohol was evaporated using rotary evaporator. After adding a phosphate buffer saline at physiologic pH, the mixture was subjected to ultra-sonication at 40 °C to produce nano-sized niosomes (101). The obtained formulation achieved a relatively high entrapment efficiency of LTZ (66.6%). In addition, in vitro release of LTZ was seen to follow first-order kinetics, reflecting the ability of the system to sustain the release of LTZ over 48 hours (91). More importantly, this formulation demonstrated less toxic effects than pure LTZ according to the in vitro studies. Although the results of this

study showed promising findings, it failed to report several important characteristics of the prepared formulation such as particle size distribution, thermal analyses, and stability studies which are needed to have a clear picture about the proposed claims. Moreover, the reproducibility of this formulation is somewhat doubtable since the authors just reported the results of one experiment only. Therefore, it is advisable to run more experiments in order to increase the reliability of their results. This, however, should not prevent other researchers from considering the use of the niosomal carriers as a viable option for effective drug delivery system.

1.3 Monodisperse Microparticles as Drug Delivery Systems

The term ‘monodisperse’ refers to particles with a narrow size distribution. This entails that the particles have nearly similar shape and size, appearing almost identical under microscopic analysis (102–107). Such highly uniform particles are highly favored for drug delivery purposes over polydisperse particles which have a wider particle size distribution and heterogeneous nature (106,108,109). This is because the behavior of monodisperse particles in both in vitro and in vivo systems can be predicted with high accuracy. This means that when monodisperse particles are used as drug carriers, they can deliver equal amounts of drug per particle, resulting in optimized release profile kinetics for the delivered drug. This is mainly due to the fact that drug release from highly uniform particles can be accurately determined from the previously calculated surface area with respect to the volume and the equivalent distances between the diffused

drug particles and/or rate of degradation of the polymeric carrier (110–122). Therefore, the progression towards in-vivo studies would maintain its repeatability as that of in vitro testing. This is of high importance since such constant drug delivery to target sites inside the body would offer controlled drug release over extended periods of time, preventing the fluctuations of the drug's levels, which would eventually maintain the concentrations of the drug within its therapeutic range. The ultimate goal of this is to minimize the undesirable adverse effects of the drug and increase patient compliance (122–127).

In any drug delivery system, monodisperse particles present an outstanding performance over polydisperse counterparts. In pulmonary drug delivery systems, for instance, the administration of monodisperse particles would ensure their delivery to the specific site as minor differences in size distribution would result in particles being deposited in unwanted regions of the pulmonary systems (77,128). Likewise, systemic routes of administration such as intravenous (IV) and intramuscular (IM) routes of anticancer drugs in a monodisperse fashion would facilitate the targeted embolization of tumor vessels (129).

Although monodispersity has been discussed extensively in literature, universal standardization for the term 'monodisperse' is lacking. In addition, there is a scarcity in the well-established measures for assessing how truly the produced particles meet the criteria of monodispersity (130). Thus, it is essential to define a set of criterion for monodispersity in order to be able to evaluate the success of a method in producing actual monodisperse microparticles. Upon extensive literature review, particles are thought to be

monodispersed if their median size distribution expressed in ‘span’ values is <0.3, or if the coefficient variation of their size distribution is <3.001%. Now, the span refers to a well-known parameter used to measure the width of the size distribution. It is calculated as: Span= (D90 - D10)/ D50.

Where D90, D10, and D50 represent the median diameter by which 90%, 10%, and 50% of the size distribution has a smaller particle size than the given value of the equation (111,116,118,121,122,131,132).

1.4 Vibrating Orifice Aerosol Generator (VOAG)

Vibrating Orifice Aerosol Generator (VOAG) is an instrument that was developed by Berglund-Liu in 1973 (133). The instrument was designed originally to produce a constant jet of monodisperse liquid droplets that would dry off upon passing a drying column, leaving the solutes that were dissolved in that liquid in the form of monodisperse microparticles (Figure 3) (134). The VOAG could also be operated in an inverted position where the liquid jet stream would fall down instead of travelling up the column. In order to use the VOAG in generating monodisperse microparticles, an organic solution of LTZ along with a polymeric carrier; either Polycaprolactone (PCL), or Poly(D,L-Lactide) (PDLLA) would be injected into the VOAG, and upon passing an extremely narrow orifice, vibrating at frequency of 100-1000 kHz, a monodisperse cylindrical liquid jet would be formed. Afterwards, this jet would eventually get broken down into microdroplets as a result of the orifice vibration. With the flow of a dry air, the

microdroplets would be dried, forming the intended monodispersed microparticles which would be collected in the cylindrical chamber.

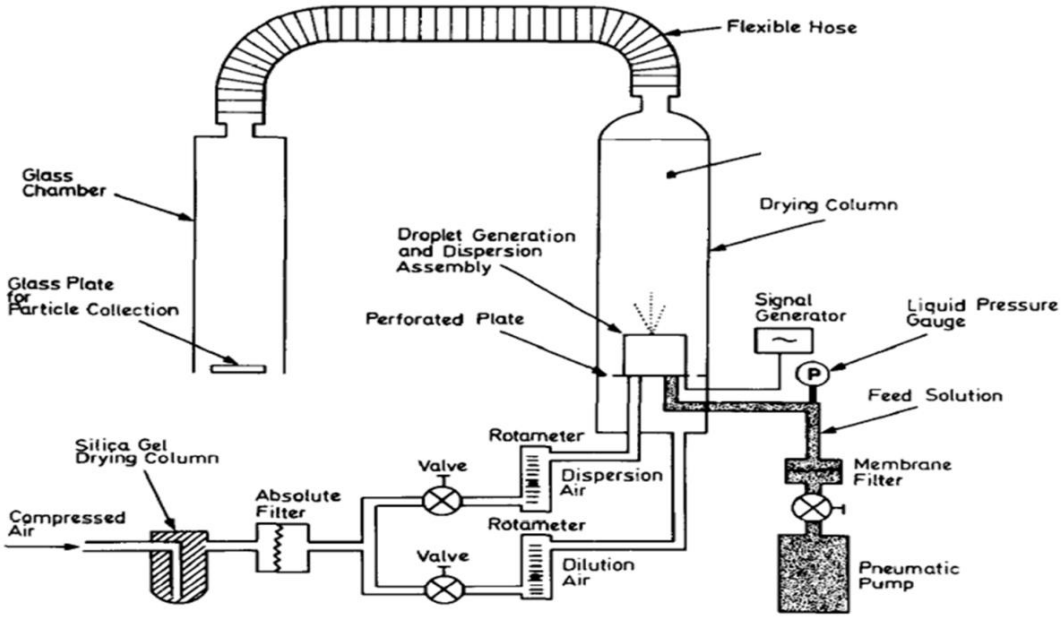

Figure 3. Schematic representation of the VOAG (135).

1.5 Study Hypothesis

This study hypothesized that if LTZ was incorporated into monodisperse polymeric microparticles either using PCL or PDLLA, the new complex would possess improved release kinetics profile, and hence, the safety of LTZ would be potentially improved.

1.6 Study Objectives

1. To prepare monodispersed LTZ-loaded polymeric-based microparticles via the VOAG instrument using either PCL or PDLLA as drug carriers.

2. To screen for and identify the significant factors affecting particle size distribution in order to optimize the prepared formulations.

3. To characterize the optimized formulations in terms of yield, morphology, particle size, zeta potential, thermal properties, physical state, drug loading, and entrapment efficiency.

4. To investigate the drug release profile through in vitro dissolution study.

5. To investigate the cellular cytotoxicity of the optimized formulations against conventional LTZ on MCF-7cells.

Chapter 2: Materials and Methods

2.1 Materials and Equipment

Table 2 summarizes the materials used in conducting the experiments. All chemicals were used as supplied without any further purification or chemical modification.

Table 2. *Summary of the Chemicals Used in the Study*

Substance	**Suppling company**
Letrozole	Jiangsu Ainty Handsome CO., LTD (China)
Poly(D,L-Lactic acid), MW 15000, IV 0.2 dl/g	Polysciences, Inc. (PA, USA)
Polycaprolactone, MW 50000, powder	Polysciences, Inc. (PA, USA)
Dichloromethane (HPLC gradient grade, 99.8%)	Sigma-Aldrich Co. LLC (Germany)
Polyvinyl alcohol (88% hydrolyzed)	Sigma-Aldrich Co. LLC (Germany)
Polystyrene monodisperse microparticles, 20 µm	Sigma-Aldrich Co. LLC (Germany)
Transcutol® HP	Gattefossé (Lyon, France)
Acetonitrile gradient grade	Merk Co. (Germany)
Potassium chloride (purity: 99.9%)	BDH LLC. (UK)
Dialysis tubing cellulose membranes (MW cut-off = 14,000)	Sigma-Aldrich Co. LLC (Germany)
MCF7 (ATCC® HTB-22™) cell line	ATCC®, VA, USA
Primary Mammary Epithelial Cells; Normal	ATCC®, VA, USA
Eagle's Minimum Essential Medium (EMEM)	ATCC®, VA, USA
Mammary Epithelial Cell Basal Medium	ATCC®, VA, USA
Mammary Epithelial Cell Growth Kit	ATCC®, VA, USA
Penicillin-Streptomycin-Amphotericin B Solution	ATCC®, VA, USA
Trypsin-EDTA Solution, 1X	ATCC®, VA, USA
Trypsin Neutralizing Solution	ATCC®, VA, USA
Dulbecco's Phosphate Buffered Saline (D-PBS), 1X	ATCC®, VA, USA

2.2 Optimization of the Monodisperse Microparticles Production Process

The use of the VOAG in producing monodisperse microparticles was accompanied with several challenges that restricted the operational process and resulted in a very low yield. These included instability in liquid pressure that builds up upon passing through the tubes of the instrument, persistent clogging of the orifice which prevented the consistent liquid feed, inefficient drying system, and difficulty in collecting the particles. Therefore, a number of modifications were implemented in order to optimize the production process, facilitate handling of the instrument, maximize the percentage yield, and minimize material loss. To stabilize liquid pressure, the Teflon O-ring (0.075 mm in thickness) that holds the orifice disc was replaced with a rubber O-ring (2 mm in thickness). To overcome the issue of persistent clogging of the orifice, the orifice disc that had a hole diameter of 20 µm was replaced with a specially manufactured orifice disc purchased from Lenox Laser, Inc. (MD, USA) with the following parameters:

Disc diameter: 9.5 mm ± 0.26% mm

Hole diameter: 300 µm ± 5% µm

Thickness: 0.05 mm ± 5% mm

Centering: ± 0.25 mm

Finally, in an effort to overcome the inefficient drying system that led to the difficulty in collecting the particles, the drying column was removed and the liquid chamber base was inverted and mounted on a beaker where the dispersion cap was totally immersed in the

collecting medium inside the beaker. The collecting medium consisted of 0.04-1% Polyvinyl Alcohol (PVA) aqueous solution.

2.3 Preparation of Polymeric Monodisperse Microparticles Loaded with Letrozole

An amount of 1 g PCL or PDLLA was mixed with 5-30% w/w LTZ in 1-2 % w/v ml dichloromethane. The resulting organic solution was filled into the syringe connected to the pump of the VOAG to flow at a rate of 0.17-1.7 ml/min. Upon passing the 300 µm orifice vibrating at a frequency of 100-1000 KHz, a constant stream of monodispersed microdroplets was generated. These droplets were collected in a 0.04-1% Polyvinyl Alcohol (PVA) aqueous medium which served as a stabilizer to prevent particles aggregation (75). Before choosing PVA to prevent particles aggregation, different surfactants were tried such as Tween 20, Tween 80, Span 20, Span 80, and sodium lauryl sulfate. However, all of these surfactants did not maintain an adequate dispersion of the particles, therefore, PVA was selected as it appeared to efficiently prevent particles aggregation. The ratio of the organic medium: aqueous medium was 1:4-1:8 v/v. The formed dispersion was stirred at 250-500 rpm, ambient temperature for 24 hours to ensure complete solvent evaporation. Solidified microparticles were collected through filtration, washed several times with distilled water to remove residual PVA, and then centrifuged at 5°C, 8500 rpm for 10 minutes, and finally dried under vacuum at -19 Kpa at 35°C over 48 hours.

Production parameters such as drug loading, organic phase concentration, liquid flow rate, frequency, PVA concentration, organic: aqueous phase ratio, and stirring rate were screened to explore their effects on particle size and particle size distribution using a 12-run Plackett-Burman design (136). The optimal parameters as revealed by the Plackett-Burman design were used in further experiments in order to produce the most homogenous monodisperse microparticles possible. These optimized particles obtained were characterized for percentage yield, microscopic morphology, particle size, zeta potential, drug loading, drug entrapment efficiency, thermal properties, physical characteristics, drug release kinetics, and in vitro cytotoxicity.

2.1 Experimental Design for Optimizing the Production Parameters

Multiple factors involved in the production process of monodisperse particles were thought to have an effect on particle size distribution including drug loading, organic phase concentration, organic: aqueous phase ratio, PVA concentration, frequency of the vibrating orifice, liquid flow rate, and stirring rate (137). Therefore, it was essential to study the effects of these factors on particle size distribution in order to determine the optimal values of each one that would yield optimal monodisperse particles. Thus, a screening of the 7 factors that were thought to have an impact on particle size distribution was constructed based on Plackett-Burman design which is a powerful tool that allows the accurate identification of major factors influencing an outcome with a minimal number of experiments. This is because Plackett-Burman design is a fractional factorial

design that combines the advantage of accuracy of full factorial designs and the few experimental runs of fractional factorial designs. Therefore, the use of Plackett-Burman design is very reasonable in determining the factors that significantly affect the particle size distribution and specify the optimal values that would result in the desired outcomes. Using Minitab® 17 Statistical Software (Coventry, UK), a 12-run, 2-level Plackett-Burman design was created with each run containing a combination of the different levels of the following factors: drug loading (X1), organic phase concentration (X2), organic: aqueous phase ratio (X3), PVA concentration (X4), frequency of the vibrating orifice (X5), liquid flow rate (X6), and stirring rate (X7). The highest and lowest levels for each factor were selected based on the reported results of previous studies in literature (136,138,139). Table 3 illustrates the 12-run Plackett-Burman design with all different combinations. Each run was done in triplicate for each polymeric carrier; PCL and PDLLA. Particles generated from each run were analyzed for their particle size distribution where the average span values were calculated and reported. The main effects of each of the 7 factors on the average span values were examined using Minitab® 17 Statistical Software.

Table 3. *Plackett-Burman Design for Optimizing PCL- and PDLLA-based Formulations*

Formulation	Drug loading (%w/w)	Organic phase concentration (%w/v)	Organic: aqueous phase ratio	PVA concentration (%w/v)	Frequency (KHz)	Liquid flow rate (ml/sec)	Stirring rate (rpm)
F1	5	1	1: 8	0.1	1000	0.17	500
F2	30	2	1: 4	0.1	100	0.17	250
F3	30	1	1: 8	0.04	100	0.17	500
F4	5	2	1: 8	0.04	1000	0.17	250
F5	30	2	1: 4	0.1	1000	0.17	500
F6	5	2	1: 8	0.1	100	1.7	500
F7	30	2	1: 8	0.04	1000	1.7	250
F8	5	2	1: 4	0.04	100	1.7	500
F9	5	1	1: 4	0.04	100	0.17	250
F10	5	1	1: 4	0.1	1000	1.7	250
F11	30	1	1: 4	0.04	1000	1.7	500
F12	30	1	1: 8	0.1	100	1.7	250

2.2 Ultra-Performance Liquid Chromatography (UPLC) Validation

2.2.1 UPLC Specifications

International Council for Harmonization (ICH) guidelines were followed in the validation process (140). Table 4 summarizes the specific instrument, accessories, and parameters used during the validation process.

Table 4. *Summary of the UPLC Specifications*

Component	**Description**
Instrument	ACQUITY UPLC® H-Class System
Column	ACQUITY UPLC® BEH C-18 (2.1 x 50 mm, 1.7 µm particle size)
Detector	ACQUITY UPLC® Tunable UV Detector, set at λ= 240 nm
Mobile phase	Acetonitrile: Water (35:65, v/v) under isocratic conditions
Diluent and solvent	Acetonitrile
Flow rate	0.3 ml/min
Injection volume	1 µl
Column temperature	25 °C
Sample temperature	20 °C
Retention time	Approximately 1.8 min
Filter	Polytetrafluoroethylene (PTFE) 0.2 µm

Standard and sample solutions were both prepared by dissolving 25 mg LTZ in 50 ml acetonitrile in a volumetric flask through vigorous shaking followed by 5 minutes of sonication, and then diluting 5.0 ml of this solution using the mobile phase in a 50.0 ml volumetric flask to make up a final concentration of 50.0 µg/ml. Before injection, the solutions were filtered using 0.2 µm PTFE filters. For accurate measurements, fresh standard and sample solutions were prepared on the day of injection.

2.2.2 System Suitability

It was essential to confirm that the UPLC system would be appropriate for the detection of LTZ from its formulations. In order to do so, peak area, tailing factor, retention time, and theoretical plates were quantified.

2.2.3 Forced Degradation Studies

These studies were very important as they provide an evidence of how stable and specific the method is in analyzing LTZ content from the prepared formulations. Stock solutions were prepared by dissolving 25.0 mg LTZ in 50.0 ml acetonitrile (500 µg/ml) in a volumetric flask which was placed in a cold water bath for 30 minutes of sonication to ensure complete dissolution of LTZ. These solutions were then filtered using double 0.2 µm PTFE filters, subjected to freezing at -4 °C for 3 hours, removed from the freezer and kept at room temperature for 15 minutes, and finally filtered again using 0.2 µm PTFE

filters. This step was done to ensure that all impurities got precipitated in order to minimize the blockage of the UPLC column as it was found to be effective in our preliminary trials while working with the UPLC system. However, this was not validated in this study as the time did not permit for that. In addition, it was very important to conduct the forced degradation studies in the presence of the two polymers; PCL and PDLLA to provide a comprehensive stability profile of the produced formulations. However, due to time limitation, this was done only on LTZ alone, and as such this was a limitation in this study. Therefore, these experiments should be incorporated in our future studies.

2.2.3.1 Acidic Stability

A 5.0 ml of the stock solution (500 µg/ml) was placed in a round bottom flask to which 5.0 ml of 0.1 N HCL was added. The mixture was refluxed for 2 hours at 80 °C. After that, the solution was allowed to cool down, and then transferred to a 50.0 ml volumetric flask to be neutralized by adding 5.0 ml 0.1 N NaOH and toped up with acetonitrile to yield a final concentration of 50 µg/ml. Another 5.0 ml of the stock solution (500 µg/ml) was also diluted with acetonitrile in a 50.0 ml volumetric flask to yield a final concentration of 50 µg/ml. This solution served as a standard to measure the difference in LTZ concentration after being exposed to a stress acidic environment. The percentage of LTZ degradation was calculated using the following formula:

$$\% \text{ LTZ degradation} = \frac{\text{LTZ concentration after acidic stress}}{\text{LTZ concentration without any stressful condition}} \times 100$$

2.2.3.2 Basic Stability

A 5.0 ml of the stock solution (500 µg/ml) was placed in a round bottom flask to which 5.0 ml of 0.1 N NaOH was added. The mixture was refluxed for 2 hours at 80 °C. After that, the solution was allowed to cool down, and then transferred to a 50.0 ml volumetric flask to be neutralized by adding 5.0 ml 0.1 N HCL and toped up with acetonitrile to yield a final concentration of 50 µg/ml. Another 5.0 ml of the stock solution (500 µg/ml) was also diluted with acetonitrile in a 50.0 ml volumetric flask to yield a final concentration of 50 µg/ml. This solution served as a standard to measure the difference in LTZ concentration after being exposed to a stress basic environment. The percentage of LTZ degradation was calculated using the following formula:

$$\% \text{ LTZ degradation} = \frac{\text{LTZ concentration after basic stress}}{\text{LTZ concentration without any stressful condition}} \times 100$$

2.2.3.3 Oxidative Stability

A 5.0 ml of the stock solution (500 µg/ml) was placed in a round bottom flask to which 5.0 ml of 3% H2O2 was added. The mixture was refluxed for 2 hours at 80 °C. After that, the solution was allowed to cool down, and then transferred to a 50.0 ml volumetric flask and toped up with acetonitrile to yield a final concentration of 50 µg/ml. Another 5.0 ml of the stock solution (500 µg/ml) was also diluted with acetonitrile in a 50.0 ml volumetric flask to yield a final concentration of 50 µg/ml. This solution served as a standard to measure the difference in LTZ concentration after being exposed to an oxidative stress. The percentage of LTZ degradation was calculated using the following formula:

$$\% \text{ LTZ degradation} = \frac{\text{LTZ concentration after oxidative stress}}{\text{LTZ concentration without any stressful condition}} \times 100$$

2.2.3.4 Thermal Stability

A 5.0 ml of the stock solution (500 µg/ml) was diluted with acetonitrile in a 50.0 ml volumetric flask to yield a final concentration of 50 µg/ml. This solution was heated at 80 °C for 4 hours, then cooled down and injected in the UPLC to measure LTZ concentration. LTZ concentration detected from this solution was compared with a diluted stock solution (50 µg/ml) to calculate the percentage of LTZ degradation after

being exposed to excessive heating. The percentage of LTZ degradation was calculated using the following formula:

$$\% \text{ LTZ degradation} = \frac{\text{LTZ concentration after heating}}{\text{LTZ concentration without any stressful condition}} \times 100$$

2.2.3.5 UV-radiation Stability

A 5.0 ml of the stock solution (500 µg/ml) was diluted with acetonitrile in a 50.0 ml volumetric flask to yield a final concentration of 50 µg/ml. This solution was exposed to UV light (λ= 365 nm) at room temperature for 4 hours, then injected in the UPLC to measure LTZ concentration. LTZ concentration detected from this solution was compared with a diluted stock solution (50 µg/ml) to calculate the percentage of LTZ degradation after being exposed to UV light. The percentage of LTZ degradation was calculated using the following formula:

$$\% \text{ LTZ degradation} = \frac{\text{LTZ concentration after UV light exposure}}{\text{LTZ concentration without any stressful condition}} \times 100$$

2.2.3.6 Photo-stability

A 5 ml of the stock solution (500 µg/ml) was diluted with acetonitrile in a 50 ml volumetric flask to yield a final concentration of 50 µg/ml. This solution was exposed to visible light for at room temperature 24 hours, then injected in the UPLC to measure LTZ concentration. LTZ concentration detected from this solution was compared with a diluted stock solution (50 µg/ml) to calculate the percentage of LTZ degradation after being exposed to visible light. The percentage of LTZ degradation was calculated using the following formula:

$$\% \text{ LTZ degradation} = \frac{\text{LTZ concentration after visible light exposure}}{\text{LTZ concentration without any stressful condition}} \times 100$$

2.2.4 Selectivity and Specificity

The selectivity and specificity of the analytical procedure was assessed by comparing the purity chromatograms of LTZ peaks obtained from the acidic, basic, oxidative, UV-radiation, and photo-stability studies. The chromatograms were compared with that of a pure LTZ standard solution (50 µg/ml), freshly prepared without being exposed to any stressful condition. The ability of the analytical method to separate LTZ peak from other peaks pertaining to the degradation products was an indication of its selectivity and specificity.

2.2.5 Precision

An accurately weighed amount of 25 mg LTZ was dissolved in 50 ml of acetonitrile in a volumetric flask. The solution was sonicated for 30 minutes in a cold water bath to ensure complete dissolution of LTZ. Then it was filtered using 0.2 µm PTFE filters and put in the freezer at approximately -8 °C for 3 hours. Afterwards, the solution was allowed to warm up by leaving it at room temperature for 15 minutes. This was followed by another round of filtration using 0.2 µm PTFE filters, and finally the solution was diluted with acetonitrile to make up a final concentration of 50 µg/ml. The solution was then injected in the UPLC system to measure LTZ concentration to explore intra-day precision. For inter-day precision, similar procedure has been followed across two days. The test was made in 6 replicates with each being injected twice. The mean and RSD were reported.

2.2.6 Limit of Detection (LOD) and Limit of Quantitation (LOQ)

Limit of Detection (LOD) represents the least concentration of the substance in a sample (i.e., LTZ in this case) that can be detected by the analytical procedure but not necessarily quantified. Limit of Quantitation (LOQ), on the other hand, represents the least concentration of the substance in a sample that can be accurately and precisely calculated and quantified (140). LOD and LOQ were determined from the calibration curve where different known concentrations of LTZ (n=11) were injected in UPLC and plotted against

their corresponding areas as measured by the UPLC system. LOD and LOQ were calculated using the following equations:

LOD = (3.3 * SD)/ Slope

LOQ= (10 * SD)/ Slope

Where the slope was obtained from the linear equation of the calibration curve, and the SD was computed for the residuals of the regression line.

2.2.7 Linearity

A stock solution was prepared by dissolving 25 mg LTZ in 50 ml acetonitrile in a volumetric flask (500 µg/ml), followed by sonication for 5 minutes. A total of 11 solutions with different concentrations were made from that stock solution (0.5, 1, 2.5, 5, 10, 25, 50, 100, 150, 200, 250 µg/ml) and injected in UPLC for analysis. The concentrations were plotted against their corresponding areas obtained from the UPLC system. A fitted regression line having least residual sum of squares was drawn and its equation displaying the slope and y-intercept was reported.

2.2.8 Accuracy

Accuracy was assessed by measuring the percentage recovery of 3 different LTZ concentrations (40, 50, 60 µg/ml) prepared from the stock solution (500 µg/ml) as

previously described. The solutions were injected in UPLC and their corresponding concentrations were compared with a standard solution having a LTZ concentration of 50 µg/ml. Percentage recovery was calculated by the following equation:

$$\% \text{ Recovery} = \frac{\text{LTZ concentration obtained from the sample}}{\text{LTZ concentration obtained from the standard}} \times 100$$

The experiment was done in triplicate and the mean and RSD values were reported.

2.2.9 Effect of Filtration

Filtration is an essential part of the analytical procedure. Samples must be filtered prior to their injection into the UPLC system to prevent the entry of large particles that may clog the column and damage it. At the same time, it is necessary to ensure that the filter does not interfere with the active substance to be analyzed in order to get accurate results. Two types of filters were assessed for their efficiency to be used for filtering samples containing LTZ; 0.2 µm PTFE and 0.2 µm Nylon filters. To compare between these filters, 25 mg LTZ was dissolved in 50 ml of acetonitrile in a volumetric flask (500 µg/ml). The solution was sonicated for 30 minutes in a cold water bath to ensure complete dissolution of LTZ. Then it was filtered using either PTFE or Nylon filters and put in the freezer at around -8 °C for 3 hours. Subsequently, the solution was allowed to warm up by leaving it at room temperature for 15 minutes. This was followed by another round of filtration using either PTFE or Nylon filters, and finally the solution was diluted

with acetonitrile to make up a final concentration of 50 µg/ml. The solution was then injected in the UPLC system to measure LTZ concentration and this was compared with a standard LTZ solution (50 µg/ml) prepared similarly, but without filtration in order to calculate the percentage recovery. The experiment was done in 7 replicates and the mean and RSD were reported.

2.2.10 Solution Stability

Stability of LTZ solutions was evaluated at two storing conditions; at room temperature and in refrigerator (5 °C). Standard and sample solutions having LTZ concentrations of 50 µg/ml were prepared as previously described and stored in tightly closed unwrapped containers at room temperature and in refrigerator (5 °C) for 48 hours. The solutions were assayed using the UPLC system at 24 and 48 hours and percentage recovery was calculated by dividing LTZ concentrations obtained from the samples over LTZ concentrations obtained from the standards, multiplied by 100. The experiment was done in 6 replicates and the mean and RSD were reported.

2.3 Characterization of the Optimized Polymeric Monodisperse Microparticles Loaded with Letrozole

2.3.1 % Yield

Produced monodisperse microparticles were collected from the filter papers using a clean spatula, then weighed to observe how much was obtained from the initial amount used in preparing the formulations. The yield was calculated using the following formula:

% Yield= (Actual weight of the obtained microparticles)/ (Theoretical weight of the microparticles) x 100

2.3.2 Morphological Analysis

Approximately 5-10 mg of the dried monodisperse microparticles were spread on a double-sided tape fixed on an aluminum holder and then sprayed with a gold layer of around 20 nm in thickness. Imaging was carried out at 15.0 kV using Nova NanoSEM 450™ scanning electron microscope (FEI, California, USA).

2.3.3 Particle Size Analysis

Samples were appropriately diluted using distilled water and analyzed at a temperature of 25°C by the dynamic light scattering technology offered by the Mastersizer 2000 (Malvern Instruments Ltd., UK). Particle size and size distribution were determined by

measuring the mean hydrodynamic diameter and the span, respectively. The mean value of 3 replicates was calculated for each formulation.

2.3.4 Zeta Potential Analysis

Zeta potential was determined using laser Doppler micro-electrophoresis offered by Zetasizer Nano ZS (Malvern Instruments, Ltd, UK). Distilled water or 0.1 M KCL solution were used to dilute the samples (2-3 mg) which were analyzed through the instrument's software. Each value reported represented the mean of 3 replicates for each formulation.

2.3.5 Thermal Properties

Thermal characteristics of the obtained formulations were attained via Differential Scanning Calorimetry using the DSC 8000 instrument (Perkin Elmer Co., USA) equipped with the intra-cooling system (Intracooler II, Perkin Elmer Co., USA). Approximately 2-4 mg of each formulation was placed into an aluminum pan tightly sealed with an aluminum cover and scanned over a temperature range of 0 - 200°C or -70 - 200°C for PDLLA- and PCL-based formulations, respectively, with a rate of 10°C/min. Nitrogen gas flow was set at 40 ml/min to eliminate humidity that might affect the scanning. Pure LTZ, PCL, PDLLA, physical mixtures of LTZ and PCL/PDLLA, LTZ-PCL formulations, and LTZ-PDLLA formulations were analyzed through DSC.

2.3.6 Structural Characterization

Physical structure studies were performed using X-ray diffractometer (D8 Advance, Bruker Co., Germany) by employing CuKα radiation source. Pure LTZ, PCL, PDLLA, physical mixtures of LTZ and PCL/PDLLA, LTZ-PCL formulations, and LTZ-PDLLA formulations were analyzed using A1° divergence slit between the 2θ range 5-60°C with a step size of 0.1°C and step time of 1 sec. DIFFRAC.EVA software was used to obtain the resulted XRD patterns.

2.3.7 Drug Loading and Entrapment Efficiency Measurement

Drug loading was determined by solubilizing specific quantities of the different formulations in 50 ml acetonitrile, followed by sonication for 10 min to ensure complete dissolution of the drug in the solvent, and then LTZ concentration was measured via UPLC (Waters Co., USA) using the same parameters explained in UPLC validation previously. The determination of drug entrapment efficiency was carried out by dispersing certain amounts of the different formulations in 2 ml distilled water, and then centrifuging at 14,800 rpm, -5°C for 1 h. The concentration of LTZ in the supernatant was measured by UPLC and was subtracted from its corresponding initial LTZ concentration used to calculate the drug loading. The concentration of LTZ in the pellets was also measured to ensure the accuracy of determining the entrapment efficiency using

the supernatant subtraction from the initial concentration of LTZ. All experiments were conducted in triplicates for each formulation and the mean values were recorded.

2.4 In Vitro Drug Release Study and Kinetic Modeling

The design of an appropriate in vitro drug release study started with the selection of a suitable diffusion medium that would maintain a sink condition, while ensuring the stability of the drug throughout the study period. The sink condition refers to the volume of the diffusion medium that is at least larger than 3 times the volume required to generate a saturated solution of the drug (140). Therefore, a solubility study was conducted in order to determine the required volume of the medium for the drug release study. This was done by solubilizing 100 mg LTZ in 20 ml 0.1 M phosphate buffer solution (pH 6.8) with 20% v/v Transcutol®. This solution was placed in a Julabo SW22 shaking water bath (JULABO Labortechnik GmbH, Seelbach, Germany) at 37±1°C, 100 rotations per min for 3 days. After that, the solution was filtered using 0.2 µm PTFE filters, and then injected in the UPLC system to measure the concentration of LTZ which reflected its solubility in the medium. The solution was then left in the shaking water bath for 31 days at the same previous conditions in order to ensure that LTZ remained stable in the medium at the end of the study period. Thus, after 31 days, the solution was again filtered using 0.2 µm PTFE filters, and then injected in the UPLC system to measure the concentration of LTZ. The difference between the concentration of LTZ after 3 days and

that after 31 days gave an indication about the percentage of degradation that LTZ might have undergone.

In vitro release study was completed through the use of dialysis tubing cellulose membranes (MW cut-off= 14,000). Quantities of the optimized formulations having an amount of 75 mg LTZ were suspended in 10 ml of the diffusion medium and filled in the dialysis tubes that were then sealed with their specified closures. The tubes were then immersed in closed glass containers filled with 200 ml of the diffusion medium. These containers were placed in the shaking water bath at 37±1°C, 100 rotations per min for one month. At specific intervals, 5 ml was withdrawn from the external medium, filtered, and injected in UPLC for analysis. Similar volumes of fresh medium were used for replacement to maintain sufficient sink conditions. The concentrations of LTZ in the withdrawn medium were measured via UPLC as described previously. Cumulative percentage of drug release was calculated by summing the concentration of LTZ released at each time interval with the previous ones, and then dividing the total concentration by the initial drug loading used at the beginning of the experiment. Data were fitted into four different kinetic modeling: zero-order, first order, Higuchi model, Hixson-Crowell model, and Korsemeyer-Peppas semi-empirical model. For each model, both release rate constants (k) and correlation coefficients (R2) were computed via their corresponding equations. The model that provided R2 values closer to unity was considered the release order.

2.5 In Vitro Cytotoxicity Studies

2.5.1 Culture Medium

Eagle's Minimum Essential Medium (EMEM) (ATCC®) was used in culturing MCF-7 cells which contained 1500 mg/L sodium bicarbonate, Earle's balanced salt solution, 2 mM L-glutamine, nonessential amino acids, and 1 mM sodium pyruvate. An addition of 1 % v/v Penicillin-Streptomycin-Amphotericin B (ATCC®) solution was added to the medium to prevent potential microbial growth. The final pH of both media was maintained at 7.4.

2.5.2 Cell Culturing

Frozen MCF-7 cells were thawed in a water bath at 37°C with gentle shaking for 2 min. MCF-7 cell suspension was resuspended in 2 ml medium, then centrifuged at 200 g (1100 rpm) for 5 min, and supernatant was discarded. Under aseptic conditions, 1 ml of pre-warmed medium at 37°C were added to the cells. The cells were mixed properly with the medium by slowly pipetting up and down, and then the cells suspension was placed into 25 cm^2 flask with additional 4 ml of the medium being added to the flask. The cells were incubated at 37°C, 5% CO_2 with regular changing of the medium every 2-3 days. One week later, the cells were split and transferred into 75 cm^2 flasks after they reached 90-95% confluency. This was carried out by aspirating the media, washing with 5 ml 1X Dulbecco's Phosphate Buffered Saline (D-PBS), adding 3 ml 1X Trypsin-EDTA solution, and finally incubating the cells at 37°C, 5% CO_2 for 5 min. Then, the cells suspension

was normalized with 3 ml medium. This was followed by centrifuging the cells suspensions at 200 g (1100 rpm) for 5 min, discarding supernatants, and re-suspending the pellets in 1 ml of pre-warmed medium. Now, these suspended pellets were cultured in 75 cm^2 flasks with additional 14 ml of the media and incubated at 37°C, 5% CO_2. The medium was changed every 2-3 days until the cells became 90-95% confluent where they got harvested and used for cytotoxicity experiments.

2.5.3 Treatment of Cells

Cells that reached 90-95% confluency were seeded in 96-well plates at a density of 10,000 cells/well and then incubated for 24 hours 37°C, 5% CO_2 to enable them to recover and attach to the surface of the wells. Cell counting was done using a hemocytometer where 100 µL of each cell suspension was diluted with the specific medium to make up a final dilution ratio of 1:10. Approximately 10 µL of this diluted cell suspension was loaded in the hemocytometer and placed under the microscope where cells residing on the 4 corner squares were counted. Final cell count was calculated based on the following equation:

$$\text{Final cell count/ml} = \frac{\text{Total number of cells counted x dilution factor x } 10^4}{4}$$

An appropriate volume of the medium was added to the concentrated cells suspension in order to yield a cell density of 10,000 cells/well. After 24 hours of incubation, cells were treated with 5 different concentrations of LTZ from each formulation: 10 nM, 100 nM, 1 µM, 10 µM, and 100 µM. These solutions were prepared by mixing 350 ml of 1:5 v/v acetonitrile: Transcutol® with 1 g from each formulation which yielded solutions with final concentrations of 10 mM. After that, the solutions were diluted with appropriate volumes of the EMEM medium in order to get the required concentrations (10 nM, 100 nM, 1 µM, 10 µM, and 100 µM). Cytotoxicity was evaluated using DNA staining after an incubation period of 48 hours of the treated cells.

2.5.4 Cytotoxicity Measurement based on DNA Staining

DNA staining was done via adding 12 µL of 38% v/v formaldehyde to each well of the treated MCF-7 cells to make up a final concentration of 3.8% v/v formaldehyde. Cells were left for 10 minutes under room temperature inside the hood to get fixed. Then, formaldehyde was removed and 100 µL of 0.1% v/v 4′,6-Diamidino-2-phenylindole dihydrochloride (DAPI) stain was added using DPBS as diluent. Cells were left for another 10 minutes inside the hood in order to achieve a successful DNA staining. This step was followed by replacing the DAPI stain with 100 µL of DPBS, and then measuring the cell count using ArrayScan™ XTI Live High Content Platform (ThermoFisher Scientific, NY, USA) where 25 fields were selected from each well for analysis.

Chapter 3: Results and Discussion

3.1 Optimization of the Monodisperse Microparticles Production Process

The production of monodisperse microparticles was carried out using the VOAG which is an instrument mainly designed to generate monodisperse micro-droplets of the solution injected into the system (133,134,141,142). When the solvent of the dissolved solute evaporates within the drying column, the solute settles down in a solid form with narrow particle size distribution. Using the original VOAG was very challenging since the instrument was inefficient in producing dried monodisperse microparticles as a final product following the specified instructions by the manufacturer. Operating the VOAG as is failed to produce any dried microparticles, leading to a yield that was almost zero. This was due to the fact that the instrument was suffering from several technical problems including an instability in the liquid pressure that builds up as a result of the liquid passing through the liquid feed tubes to the orifice, frequent clogging of the orifice which stopped the whole production process, and inefficient drying system which made the collection of the particles extremely difficult.

In order to stabilize the liquid pressure, the Teflon O-ring (0.075 mm in thickness) that holds the orifice disc was replaced with a rubber O-ring (2 mm in thickness) supplied by Perkin Elmer Co., USA. In contrast to the thin Teflon O-ring, this thick rubber O-ring was able to sufficiently hold the orifice disc tightly in its place, prevent the leakage of the

liquid that contributes to the persistent drop in liquid pressure, and withstand several different solvents without being damaged or teared over long periods of use.

Frequent clogging of the orifice was another major issue faced while dealing with the VOAG. The orifice used to get clogged constantly during the production process which resulted in massive material loss due to the removal of the orifice disc for cleaning purposes. Two different cleaning techniques were used to remove residual particles that clogged the orifice. The first technique was suggested by the manufacturer and this was the backflush of the orifice in which the dispersion cap was placed over the piezoelectric quartz with its opening being tightly closed, allowing the air to flow while keeping the drainage valve open (133). This procedure resulted in a buildup of pressure within the cap, forcing the air to flow against the orifice and carrying the particles away through the drainage tube. Despite the technique was used several times, the clogging problem remained persistent. The second technique used was soaking the orifice disc in excess volume of dichloromethane and place it in a bath sonicator (Branson B5510, UK) at 40 kHz for 30 minutes. Such technique was only useful after few minutes of cleaning, so the instrument was run for 1-2 minutes, then another round of cleaning was required. This resulted in a huge loss of the solution between each cleaning session and also caused a damage to the orifice after a couple of cleaning sessions. More importantly, whenever the liquid jet was initiated after each cleaning session, more heterogeneous particles were generated due to changes in droplets velocities and diameters (143). Therefore, there was a need to find a way that eliminates the clogging of the orifice to maintain a consistent generation of monodisperse particles throughout the production process. The orifice disc

supplied by the manufacturer had a hole diameter of 20 µm, and such very small opening posed a high shear force against the passing solution, increasing the clogging of the orifice. This required the preparation of extremely dilute solutions in order to minimize the friction between the viscus solution and the orifice. However, this was not practical since large volumes of the organic solvent was required and the clogging was also experienced while using pure solvent during flushing the system. In addition, it was found out that the orifice disc was composed of two plates; a thin plate (approximately 0.085 mm in thickness) facing the liquid flow where the actual orifice was grooved in, and a thick plate (0.254 mm in thickness) on top of the thin plate with a wider hole opening (1.27 mm in diameter) supporting it as depicted in Figure 4.

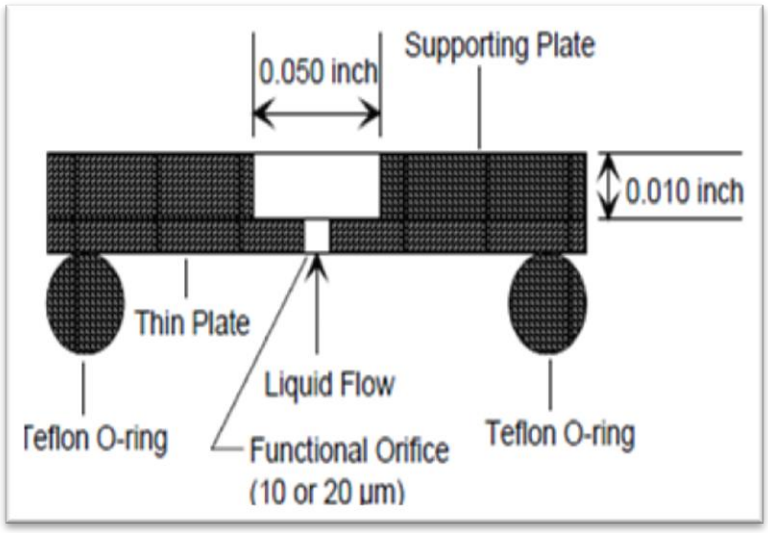

Figure 4. Orifice disc assembly supplied by the manufacturer (135).

This kind of orifice disc assembly was another contributor to the clogging of the orifice where the pressure exerted by the passing solution caused the orifice edges within the thin plate to bend over and get inside the wider opening of the above thick plate. Thus, it was more reasonable to replace the 20-µm orifice disc originally supplied by the manufacturer with a specifically manufactured orifice disc to meet our production requirements, and this was purchased from Lenox Laser, Inc. (MD, USA) with the following parameters:

Disc diameter: 9.5 mm ± 0.26% mm

Hole diameter: 300 µm ± 5% µm

Thickness: 0.05 mm ± 5% mm

Centering: ± 0.25 mm

This newly designed orifice disc consisted of only one thin plate (0.05 mm in thickness) where the orifice was grooved in with a diameter of 300 µm. This huge increase in orifice hole diameter enabled the passage of highly concentrated and viscus solutions reaching up to 10% w/v without any clogging experienced throughout the entire production process. Cleaning of the orifice was done by just wiping it off with acetone and this was only needed between the production of different formulations not within the same formulation. Hence, this new orifice disc prevented the clogging of the orifice that made the production process very frustrating, eliminated the necessity of cleaning while producing the same formulation which minimized the variation in the production

parameters, minimized the amount of solvent needed for cleaning, and also minimized the solvent used in the formulation itself.

The final issue encountered with the use of the VOAG was the inefficient drying system which made the collection of the particles almost impossible. The drying column was 60 cm in length and the dispersed droplets were supposed to be dried with the help of an air stream passing through the droplets at a maximum velocity of 100 L/min. The short length of the drying column, the rapid settling of the particles, and the absence of heat supply to fasten the drying process contributed all to the inefficiency in drying the particles. The droplets got splashed out by the air supply and settled on the side walls of the drying column before they dry which made them aggregate and lose their monodisperse properties. In an attempt to modify the drying efficiency of the VOAG, the air supply was replaced with a nitrogen gas supply, heating tapes set at 120 °C were wrapped on the external wall of the drying column as claimed to be effective in enhancing the drying process of the particles (141), and a vacuum attached to a collecting flask was mounted on the distal opening of the drying column in order to minimize particles collision and force them to be collected in the flask not on the side walls of the drying column. Unfortunately, such attempt failed to dry the particles and minimize their collision due to certain limitations. First, particles traveling velocity was much higher than that of the counteracting nitrogen gas flow and since the drying column was very short, the particles did not get a sufficient time to get dried. Second, the wide diameter of the drying column (around 20 cm) made it difficult to force the particles to line up in one direction, causing a more random movement of the particles, increasing their collision,

and ultimately residing on the side walls of the drying column. Finally, although the vacuum was operated at -19 Kpa, it could not pull out the particles towards the collecting flask due to the strong collision between the particles.

It seemed impossible to correct the various limitations of the drying system, therefore, an alternative approach to collect and dry out the particles was sought without the need to use the drying system supplied by the manufacturer. The air supply and the drying column were removed, and instead, the liquid chamber base was inverted and mounted on a beaker where the dispersion cap was totally immersed perpendicularly in the collecting medium inside the beaker. The collecting medium consisted of 0.04-1% Polyvinyl Alcohol (PVA) aqueous solution in order to prevent agglomeration of the particles and effectively produce a uniform suspension of monodisperse particles. Magnetic stirring was used in order to prevent particles settling and facilitate solvent evaporation.

The reduction of particle size generated from the 300-µm orifice was enabled through the rapid rotational movement of the collecting medium which resulted in a frictional force imposed on the surface of the droplets around the orifice edges. Such force was enough to break down the generated droplets and reduce the final particle size. Berkland et al., reported the use of an annular aqueous stream pumped concurrently with the organic stream containing the drug and the polymeric carrier in order to reduce the final particle size as produced by a 300-µm nozzle (144). They have reported that their system was able to reduce the particle size to almost 100 times smaller than the nozzle size. In our experiments, we were also able to produce similar results, however, it was noted that the

smaller the particle size achieved by this mechanism, the more heterogeneous the particles became, leading to a wider particle size distribution, and hence, loss of monodispersity. Preliminary experiments have shown that the optimal particle size distribution was seen with particle size of at least 15 µm, therefore no further reduction of the particle size was attempted.

Several studies have reported similar problems encountered while using the VOAG in the production of monodisperse microparticles from different materials (134,141,142,145–147). In these studies, different approaches have been used to overcome the limitations of the instrument in order to produce the intended monodisperse microparticles. Kreyling et al., proposed a strategy to minimize orifice clogging solution by filtering the solution using 0.5-µm PTFE filters; one was mounted on the syringe to filter the solution while being pumped, and the other one was mounted prior to the orifice disc to filter the solution before it passes through the orifice (148). Between the orifice disc and the Teflon O-ring, a metal sieve and a spacing ring were inserted to reduce the potential of clogging by reducing the volume of the accumulated solution to 0.06 ml. An aqueous solution of 1% w/v NaCl was pumped through the VOAG to test the effectiveness of this strategy. Although the authors reported that the filtering strategy was capable of minimizing orifice clogging, the study only investigated the production of a very diluted salt solution which could not be of a great value when it comes to highly viscous and concentrated polymeric solutions. In addition, the liquid feed rate had to be limited to 2.5 - 4 ml/h which indicated that in order to produce one gram of monodisperse solute particles, 25 - 40 hours would be needed. In our experiments, we were able to produce

similar amount of monodisperse particle in just 0.98 – 9.8 minutes. More importantly, the study stopped at the stage of generating monodisperse droplets without being dried and collected which prevents the utilization of the produced particles in beneficial applications.

Soon after, Leong attempted to further enhance the performance of the VOAG by adding a pressure feeding system to the model suggested by Kreyling et al (143). In his trial, the pressure feeding system replaced the syringe pump and served as a reservoir to transport the solution to the orifice. However, large volumes of the solution were required to flash the system before actual initiation of the production process. Moreover, although the liquid pressure was stable with less than 3% of variation, the liquid feed rate was significantly different among different solutions. On top of that, the liquid feed rate had to be calculated appropriately before running the instrument through manual collection of the solution coming out of the orifice which is an inaccurate procedure. Therefore, this approach was difficult to adopt since it caused lots of material loss along with the requirement of calibration before each run.

An interesting article was later published highlighting some new modifications made to overcome the reported problems of the VOAG (149). The adjustments included replacing the syringe pump with a pneumatic pump in order to stabilize liquid pressure along with replacing the acrylic drying column with a wider copper cone (0.125 m^2 cross-sectional area) to minimize particle losses due to impaction. The copper cone had steep angles to guide the particles to be collected in one direction under gravitational force. Heating

tapes were also wrapped around the walls of the copper cone providing a temperature of 20 °C to 50 °C. Despite these efforts, the authors were only able to produce smooth-surface dried monodisperse microparticles with a maximum yield of approximately 45%. This was mainly due to the electrophoretic repulsion created inside the cone among the flowing particles, leading to their deposition on the inner walls of the cone.

In summary, all previous attempts to optimize the use of the VOAG in generating monodispersed microparticles were insufficient to overcome all of its limitations. In contrast, the modifications we proposed in this study were successful in covering all of the limitations, establishing practical strategies to be implemented in order to produce the required monodisperse microparticles with a very high yield easily, efficiently, and in a timely manner.

3.2 Experimental Design for Optimizing the Production Parameters

In the process of generating monodisperse microparticles, the production parameters involved in manufacturing these particles should be studied for their effects on particle size distribution. This would ensure that these parameters would be set at their optimal values in order to produce the narrowest particles size distribution possible, which would result in a successful production of monodisperse microparticles. These parameters included drug loading, organic phase concentration, organic: aqueous phase ratio, PVA concentration, frequency of the vibrating orifice, liquid flow rate, and stirring rate (136,138,150,151). Since these parameters cannot be studied separately in which they are

involved in each production process, it was essential to study the effects of these parameters collectively in perspective of each other. Resolution 4 offered by the Placket-Burman design permitted the estimation of the main effect of each parameter considering the remaining parameters using the minimal number of experiments possible with high accuracy (136,139,152,153). A 12-run, 2-level Placket-Burman design was created with each run containing a different combination of high or low levels of each parameter/factor as shown previously in Table 3. The different factor combinations resulted in a wide variation in both particle size and particle size distribution. The average particle size was ranging from 15.6 ± 1.1 µm to 91.6 ± 2.0 µm for PCL-based formulations, whereas PDLLA-based formulations had a particle size range of 22.7 ± 0.70 µm to 99.6 ± 3.1 µm (Table 5). A huge variation in particle size distribution was also seen among the different formulations in which the span values ranged from 0.22 ± 0.02 to 1.24 ± 0.27 and from 0.29 ± 0.04 to 1.48 ± 0.36 in PCL-based and PDLLA-based formulations, respectively (Table 5). The polydispersity nature of selected formulations was also noticed in SEM images as shown in Figure 5. These images represented the most polydisperse particles obtained from PCL- and PDLLA-based formulations. Particles were mostly spherical with smooth surfaces, however, there were some irregularly shaped and doughnut-like particles with various sizes owing to their polydispersity. This representation would show the difference in morphology between these particles generated before optimization of the factors and those generated later on after optimization (highlighted in next sections).

Table 5. *Summary of the Particle Size and Particle Size Distribution Analyses for Formulations Run in Plackett-Burman Design*

Formulation	**PCL-based formulations**		**PDLLA-based formulations**	
	Mean diameter (µm)	**Span**	**Mean diameter (µm)**	**Span**
F1	47.9 ± 1.9	0.52 ± 0.03	59.2 ± 1.1	0.60 ± 0.02
F2	47.0 ± 2.4	0.56 ± 0.03	53.3 ± 3.2	0.59 ± 0.04
F3	33.4 ± 2.7	0.37 ± 0.03	44.0 ± 3.4	0.44 ± 0.04
F4	58.7 ± 1.5	0.60 ± 0.02	64.0 ± 2.3	0.59 ± 0.07
F5	15.6 ± 1.1	0.22 ± 0.02	22.7 ± 0.70	0.29 ± 0.07
F6	91.6 ± 2.0	1.24 ± 0.27	99.6 ± 3.1	1.48 ± 0.36
F7	47.1 ± 2.4	0.58 ± 0.04	58.0 ± 5.6	0.61 ± 0.05
F8	57.9 ± 1.8	0.60 ± 0.04	61.1 ± 4.8	0.61 ± 0.09
F9	61.8 ± 3.2	0.61 ± 0.05	46.6 ± 2.3	0.57 ± 0.09
F10	76.7 ± 2.4	0.88 ± 0.03	84.2 ± 2.9	0.93 ± 0.04
F11	17.4 ± 1.2	0.26 ± 0.04	24.0 ± 2.6	0.29 ± 0.04
F12	88.7 ± 1.3	1.15 ± 0.22	97.8 ± 3.0	1.46 ± 0.36

Data reported as mean ± SD, n=3.

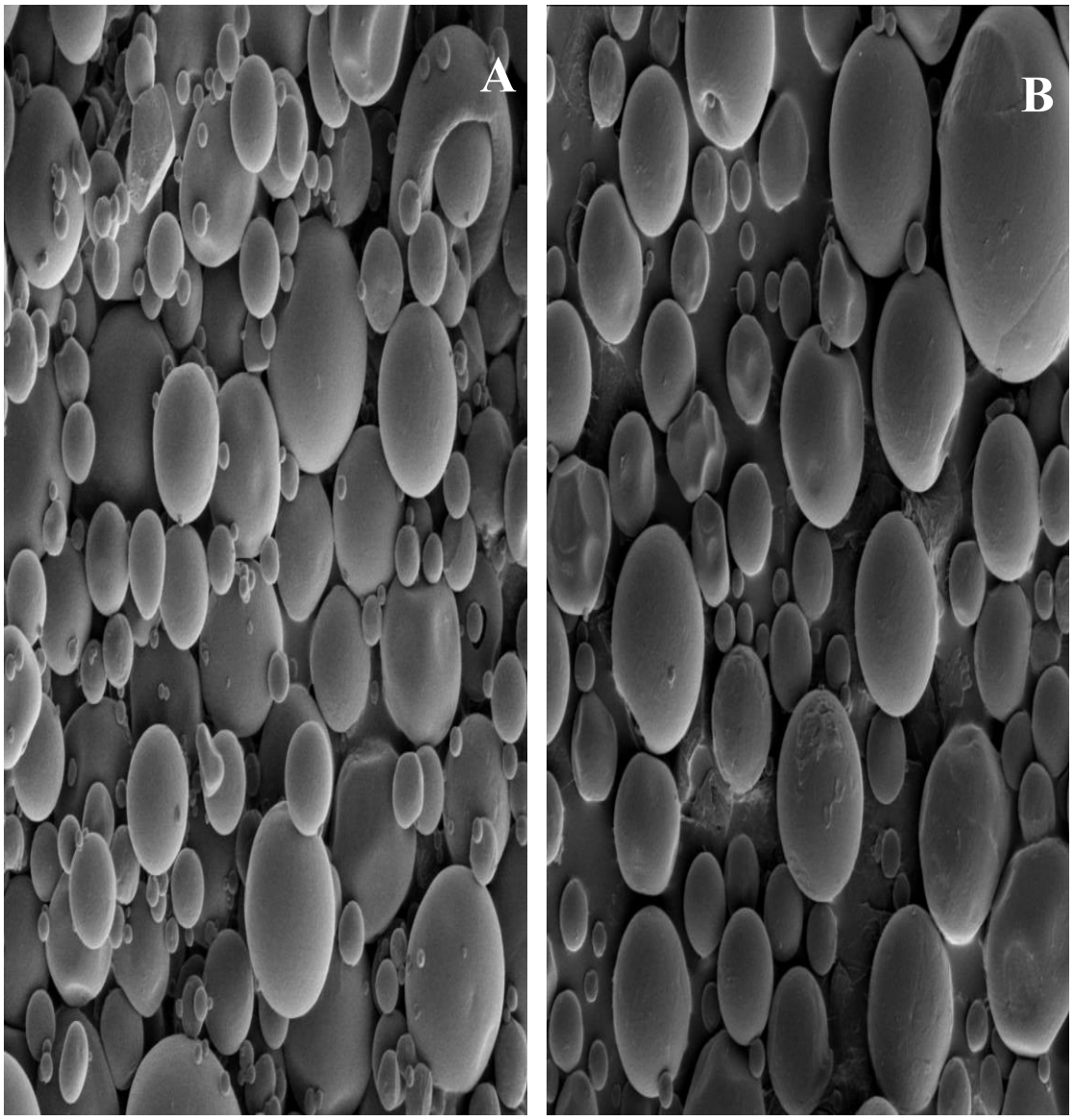

Figure 5. SEM micrographs of selected formulations from Plackett-Burman design. (A): PCL-based formulation (F6), (B): PDLLA-based formulation (F6).

Regression analysis allowed the accurate elucidation of the effects of each parameter/factor on particle size distribution; span (Y) through the following equation for PCL-based formulations:

$$Y = 0.397 - 0.00876\ X1 + 0.0033\ X2 + 0.0561\ X3 + 4.296\ X4 - 0.000273\ X5 + 0.1983\ X6 - 0.000773\ X7.$$

On the other hand, PDLLA-based formulations had a different equation, but with a similar pattern to these observed in PCL-based formulations. The equation illustrating the effects of each parameter/factor on particle size distribution; span (Y) for PDLLA-based formulations was:

$$Y = 0.169 - 0.00724\ X1 + 0.0211\ X2 + 0.0786\ X3 + 6.26\ X4 - 0.000338\ X5 + 0.2505\ X6 - 0.000702\ X7.$$

These equations were very accurate in predicting the span values for each formulation through setting the parameters/factors at their optimal levels to ensure achieving the lowest span values possible before running the experiment. This is due to the strong correlation between the predicted and observed span values using these equations where the correlation coefficient (R^2) was 0.9668 and 0.9521 for PCL- and PDLLA-based formulations, respectively (Figures 6 and 7). This facilitated the production of formulations with narrow particle size distribution using either polymer with just few selections of the parameter values.

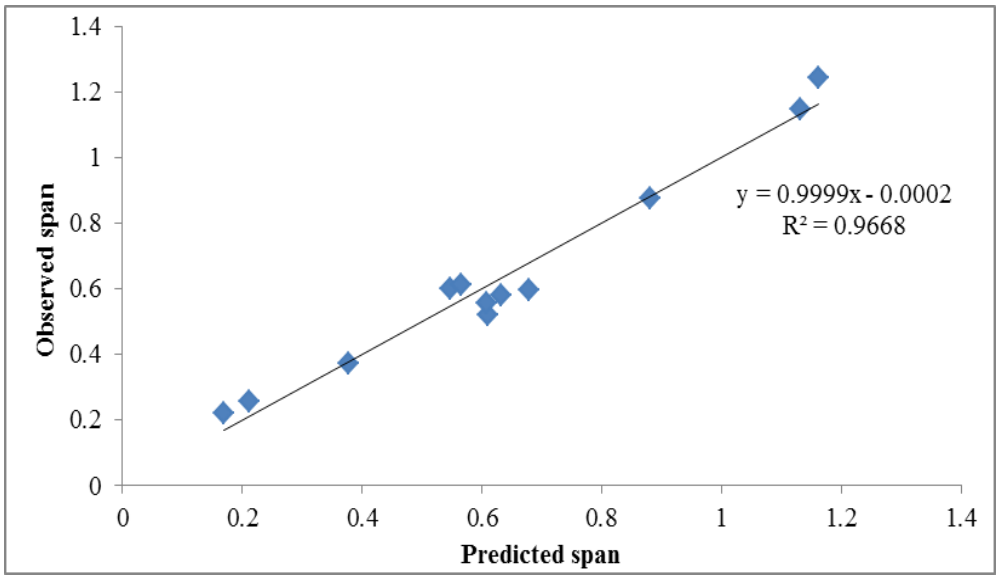

Figure 6. Correlation between observed and predicted span values by the model for PCL-based formulations.

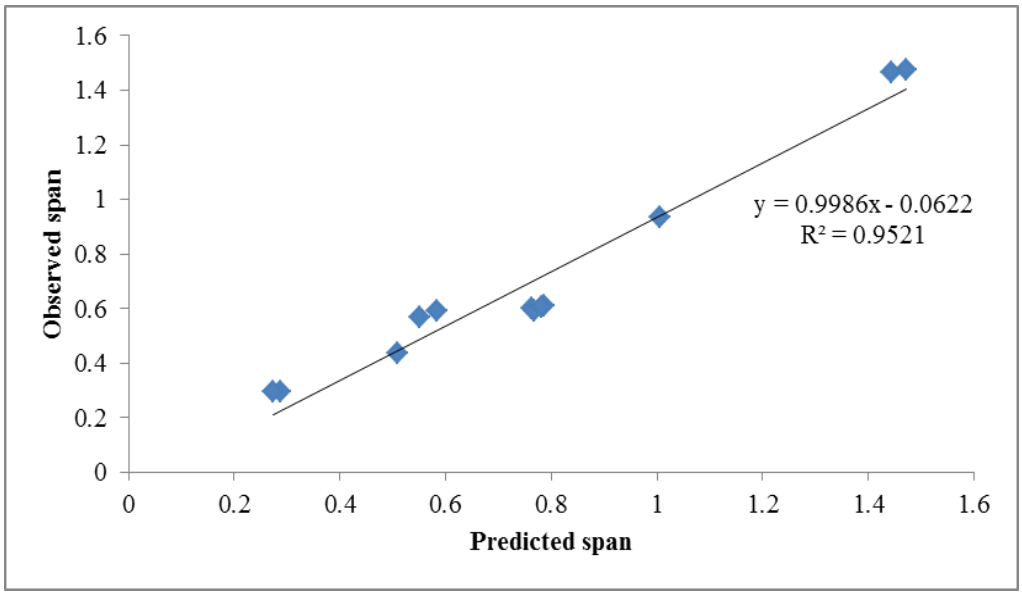

Figure 7. Correlation between observed and predicted span values by the model for PDLLA-based formulations.

One-way ANOVA analyses had revealed that all production parameters had a significant effect on particle size distribution ($p < 0.05$), except for organic phase concentration ($P = 0.955$) in PCL-based formulations (Table 6). However, drug loading, organic phase concentration, and stirring rate were found to have no significant impact on particle size distribution when PDLLA was used (Table 6). This interesting observation was also noted previously when different polymeric carriers were used owing to the differences in their intrinsic characteristics (79,136–139,150–157).

Coefficient values indicated that some of the parameters had a positive relationship with the span, meaning which the increase in these parameters led to the increase in the span. These included: organic phase concentration, organic: aqueous phase ratio, PVA concentration, and liquid flow rate. In contrast, the other parameters had an inverse relationship with the span, meaning which the increase in these parameters caused a reduction in the span, which was favorable. These included drug loading, frequency of the vibrating orifice, and stirring rate. Such findings were also in agreement with other reports (136,137).

Table 6. *Statistical Analysis of the Effects of the Different Production Factors on Particle Size Distribution as Expressed in Span*

	PCL-based formulations		PDLLA-based formulations	
Factor	**Coefficient**	**p-value**	**Coefficient**	**p-value**
Drug loading	-0.1094	0.017	-0.0906	0.086
Organic phase concentration	0.0017	0.955	0.0106	0.804
Organic: aqueous phase ratio	0.1122	0.015	0.1572	0.017
PVA concentration	0.1289	0.009	0.1878	0.009
Frequency	-0.1228	0.011	-0.1522	0.019
Liquid flow rate	0.1517	0.005	0.1917	0.009
Stirring rate	-0.0967	0.025	-0.0878	0.093

One-way ANOVA test was used, n= 3.

The mean of the triplicates has been used to compute the coefficient and p-values for each factor.

There was a general agreement between PCL- and PDLLA-based formulations in terms of the order of the production parameters affecting their particle size distribution. For PCL-based formulations, the order of the parameters from those with highest impact to those with lowest impact was:

Liquid flow rate > PVA concentration > Frequency of the vibrating orifice > Organic: aqueous phase ratio > Drug loading > Stirring rate > Organic phase concentration (Figure 8).

On the other hand, in PDLLA-based formulations, the order of the parameters was:

Liquid flow rate > PVA concentration > Organic: aqueous phase ratio > Frequency of the vibrating orifice > Drug loading > Stirring rate > Organic phase concentration (Figure 8).

This indicated that there was a minor difference between the two polymers in terms of the parameters affecting their particle size distribution. However, it would be more appropriate to consider each polymeric carrier independently during the production process in order to achieve optimal results.

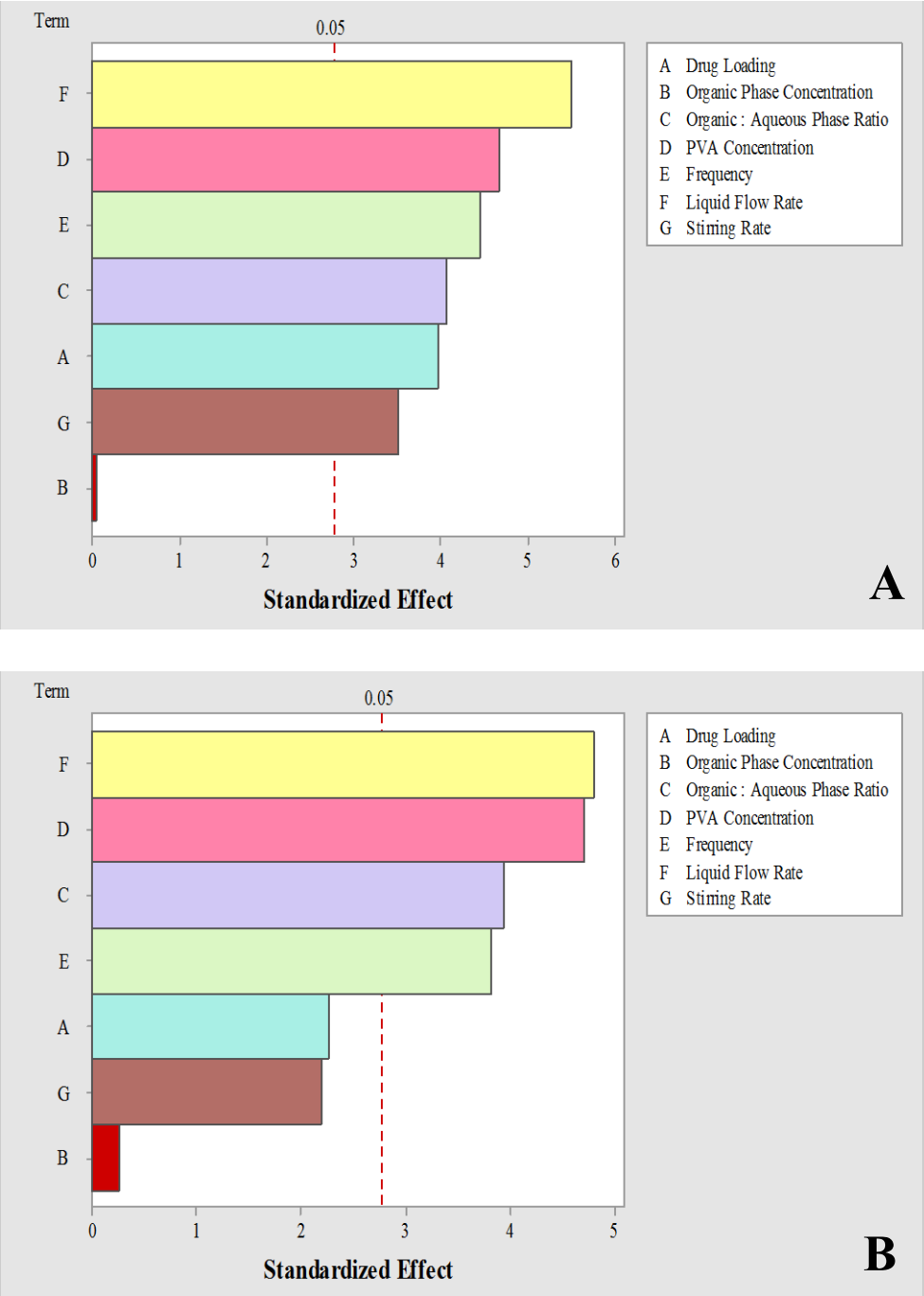

Figure 8. Pareto chart for the different production factors affecting particle size distribution as expressed in span.
(A): PCL-based formulations, (B): PDLLA-based formulations. The higher the length of the bars, the more effect the factor has on span. Bars crossing p-value= 0.05 indicate statistical significance.

Generally, the increase in drug loading caused a decrease in the span due to the subsequent increase in the viscosity of the dispersing particles. This was attributed to the fact that the content of LTZ increased in relation to the polymer (PCL or PDLLA) with higher drug loadings, causing a net increase in the overall viscosity of the formulation. As such, during partitioning to the external aqueous phase, more viscous organic droplets tend to resist the applied stirring forces as compared to the opposed dilute organic droplets, making them maintain their shape, size, and homogeneity (158–164). In contrast, the increase in organic: aqueous phase ratio led to an increased span. This was because the larger volume of aqueous external phase relative to the organic phase induced higher potential of agglomeration between the partitioning particles, resulting in non-uniform droplets, and consequently polydisperse particles (137).

The use of PVA was crucial in producing stably suspended droplets during the emulsification process. However, the concentration of PVA should be determined carefully since lower concentrations than required produce agglomerated particles, whereas higher concentrations, on the other hand, increase the external resistive forces against the droplets being emulsified (146). This what was exactly observed in this study where the lowest span achieved was obtained with PVA concentrations of 0.04% w/v, and the highest span was obtained with PVA concentrations of 0.1% w/v.

The frequency of the vibrating orifice was significantly impacting the particle size distribution. Higher frequency tend to be more effective in generating monodisperse microparticles. This was mainly to due to the intensive forces applied on the emerging

droplets from the VOAG, which produced smaller particles that were easier to get homogenously dispersed than larger counterparts (144).

Similarly, liquid flow rate, determining how much the VOAG received from the organic phase to generate the microparticles had also a significant effect on the span. This was anticipated since larger volumes supplied per unit time would produce larger particles that were less likely to get uniformly dispersed within the aqueous phase, leaving the span at its highest values (165).

Finally, higher stirring rates were more efficient in maintaining an adequately stable dispersion of the droplets, leading to narrower particle size distribution (166).

Figures 9, 10, and 11 summarized the effects of each parameter on the span in three-dimensional schemes.

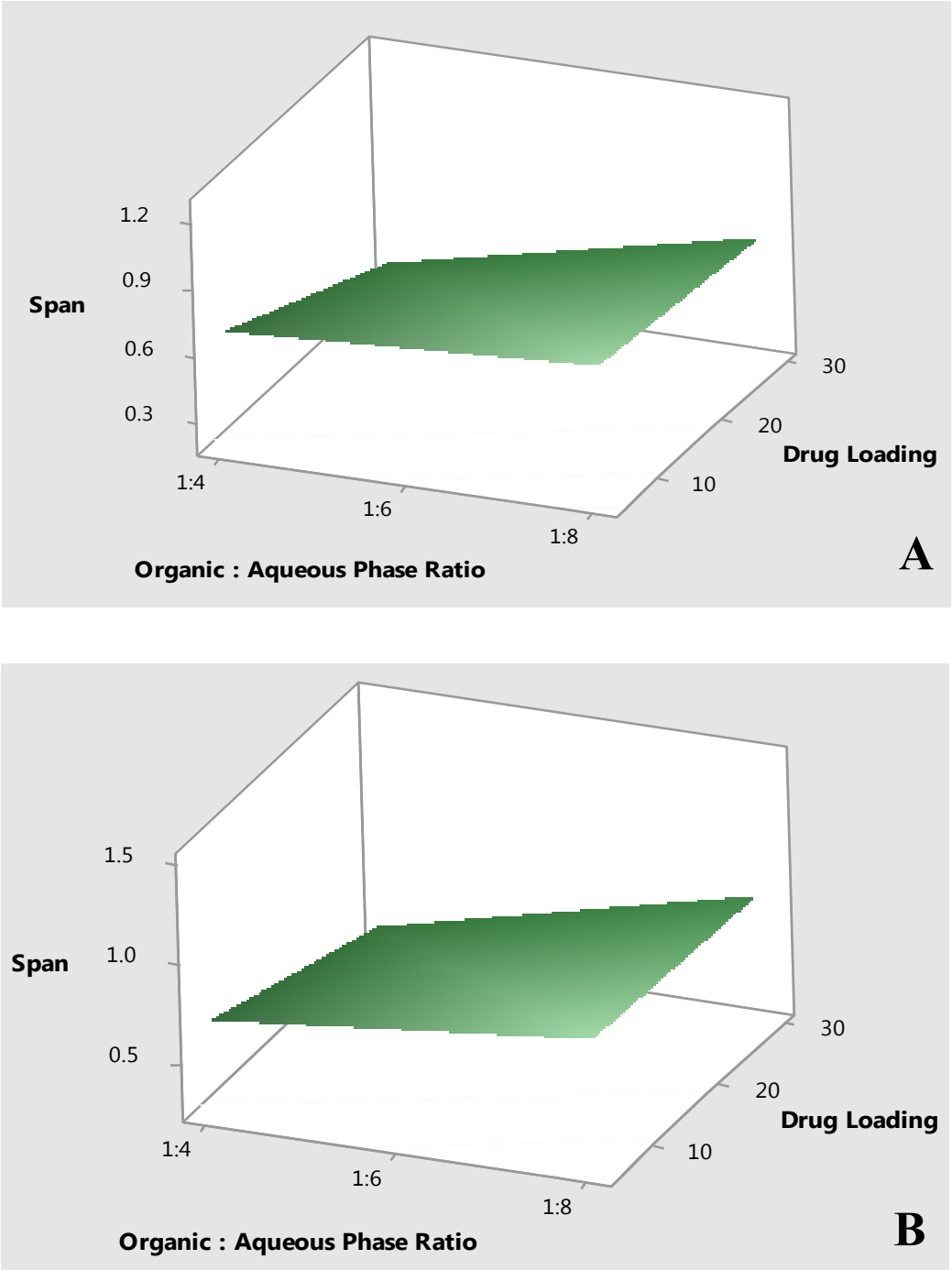

Figure 9. Three-dimensional surface plot of the main effects of drug loading and organic: aqueous phase ratio on span. (A): PCL-based formulations, (B): PDLLA-based formulations.

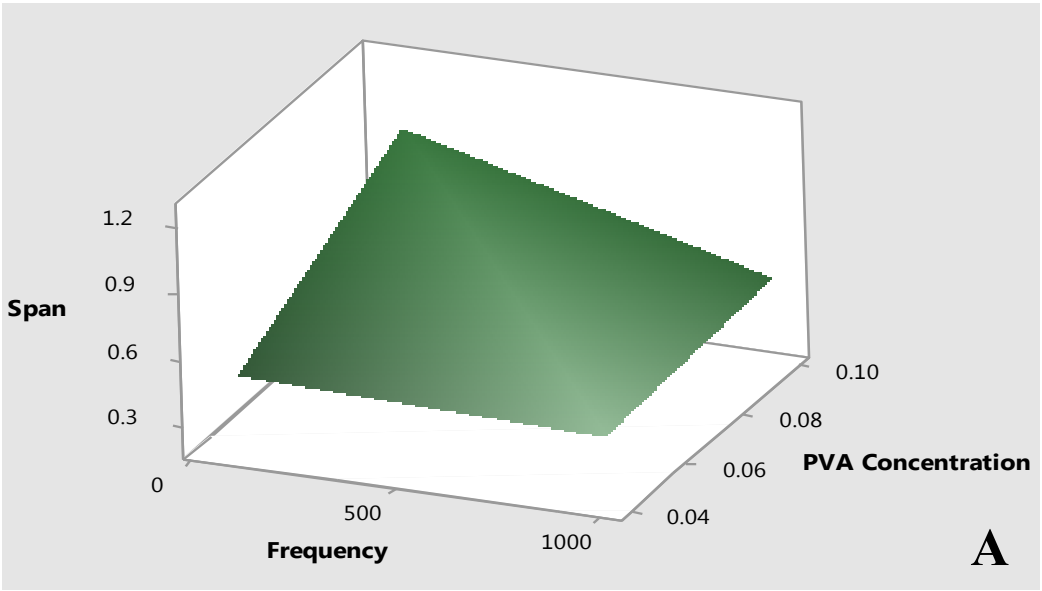

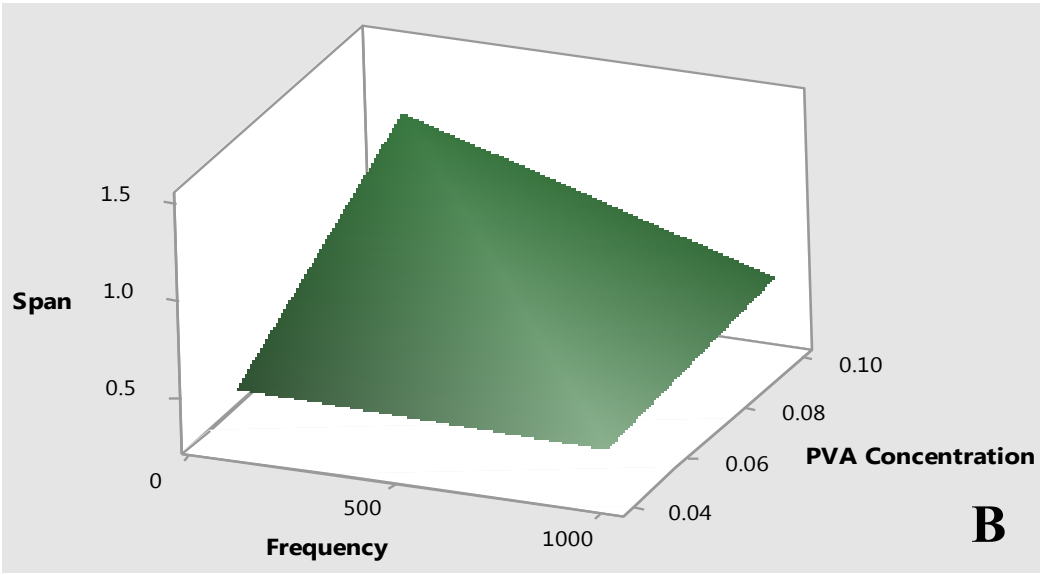

Figure 10. Three-dimensional surface plot of the main effects of PVA concentration and frequency on span. (A): PCL-based formulations, (B): PDLLA-based formulations.

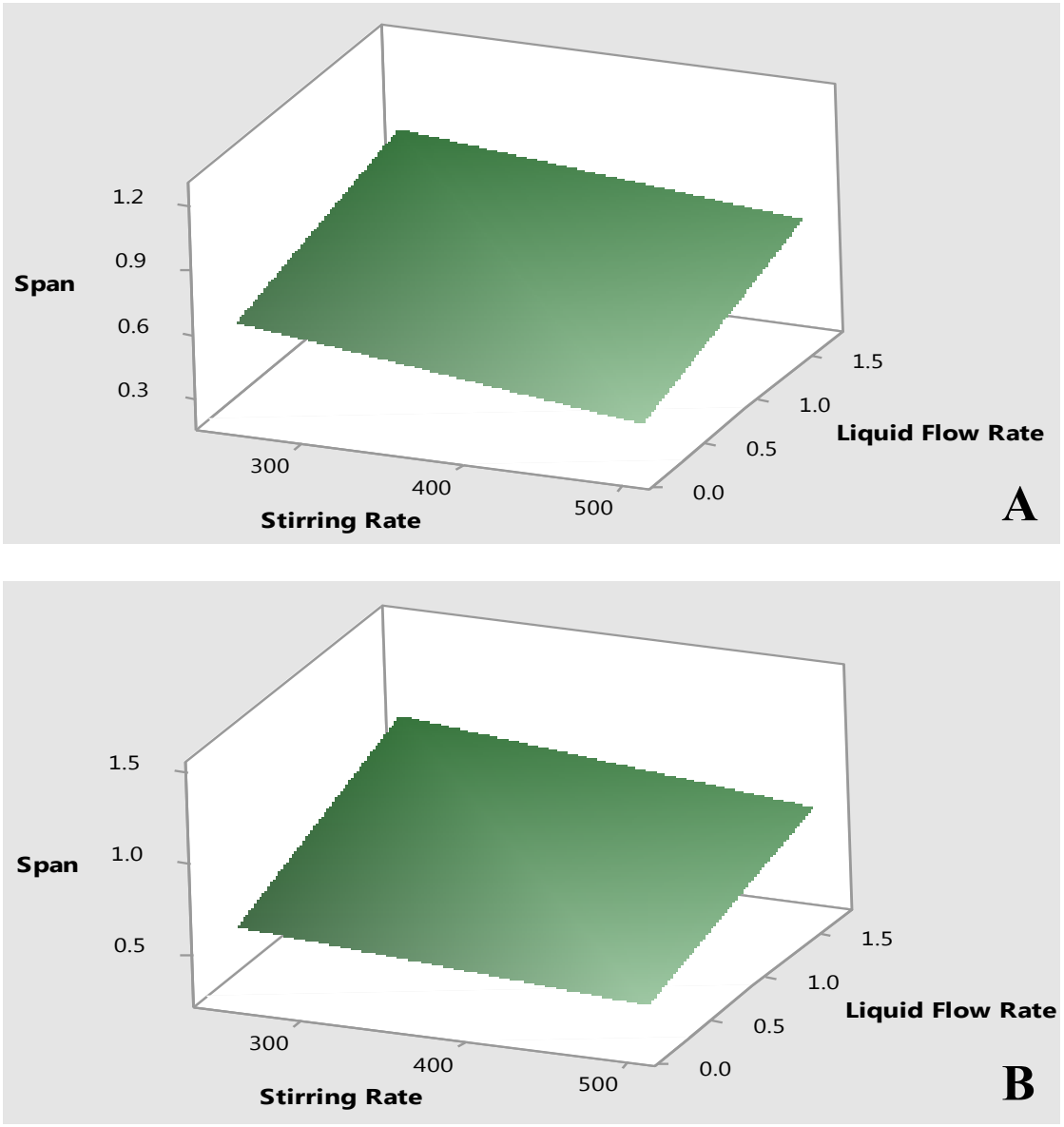

Figure 11. Three-dimensional surface plot of the main effects of liquid flow rate and stirring rate on span. (A): PCL-based formulations, (B): PDLLA-based formulations.

In a nutshell, according to the composite statistical analyses of the Plackett-Burman design, the optimal production parameters were identified by the model as shown in Table 7. These parameters were set at their specified levels for further experiments. In some experiments, however, different drug loading percentages were used in order to examine their effects on certain outcomes as would be discussed in the upcoming sections.

Table 7. *Recommended Values of the Different Production Factors for Yielding the Optimal Particle Size Distribution as Suggested by the Model Generated from Plackett-Burman Design*

Factor	**Optimal value**
Drug loading	30 %w/w
Organic phase concentration	1 %w/v
Organic: aqueous phase ratio	1:4
PVA concentration	0.04 %w/v
Frequency	1000 KHz
Liquid flow rate	0.17 ml/sec
Stirring rate	500 rpm

3.3 Ultra-Performance Liquid Chromatography (UPLC) Validation

In this study, we reported a simple, accurate, and precise method for analyzing LTZ from its pharmaceutical preparations using UPLC system. As compared with other analytical procedures reported in literature (167–172), the use of UPLC in this method offers more sensitivity, accuracy, and precision than UV spectrophotometric analyses (173), in addition to the advantage of withstanding higher pressure levels as opposed to High Performance Liquid Chromatography (HPLC) (174). Our method was able to provide a complete quantification of a sample within approximately 2 minutes, which is much more rapid than other reported methods in literature where the fastest method required a minimum of 10 minutes per sample (175). Therefore, the presenting method would offer a reliable, quick, and accurate strategy for analyzing LTZ during the development of new dosage forms, and as such, would be very useful and practical for research and development purposes.

3.3.1 UPLC Specifications

Quantification was carried out using UV at λ= 240 nm as it has been shown to be the most appropriate wavelength for accurately detecting LTZ (167,170,175). During the development of the analytical method, different ratios of acetonitrile: water was used as a mobile phase. It was found that an isocratic solution of 35:65 v/v (acetonitrile: water)

constituted the optimal ratio for extracting LTZ from its formulations. Therefore, it was used for subsequent analyses. The flow rate was also optimized at 0.3 ml/min.

3.3.2 System Suitability

It was important to ensure the developed method of analysis would be appropriate for detecting LTZ from its pharmaceutical formulations. Therefore, peak area, tailing factor, retention time, and theoretical plates were quantified in order to achieve this objective. A total of 6 samples were injected into the UPLC system, and their mean and relative standard error (RSD) were calculated and summarized in Table 8. It can be seen that mean peak area was 1105801 (RSD= 0.21; not more than 2.0), mean tailing factor was 1.235 (between 0.8-2.0), mean retention time was 1.81 (RSD= 0.05; not more than 1), and mean theoretical plates were 3676.5 (not less than 2000). This provided an evidence that all system suitability parameters were met according to ICH guidelines, and hence, the method proofed to be suitable for carrying out the analyses (140,176).

Table 8. *Summary of the System Suitability Parameters Obtained from the Developed Method of Analysis*

Parameter	**Mean ± SD**	**% RSD**	**Acceptance criteria**
Peak area	1105801 ± 2363.970	0.210	% RSD must not be more than 2.0
Tailing factor	1.235 ± 0.014	1.134	Tailing factor must be between 0.8 - 2.0
Retention time (min)	1.810 ± 0.001	0.050	% RSD must not be more than 1.0
Theoretical plates	3676.5 ± 168.690	4.588	Theoretical plates must not be less than 2000

n= 6.

3.3.3 Linearity

Linearity was assessed through assaying LTZ standard solutions at 11 different concentrations (0.5, 1.0, 2.5, 5, 10, 25, 50, 100, 150, 200, and 250 µg/ml). Each sample was injected 3 times, and the average corresponding peak area obtained from UPLC was plotted against the respective concentration to produce a calibration curve (Figure 12).

Linear regression was computed for the resulting calibration curve. It was found that the calibration curve was linear with a high correlation coefficient (R^2) of 0.9999. The regression equation explaining the relationship between the peak area and the concentration was y= 21863x – 640.58. Of note, previously reported methods of analysis had a narrow range of LTZ concentrations quantified in their linearity test such as 1-10 µg/ml (170), 2-20 µg/ml (169), 1-50 µg/ml (167), and 10-100 µg/ml (172). Such narrow ranges would limit the analysis of samples containing higher concentration levels, and thus, dilution would be needed to not exceed the specified concentrations. This would not constitute a problem in our method of analysis as a wide range of concentrations was used (0.5-250 µg/ml).

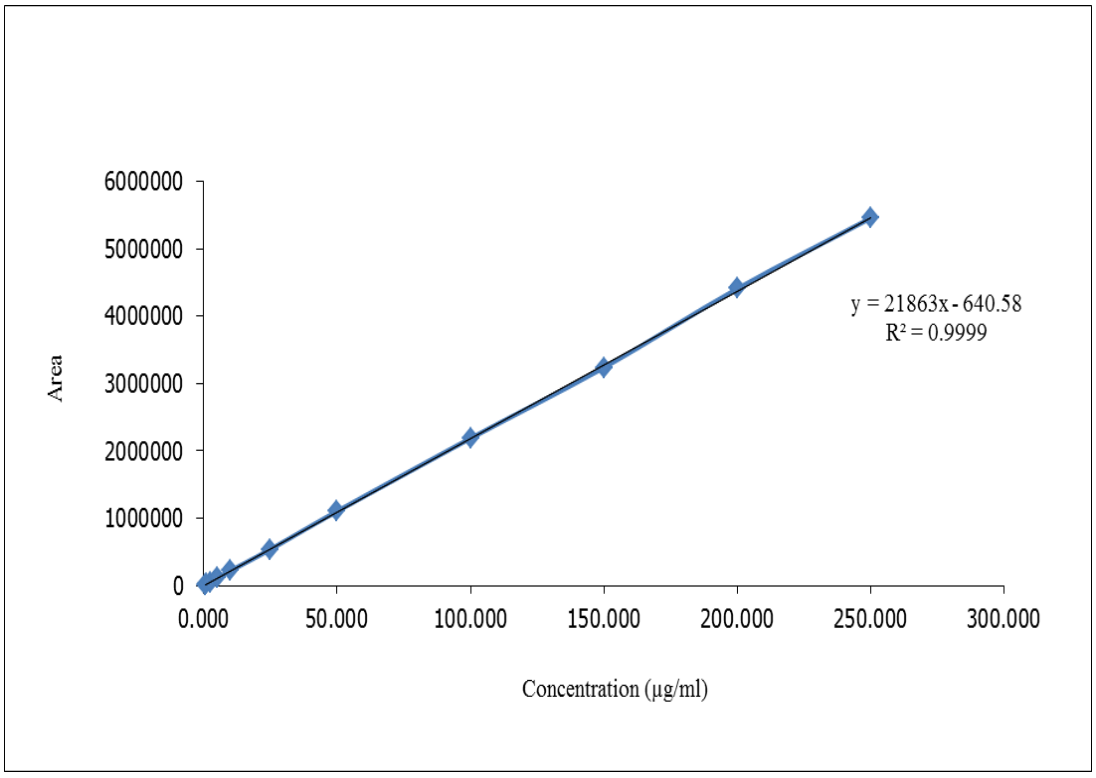

Figure 12. Calibration curve of LTZ.

3.3.4 Limit of Detection (LOD) and Limit of Quantitation (LOQ)

The calibration curve generated in the linearity test was used to calculate the LOD and LOQ. The SD of the residuals of the regression line was multiplied by 3.3 and 10 then divided by the slope to compute the LOD and LOQ, respectively. It was found that the LOD was 2.79 µg/ml, whereas the LOQ was 8.45 µg/ml. Although these very low levels would offer a high sensitivity of analysis, Annapurna et al., was able to even obtain much

lower levels with an LOD of 0.012 µg/ml, and an LOQ of 0.043 µg/ml, and this was a big advantage in their study (175).

3.3.5 Accuracy

The percentage recovery of 3 different LTZ concentrations (40, 50, 60 µg/ml) was used to assess the accuracy of the method of analysis. Table 9 presents the data obtained from the test. Percentage recovery was very high at all tested levels ranging from 99.17% to 99.70%, and %RSD was very low ranging from 0.2 to 1.1. This complies with the specifications of the ICH guidelines where percentage recovery should be within 2.0% of the actual amount, and %RSD should not exceed 2% (140).

Table 9. *Recovery Test of LTZ*

Sample	**Concentration (µg/ml)**	**% Recovery**	**% RSD**
Spiked sample (Level 80%)	39.73 ± 0.34	99.48 ± 0.18	0.2
Spiked sample (Level 100%)	51.53 ± 0.84	99.17 ± 0.49	0.6
Spiked sample (Level 120%)	60.93 ± 0.34	99.70 ± 0.92	1.1

Data reported as mean ± SD, n= 3.

3.3.6 Precision

Evaluation of how precise the method of analysis was had been accomplished through testing for intra-day and inter-day precision. Intra-day precision was done via assaying 6 samples having the same concentration (50 µg/ml) on the same day. On the other hand, inter-day precision was done via assaying 6 samples having the same concentration (50 µg/ml) on two different days. Data has shown that 98.14% and 97.53% of LTZ was recovered in intra-day and inter-day precision analyses, respectively. Percentage RSD did not exceed 2.0% for both measurements, and the difference between intra- and inter-day precision was only 0.61% (Table 10). This entails that the method was precise as it successfully met the ICH acceptance criteria (140).

Table 10. *Precision of the Method of Analysis*

Intra-day precision			**Inter-day precision**		
Area	**% Recovery**	**%RSD**	**Area**	**% Recovery**	**%RSD**
1145319 ± 82852.3	98.14 ± 1.48	1.70	1096742 ± 45944.3	97.53 ± 1.14	0.70

Data reported as mean ± SD, n=6.

3.3.7 Forced Degradation Analyses

In order to perform a complete profile of the stability of LTZ, 6 standard solutions of LTZ (50 µg/ml) were placed under different stress conditions including acidic, basic, oxidative, and thermal conditions. Photo-degradation was also assessed under both UV and visible light. Results has shown that LTZ was most sensitive to the basic stress condition where 34.11% of the drug was decomposed into 5 degradation products. This was probably due to the hydrolytic degradation of the liable cyano-phenyl group in LTZ (175). Oxidation was found to be the second condition affecting the stability of LTZ as 11.12% of the drug was degraded. Acidic medium had lesser effects on LTZ where 98.66% of the drug was recovered. LTZ was noticed to be less likely affected by heat, visible light, and UV. Resistance against these conditions would make the drug maintain its stability under such stresses. Table 11 summarizes the results of all forced degradation studies which were found to be compatible with previously reported results (175). It can be concluded that the method of analysis was sensitive as it was able to accurately detect the LTZ peak with no interference with other peaks related to the degradation products as depicted in Figures 13, 14, 15, 16, and 17.

Table 11. *Summary of Forced Degradation Analyses of LTZ*

Stress condition	% Degradation	% Recovery
Standard sample	-	100
Acidic	1.34	98.66
Basic	34.11	65.89
Oxidative	11.12	88.88
Thermal	0.79	99.21
Photolysis (UV)	0.44	99.56
Photolysis (Visible light)	0.09	99.91

The mean of the 6 replicates has been used to compute the % recovery and % degradation.

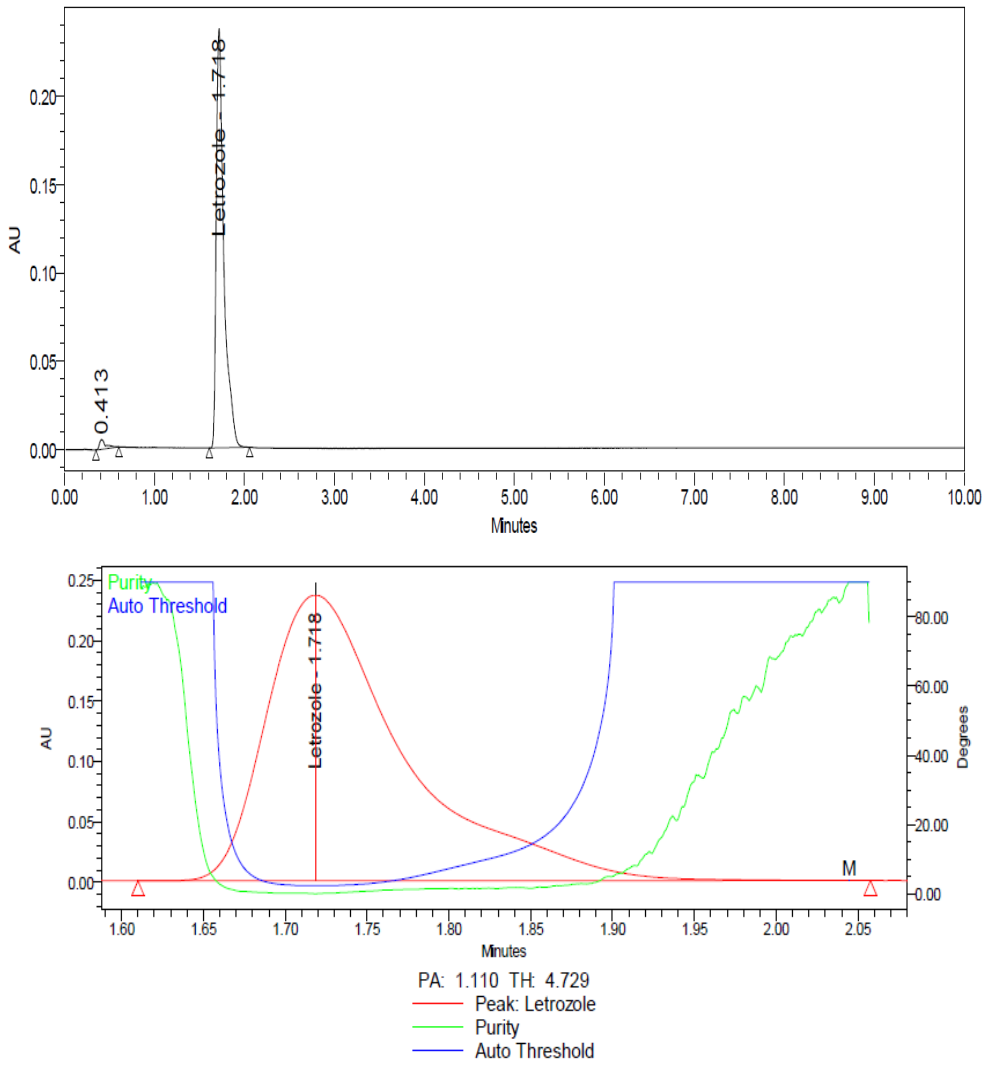

	Peak Name	RT	Area	%Area	USP Plates	Resolution	Tailing	Purity1 Angle	Purity1 Threshold	Purity1 Flag
1		0.413	26997	1.91	334		1.80	42.638	90.000	No
2	Letrozole	1.718	1384071	98.09	2421	11.26	1.92	1.110	4.729	No

Figure 13. Chromatogram of LTZ peak and purity plot under acidic degradation.

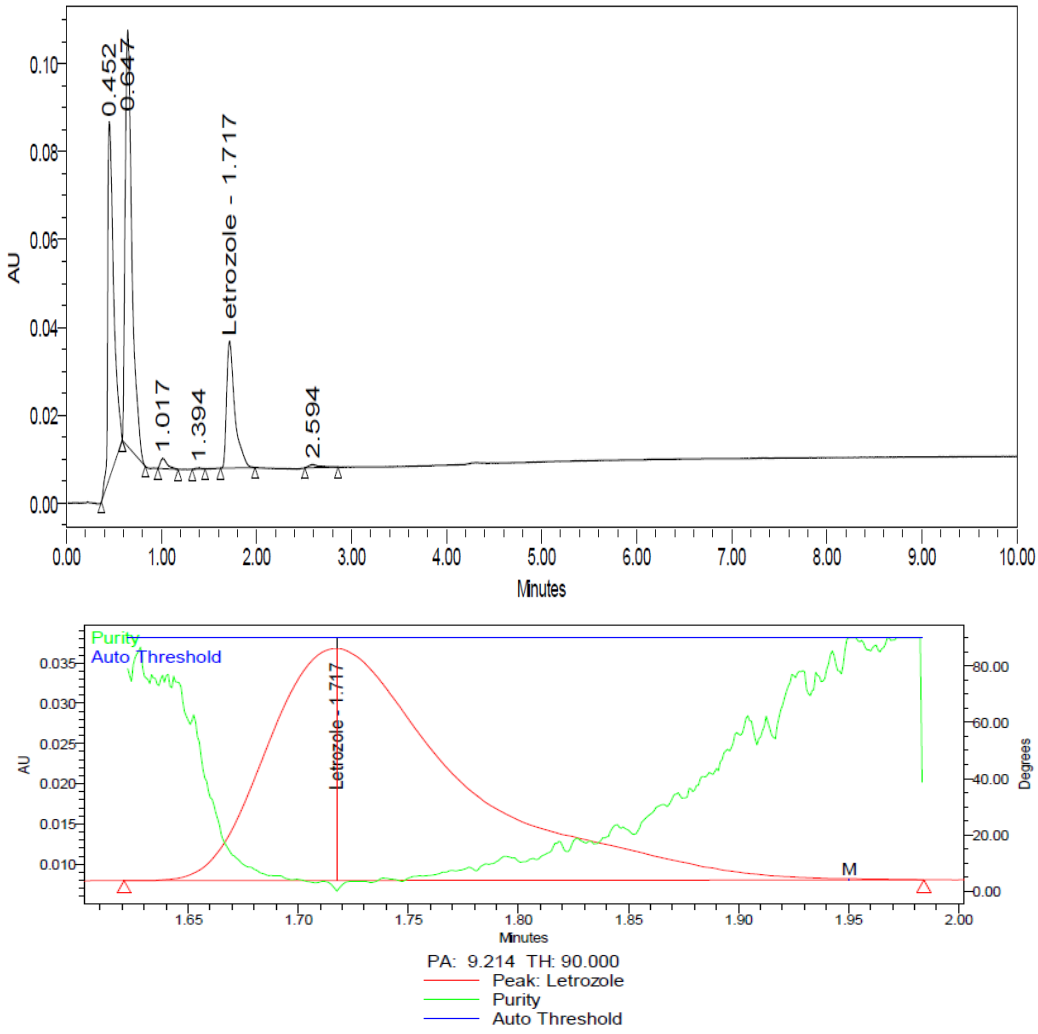

	Peak Name	RT	Area	%Area	USP Plates	Resolution	Tailing	Purity1 Angle	Purity1 Threshold	Purity1 Flag
1		0.452	352331	34.83	304		1.55	45.829	90.000	No
2		0.647	467882	46.26	444	1.65	1.85	11.460	90.000	No
3		1.017	11289	1.12	1136	2.86	1.88	11.435	90.000	No
4		1.394	1090	0.11	1215	3.15	0.92	69.061	90.000	No
5	Letrozole	1.717	173362	17.14	2261	2.50	1.89	9.214	90.000	No
6		2.594	5532	0.55	3779	5.50	1.42	66.545	90.000	No

Figure 14. Chromatogram of LTZ peak and purity plot under basic degradation.

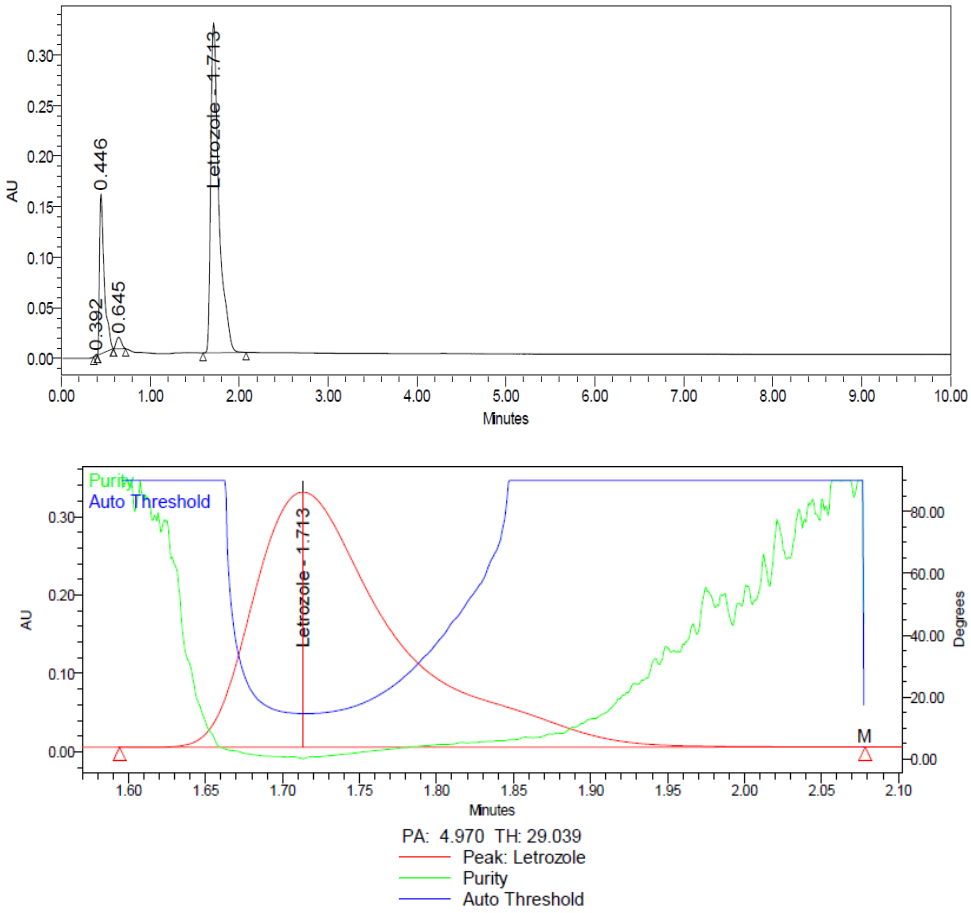

	Peak Name	RT	Area	%Area	USP Plates	Resolution	Tailing	Purity1 Angle	Purity1 Threshold	Purity1 Flag
1		0.392	1883	0.07	1894		0.74	42.067	90.000	No
2		0.446	586228	21.59	382	0.83	2.34	21.282	73.503	No
3		0.645	45915	1.69	535	1.95	1.18	41.679	90.000	No
4	Letrozole	1.713	2080751	76.65	2003	7.88	1.95	4.970	29.039	No

Figure 15. Chromatogram of LTZ peak and purity plot under oxidative degradation.

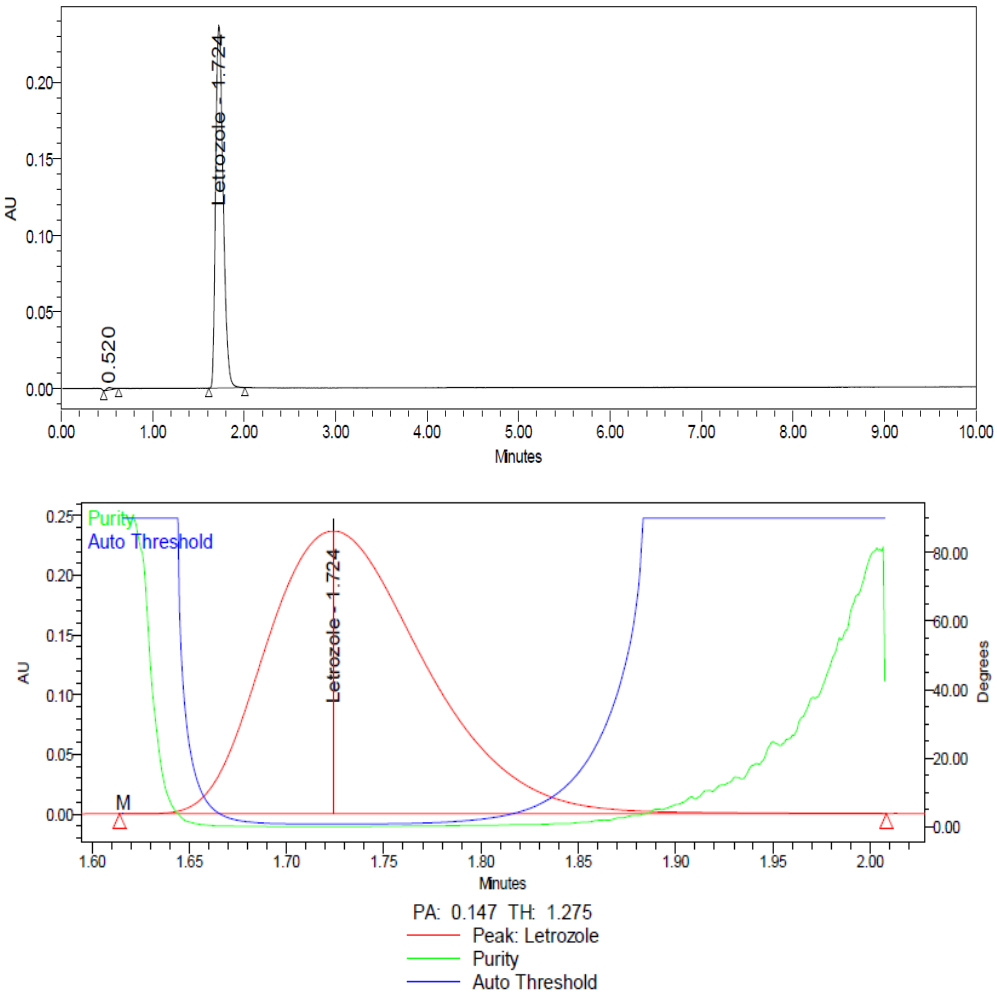

	Peak Name	RT	Area	%Area	USP Plates	Resolution	Tailing	Purity1 Angle	Purity1 Threshold	Purity1 Flag
1		0.520	7616	0.56	233		1.19	17.276	66.330	No
2	Letrozole	1.724	1345136	99.44	2115	8.37	1.34	0.147	1.275	No

Figure 16. Chromatogram of LTZ peak and purity plot under thermal degradation.

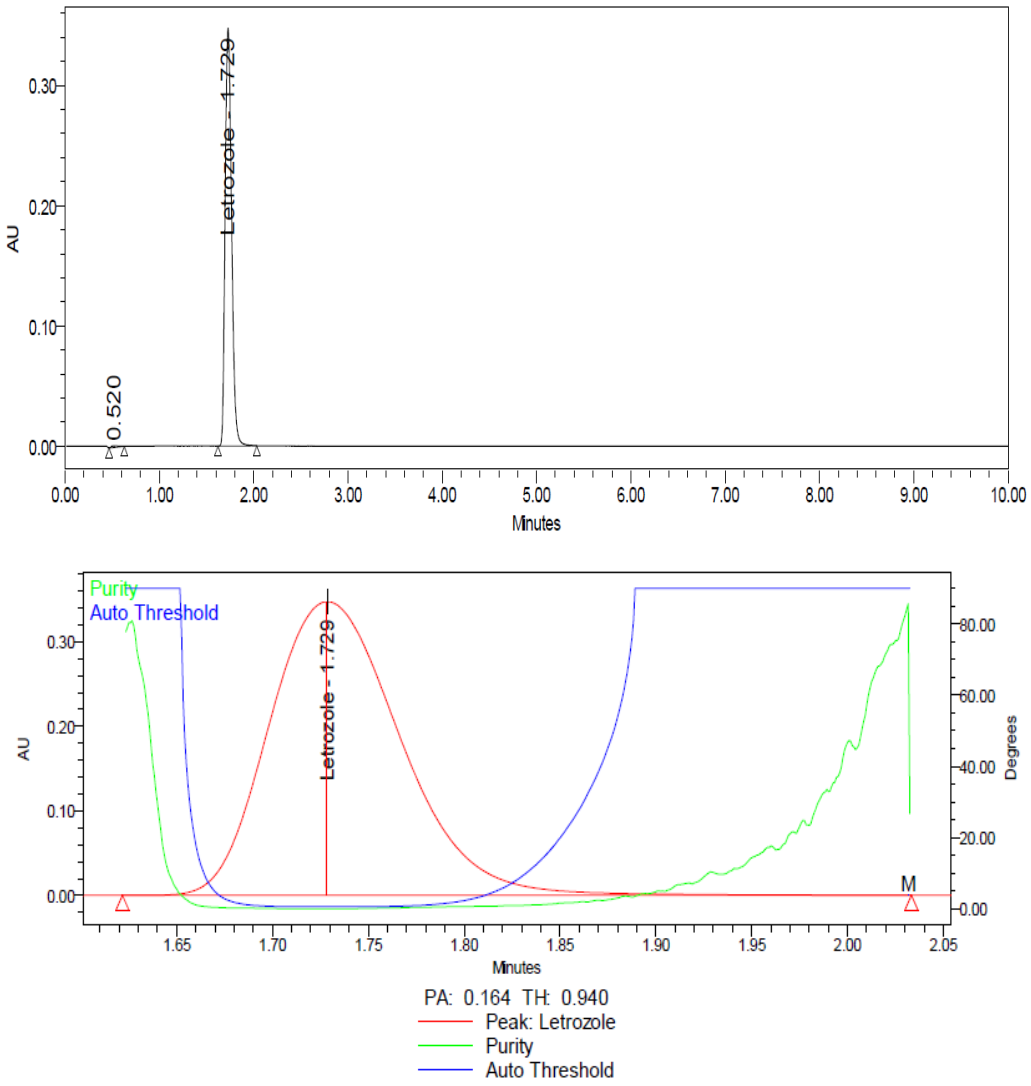

	Peak Name	RT	Area	%Area	USP Plates	Resolution	Tailing	Purity1 Angle	Purity1 Threshold	Purity1 Flag
1		0.520	7014	0.42	204		1.15	14.858	55.125	No
2	Letrozole	1.729	1649587	99.58	3116	9.82	1.25	0.164	0.940	No

Figure 17. Chromatogram of LTZ peak and purity plot under UV-photolysis.

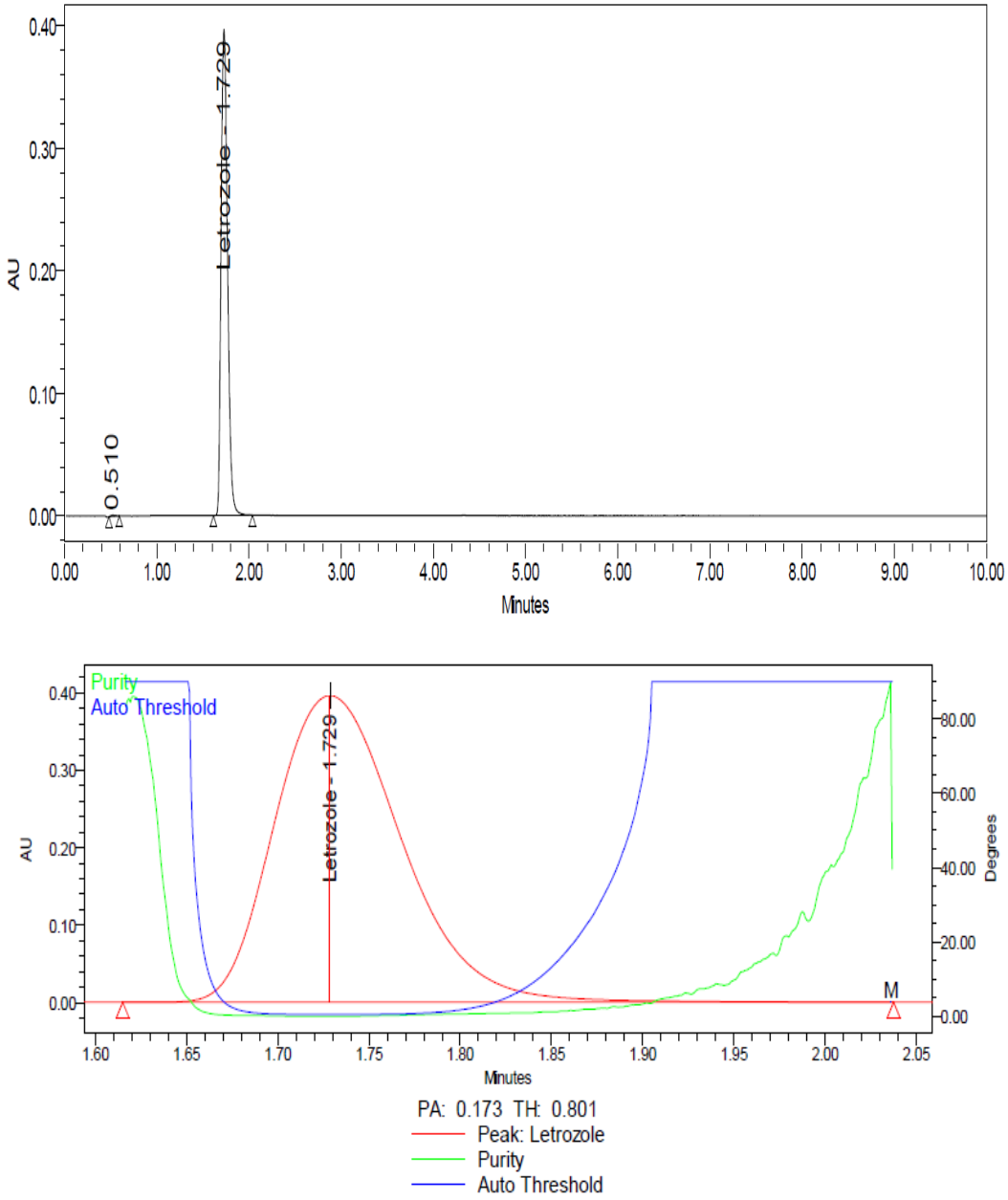

	Peak Name	RT	Area	%Area	USP Plates	Resolution	Tailing	Purity1 Angle	Purity1 Threshold	Purity1 Flag
1		0.510	3163	0.16	402		1.87	10.629	90.000	No
2	Letrozole	1.729	1913842	99.84	3037	10.70	1.29	0.173	0.801	No

Figure 18. Chromatogram of LTZ peak and purity plot under visible light degradation.

3.3.8 Solution Stability

Two storing conditions were used to assess the stability of LTZ solutions; at room temperature and in refrigerator (5°C). Standard and sample solutions having LTZ concentrations of 50 µg/ml were stored in tightly closed unwrapped containers at room temperature and in refrigerator (5°C) for 48 hours. Percentage recovery was measured through assaying 6 samples for each storing condition at 24 and 48 hours. Table 12 summarized the results obtained from the UPLC analysis. Samples were found to be stable at both storing conditions over 48 hours. Percentage recovery was not less than 98.0% for both storing conditions at the two time points of analysis. The respective %RSD values were also very low (1.1-1.7%), not exceeding 2.0% at any storing condition and time point. This provided as evidence that LTZ solutions were stable at room temperature and refrigerator for 48 hours.

Table 12. *Stability of LTZ Solutions under Two Different Storing Conditions*

	Room temperature		**Refrigerator (5°C)**	
	24 hrs	**48 hrs**	**24 hrs**	**48 hrs**
% Recovery	98.8 ± 1.35	99.4 ± 1.56	99.8 ± 0.97	99.9 ± 1.20
% RSD	1.5	1.7	1.1	1.3

Data reported as mean ± SD, n=6 .

3.3.9 Effect of Filtration

Two different types of filters were used to assess the changes in percentage recovery of LTZ standard solutions; 0.2 µm PTFE and 0.2 µm Nylon filters. A total of 7 standard solutions were assayed prior to and after filtration through either PTFE or Nylon filters. The percentage recovery did not change significantly using either filter (Table 13). The difference between the percentage recovery prior to filtration and after using PTFE and Nylon filters was only 0.6% and 0.4%, respectively. The corresponding %RSD values were also within the acceptable limits (not more than 2.0%) when either filter was used (140).

Table 13. *Effect of the Different Filters on Percentage Recovery of LTZ*

	Prior to filtration	**PTFE filter**	**Nylon filter**
% Recovery	99.2 ± 0.49	98.6 ± 0.48	98.8 ± 0.69
% RSD	0.6	0.40	0.80

Data reported as mean ± SD, n= 7.

3.4 Characterization of the Optimized Polymeric Monodisperse Microparticles Loaded with Letrozole

3.4.1 % Yield

The yield of the monodisperse microparticles produced by the VOAG constituted the biggest challenge in this study. The persistent clogging of the orifice made it impossible to produce particles with a sufficient yield. Nevertheless, the implemented modifications of the VOAG discussed earlier resulted in a huge change in the yield from almost 0% to 88.2- 96.1% (Table 14). The use of an aqueous medium to collect the generated droplets protected them from being exposed to the electrophoretic collision inside the original drying column of the VOAG (141) which also contributed to the very low yield and difficulty in collecting the particles. This was because the collision forces resulted in the disposition of the droplets on the walls of the drying column, thus, no monodisperse

particles were generated. In our proposed method, we combined the ability of the VOAG to generate monodisperse microparticles with the advantage of the efficient collection of particles using the dispersion-solvent evaporation technique. This enabled the production of monodisperse microparticles with very high yield in an easy manner. This was considered a huge achievement since such high yield percentages have never been reported previously using the VOAG (134,141,142,145–147,177,178). The maximum yield obtained from the VOAG that was reported in literature was only 45% (149). This reflects the how much this study added to the current literature in terms of enhancing the efficacy of the VOAG and turning it from an instrument capable of only producing monodisperse stream of liquid droplets into dried monodisperse microparticles of various applications and uses.

Table 14. *Summary of the Percentage Yield of the Monodisperse Microparticles Obtained Using the VOAG*

Sample/Formulation	% Yield (Before optimization)	% Yield (After optimization)
LTZ	-	88.2 ± 1.1
PCL	-	92.3 ± 1.5
PCL 5% LTZ	-	93.5 ± 2.6
PCL 10% LTZ	-	96.1 ± 0.9
PCL 20% LTZ	-	92.2 ± 2.2
PCL 25% LTZ	-	92.3 ± 2.6
PCL 30% LTZ	-	90.4 ± 0.2
PDLLA	-	94.4 ± 0.3
PDLLA 5% LTZ	-	95.2 ± 4.1
PDLLA 10% LTZ	-	93.2 ± 3.2
PDLLA 20% LTZ	-	94.0 ± 4.0
PDLLA 25% LTZ	-	90.4 ± 0.4
PDLLA 30% LTZ	-	94.2 ± 2.8

Data presented as mean ± SD, n=3.

3.4.2 Morphological Analysis

Using SEM, the optimized formulations using either PCL or PDLLA as a carrier appeared to be completely spherical in shape with fine smooth surfaces, regardless of LTZ concentration in the formulation (Figures 19 and 20). All particles seemed to be extremely uniform in size and dimensions, reflecting the high degree of monodispersity. Particles with lower LTZ loading (5%) were smaller than those with higher LTZ loading (30%) and this was normal due to the increase in their viscosity and apparent volume (163). Agglomeration of particles was not detected in all formulations, indicating that the PVA concentration was sufficient to provide adequate homogeneous dispersion of the particles. Similar morphology was reported previously with those succeeded in producing highly monodisperse microparticles (120,179–181).

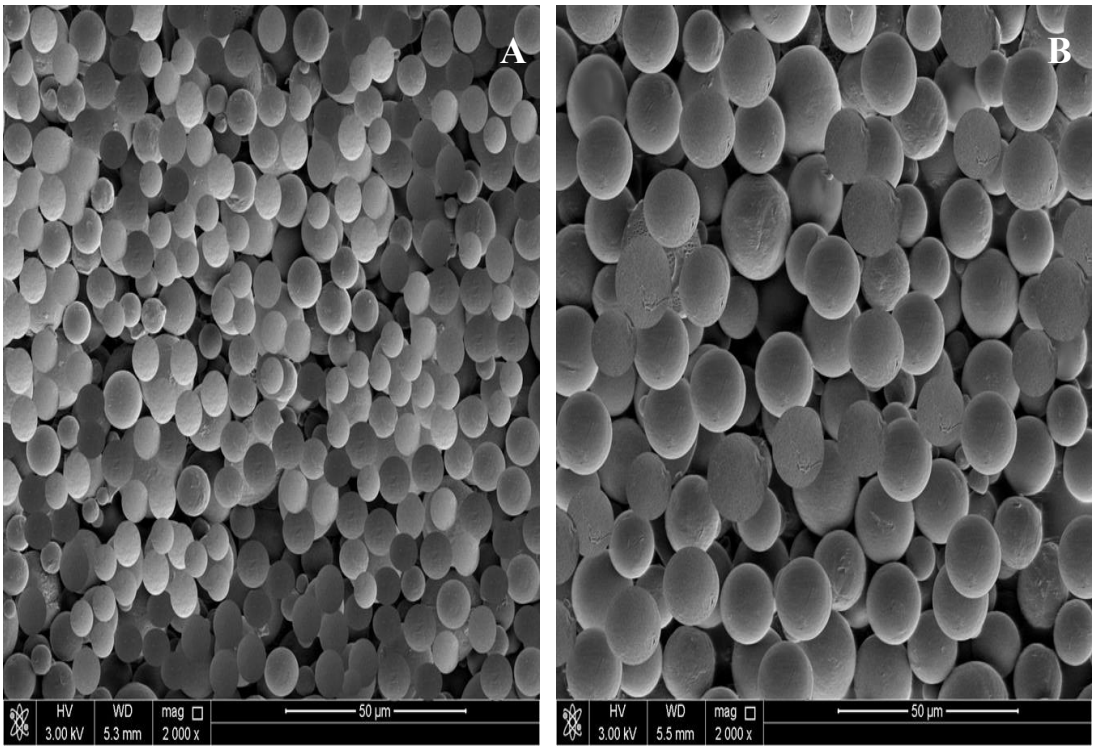

Figure 19. SEM micrographs of optimized PCL-based formulations. (A): PCL 5% LTZ, (B): PCL 30% LTZ.

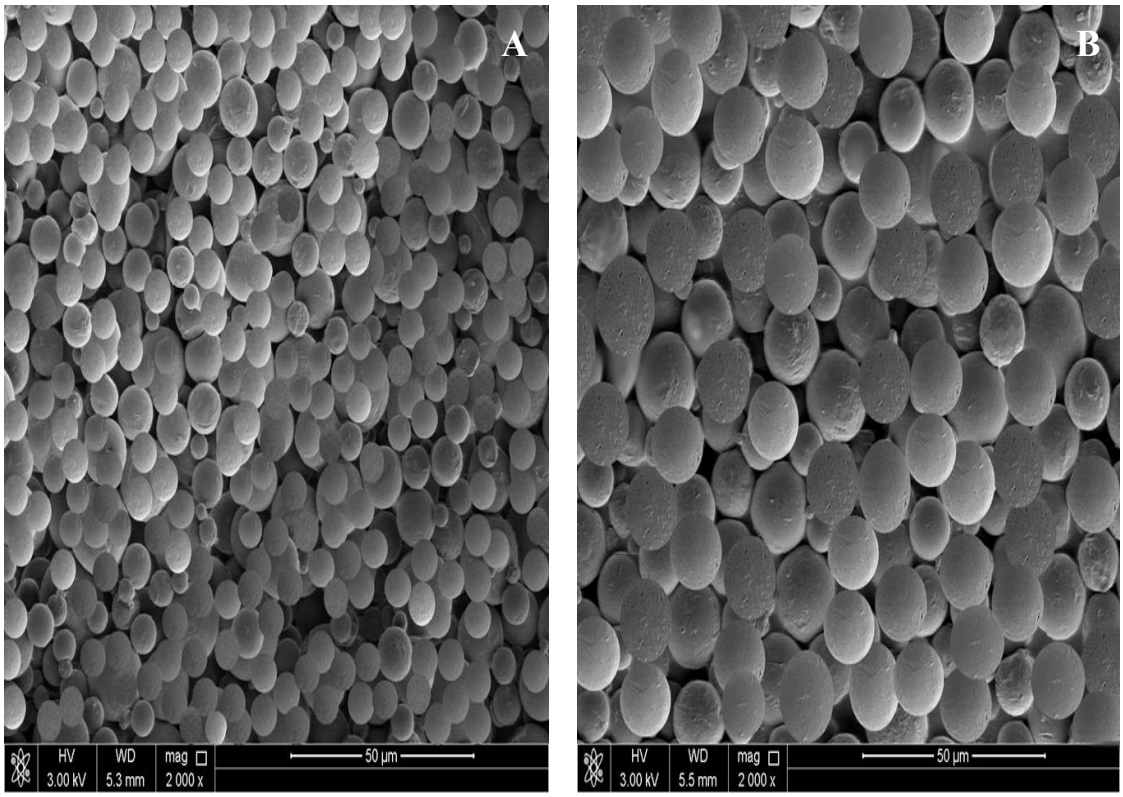

Figure 20. SEM micrographs of optimized PDLLA-based formulations. (A): PDLLA 5% LTZ, (B): PDLLA 30% LTZ.

3.4.3 Particle Size Analysis

Solidified monodisperse microparticles were formed when the organic solvent partitioned to the external aqueous medium with subsequent evaporation through stirring, leaving the microparticles in the aqueous phase to be extracted via filtration and dried thereafter (182). The median particle size increased from 10.9 ± 0.21 µm to 24.7 ± 0.82 µm when LTZ loading was increased from 0% to 30% in PCL-based formulations (Table 15). Likewise, there was an increase in median particle size from 12.9 ± 0.49 µm to 27.3 ± 0.87 µm when LTZ loading was increased from 0% to 30% in PDLLA-based formulations (Table 15). This significant increase in particle size ($P < 0.05$) might be attributed to the increase in organic phase concentration which produced a more viscous solution that was more resistant to the force applied by the stirring that broke up the large droplets into smaller ones (183). However, there was no significant difference between the particle size of PCL- and PDLLA-based formulations that had similar LTZ loadings. Similarly, particle size distribution showed a comparable pattern in which the span decreased with the increase in LTZ concentration in the formulations (Table 15). Although the difference between the span values did not reach statistical significance, it could be also related to the fact that the more viscous the organic phase became with the additional LTZ content, the more difficult the droplets got affected by the resistive forces of stirring, which maintained their original size and shape, resulting in narrower particle size distribution (184). Size analysis findings came in agreement with what was previously observed with SEM analysis, confirming the successful production of

monodisperse microparticles (Figures 19 and 20). In comparison to the previous studies which reported the production of LTZ formulations with polydisperse particles (76,89), our formulations had much narrower particle size distribution ranging from 0.162 ± 0.01 to 0.195 ± 0.01 which was comparable to that of standard polystyrene monodisperse microparticles (span= 0.167 ± 0.02) manufacture by Sigma-Aldrich Co. LLC (Germany). This indicated that we were successful in producing the intended monodisperse microparticles which demonstrated for long an advantage over the polydisperse counterparts (185).

Table 15. *Summary of the Particle Size and Particle Size Distribution Analyses for Optimized Formulations*

Formulation	Median diameter (µm)	Span
PCL	10.9 ± 0.21*	0.171 ± 0.002
PCL 5% LTZ	14.7 ± 0.67*	0.185 ± 0.01
PCL 30% LTZ	24.7 ± 0.82*	0.162 ± 0.01
PDLLA	12.9 ± 0.49*	0.179 ± 0.002
PDLLA 5% LTZ	16.3 ± 1.1*	0.195 ± 0.01
PDLLA 30% LTZ	27.3 ± 0.87*	0.178 ± 0.01
Polystyrene monodisperse microparticles (Control)	23.4 ± 2.50	0.167 ± 0.02

Data presented as mean ± SD, n=3.

(*): Indicates statistical significance at P= 0.05 between same polymer-based groups.

3.4.4 Zeta Potential Analysis

Particles surface charge measurements, also referred to as zeta potential, was negative in all formulations which was possibly attributed to the free ester groups of PCL and PDLLA that constitute the outer layer of the microparticles (Table 16). This had been

stated previously by Mandal et al., who reported negative zeta potential values when incorporating LTZ in Poly (Lactide-co-Glycolide) nanoparticles (186). When KCL solution was used as dispersant instead of distilled water, there was a significant decrease in the zeta potential by 3-5 absolute digits. This is due to the fact that free ions of KCL had neutralized some of the charges of the floating particles (187,188). A significant decrease in the absolute value of zeta potential was observed with the increase in LTZ concentration as opposed to the pattern seen with particle size. Such observation could be explained by the fact that zeta potential is affected by the rate of particles movement in the system in which particles travelling slowly tend to have a decrease in the zeta potential, whereas those moving rapidly tend to have higher zeta potential values, irrespective of the charge type (i.e. negative or positive). Larger particles which are likely to move slowly within the system had much lower absolute zeta potential values than those which are smaller in size (189).

Table 16. *Summary of the Zeta potential Analysis Using Two Different Dispersants for LTZ, PCL, PDLLA, and the Different Formulations*

Sample/Formulation	Zeta potential (mV) in distilled water	Zeta potential (mV) in KCl aqueous solution
LTZ	-20.4 ± 0.5	-14.6 ± 0.5 *
PCL	-32.8 ± 1.4	-26.5 ± 1.2
PCL 5% LTZ	-26.4 ± 0.8	-23.5 ± 0.4
PCL 10% LTZ	-24.6 ± 0.4	-20.6 ± 0.6 *
PCL 20% LTZ	-21.2 ± 0.7	-17.9 ± 0.2 *
PCL 25% LTZ	-18.6 ± 0.3	-14.9 ± 0.3 *
PCL 30% LTZ	-14.8 ± 0.3	-11.1 ± 0.2 *
PDLLA	-31.1 ± 1.9	-24.8 ± 0.2 *
PDLLA 5% LTZ	-27.3 ± 0.4	-23.0 ± 0.2 *
PDLLA 10% LTZ	-24.3 ± 0.4	-21.0 ± 0.4 *
PDLLA 20% LTZ	-22.1 ± 0.3	-18.2 ± 0.4 *
PDLLA 25% LTZ	-19.4 ± 0.7	-15.8 ± 0.5 *
PDLLA 30% LTZ	-15.9 ± 0.5	-12.6 ± 0.5 *

Data presented as mean ± SD, n=3, number of measurements for each n= 15.

(*): Indicates statistical significance at $P < 0.05$.

3.4.5 Thermal Properties

DSC thermograms of pure LTZ indicated its crystalline nature with a melting point at 186 °C, while PDLLA was confirmed to be amorphous with no melting point peak. On the other hand, PCL was confirmed to be crystalline with a melting point of 63.5 °C. The physical mixture of LTZ and PCL or PDLLA had significantly reduced its crystallinity (Tables 17 and 18, and Figures 21 and 23). The incorporation of LTZ into PCL or PDLLA in the formulation resulted in a conversion of its crystalline form into an amorphous form where the melting point disappeared from all formulations (Tables 17 and 18, and Figures 22 and 24).

Table 17. *Thermal Properties of LTZ, PDLLA, and the Different Formulations with their Physical Mixtures*

	Polymer properties		LTZ properties		
Material	**Tg (°C)**	**ΔH (J/g)**	**Tm (°C)**	**ΔH (J/g)**	**% Crystallinity**
LTZ	-	-	186.0	105.4	100%
PDLLA	60.5	11.5	-	-	-
PDLLA 5% LTZ (physical mix)	60.1	10.8	184.1	0.1	0.09%
PDLLA 10% LTZ (physical mix)	59.3	11.0	184.1	0.6	0.57%
PDLLA 20% LTZ (physical mix)	61.4	7.1	186.8	2.3	2.18%
PDLLA 25% LTZ (physical mix)	61.2	8.1	187.6	5.3	5.03%
PDLLA 30% LTZ (physical mix)	59.7	8.2	185.6	5.7	5.41%
PDLLA 5% LTZ (formulation)	57.0	2.1	-	-	0%
PDLLA 10% LTZ (formulation)	50.2	2.3	-	-	0%
PDLLA 20% LTZ (formulation)	53.2	1.8	-	-	0%
PDLLA 25% LTZ (formulation)	51.9	0.9	-	-	0%
PDLLA 30% LTZ (formulation)	52.4	2.7	-	-	0%

Table 18. *Thermal Properties of LTZ, PCL, and the Different Formulations with their Physical Mixtures*

	Polymer properties		**LTZ properties**		
Material	**Tm (°C)**	**ΔH (J/g)**	**Tm (°C)**	**ΔH (J/g)**	**% Crystallinity**
LTZ	-	-	186.0	105.42	100%
PCL	63.5	48.1	-	-	-
PCL 5% LTZ (physical mix)	64.6	68.7	190.5	0.5	0.47%
PCL 10% LTZ (physical mix)	63.7	51.7	186.8	0.7	0.66%
PCL 20% LTZ (physical mix)	64.4	37.7	187.9	1.3	1.23%
PCL 25% LTZ (physical mix)	62.2	46.6	184.9	2.9	2.75%
PCL 30% LTZ (physical mix)	64.1	37.2	188.0	8.3	7.87%
PCL 5% LTZ (formulation)	57.8	34.2	-	-	0%
PCL 10% LTZ (formulation)	56.1	29.6	-	-	0%
PCL 20% LTZ (formulation)	58.6	39.1	-	-	0%
PCL 25% LTZ (formulation)	57.9	39.9	-	-	0%
PCL 30% LTZ (formulation)	60.3	41.6	-	-	0%

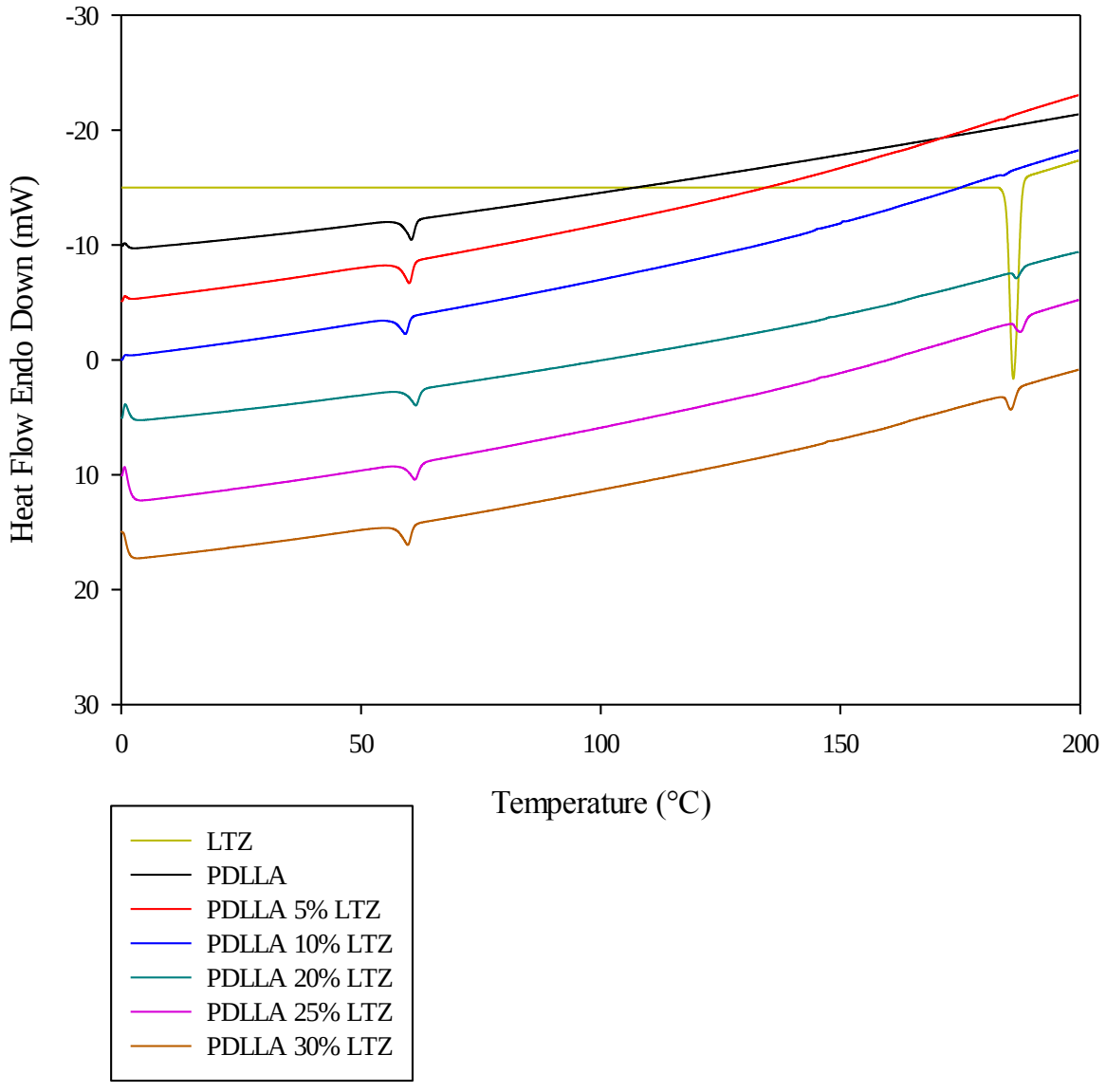

Figure 21. DSC thermograms of LTZ, PDLLA, and their physical mixtures.

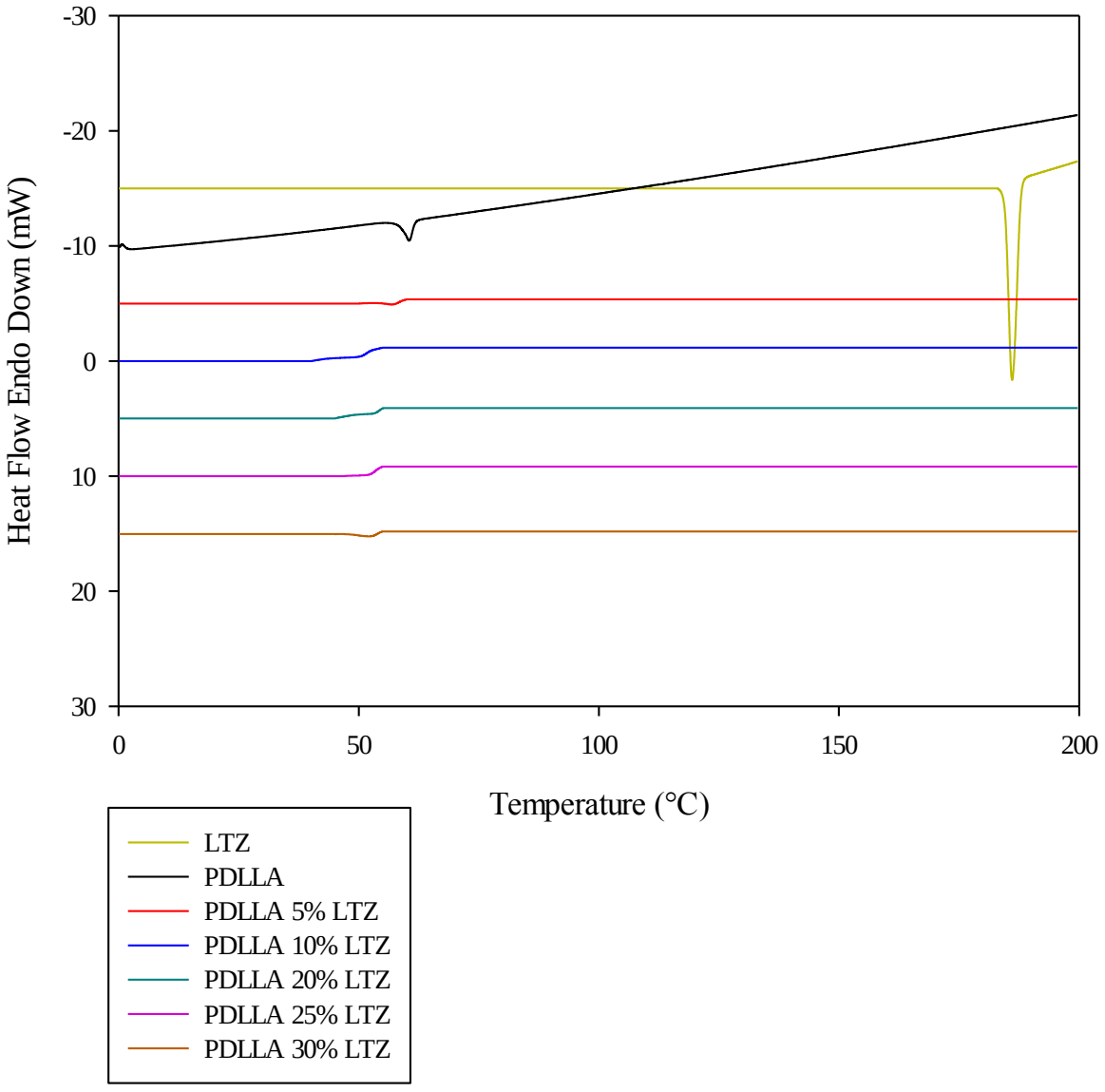

Figure 22. DSC thermograms of LTZ, PDLLA, and their formulations.

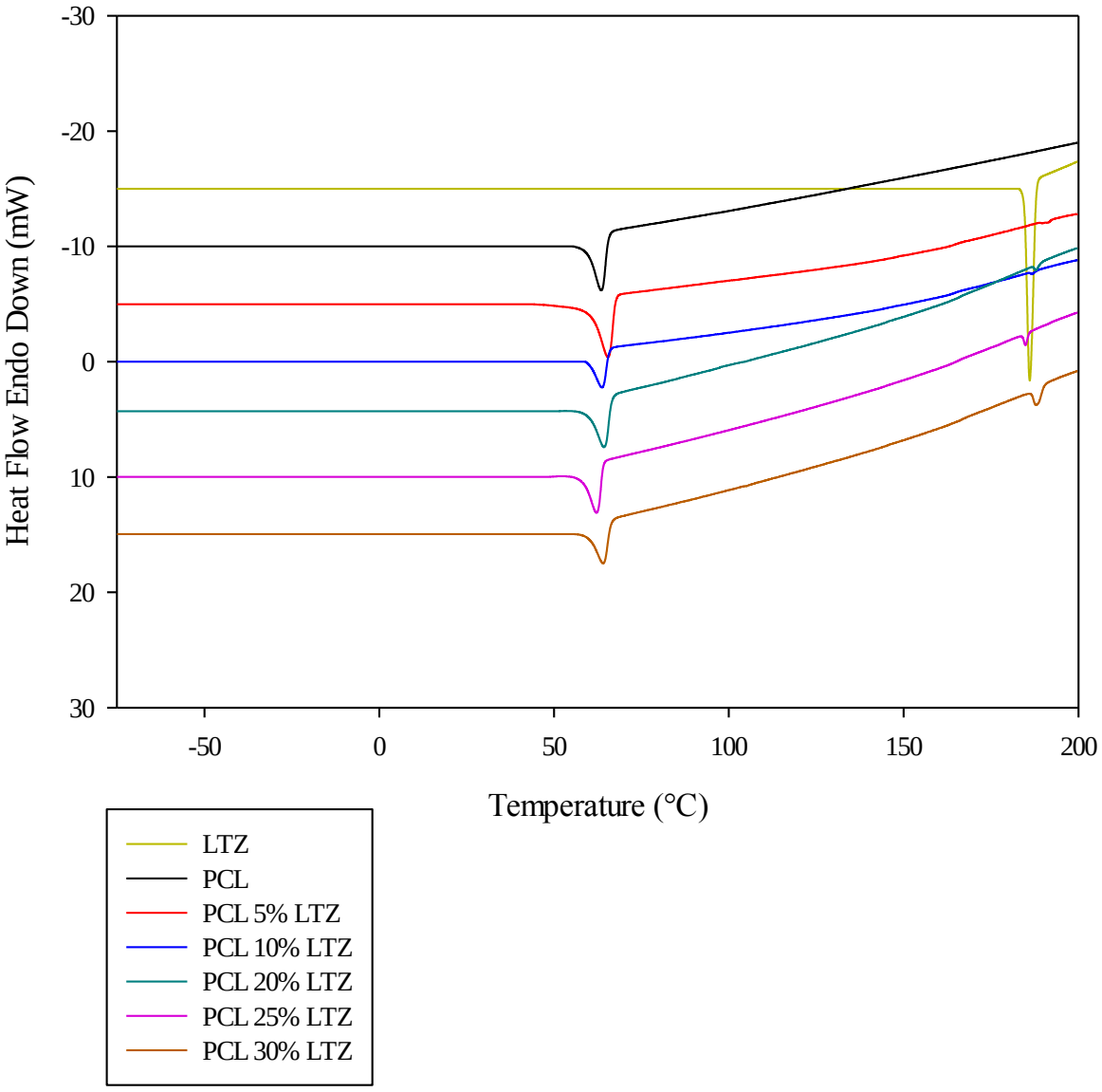

Figure 23. DSC thermograms of LTZ, PCL, and their physical mixtures.

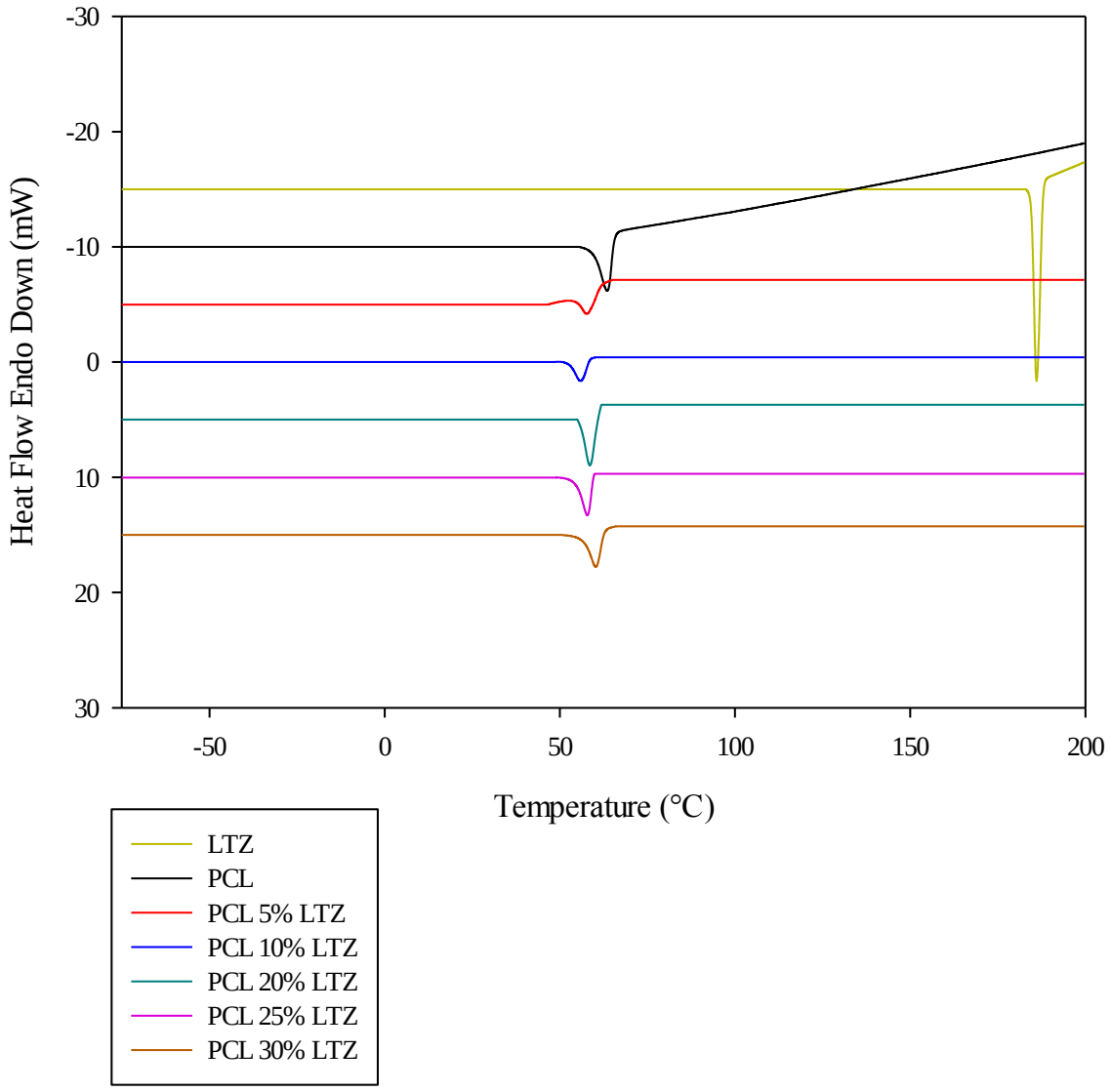

Figure 24. DSC thermograms of LTZ, PCL, and their formulations.

3.4.6 Structural Characterization

XRD analysis, however, showed some dissimilarities to those observed with DSC. As a more powerful technique in elucidating the physical structure of materials, XRD was able to show some of the distinctive peaks of LTZ crystals in PDLLA-based formulations containing 20%, 25%, and 30% LTZ (Figures 25 and 26). This could be possibly attributed to some drug crystals lying on top of particle surfaces. Although drug entrapment efficiency was higher in these formulations as compared to the one having only 5-10% LTZ, these proposed drug crystals on the surface of particles might indicate that the drug concentration exceeded its solubility in the polymeric matrix, leaving some particles in their crystalline form near or on the top of the surface (190). On the other hand, LTZ was found to be totally amorphous in all PCL-based formulations (Figures 27 and 28), and this is may be due to its high hydrophobic nature (191). Of note, some of LTZ peaks were overlapping together which was not reported previously in literature (192), and this was mainly due to some technical issues found in our XRD instrument.

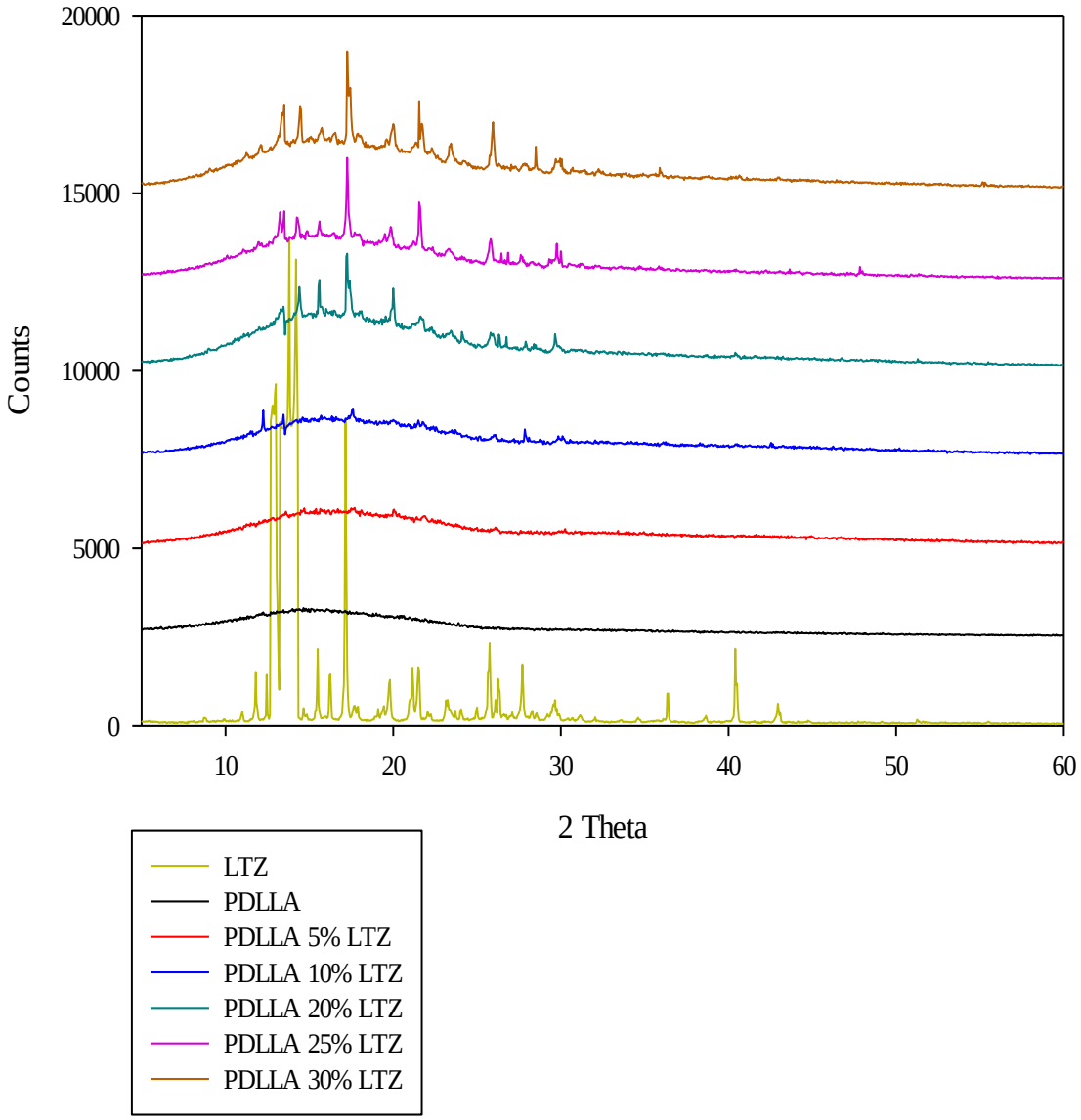

Figure 25. XRD patterns of LTZ, PDLLA and their physical mixtures.

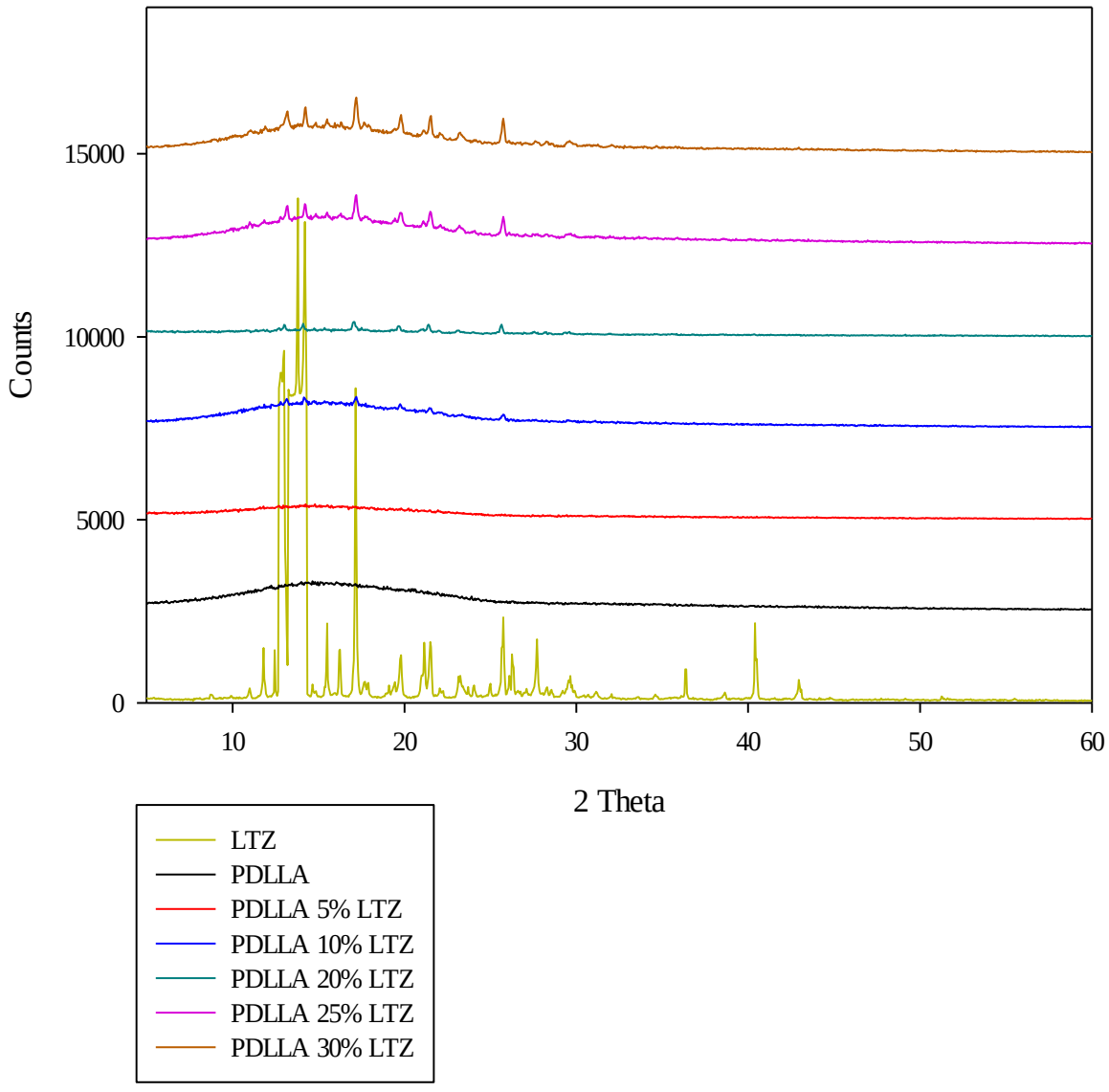

Figure 26. XRD patterns of LTZ, PDLLA and their formulations.

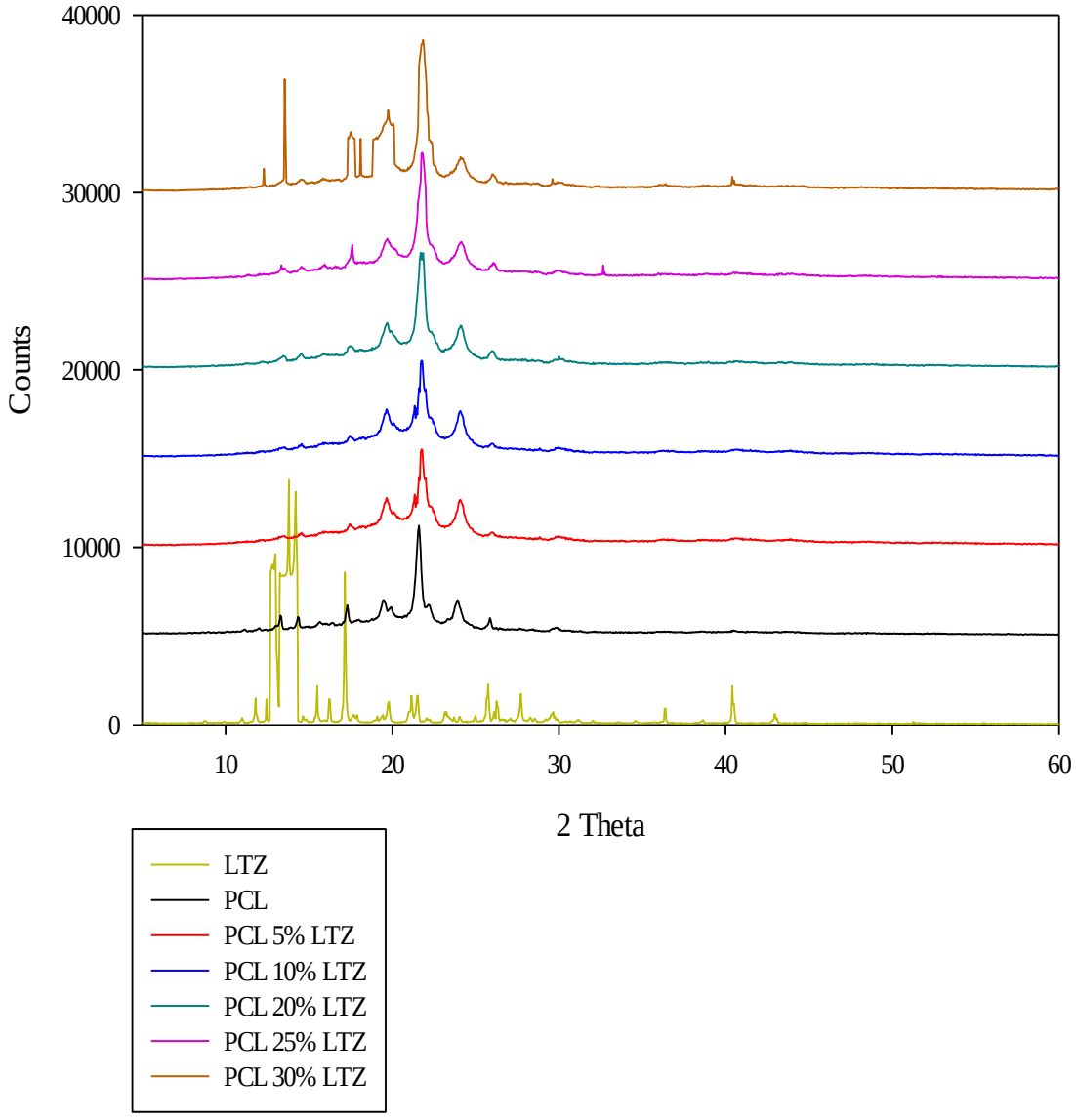

Figure 27. XRD patterns of LTZ, PCL and their physical mixtures.

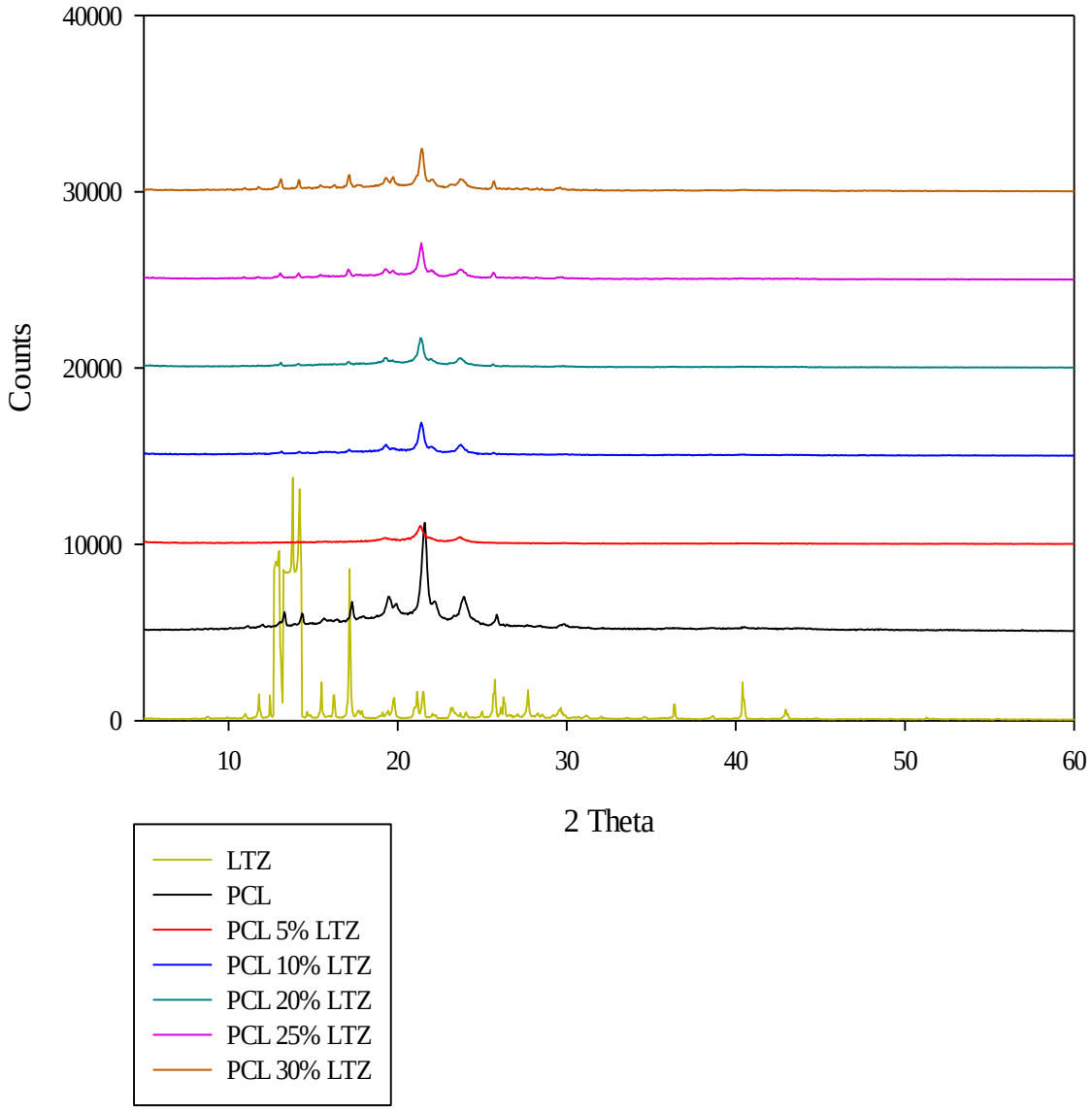

Figure 28. XRD patterns of LTZ, PCL, and their formulations.

3.4.7 Drug Loading and Entrapment Efficiency Measurement

Drug loading approached 100% (98.1 to 99.3%) in all formulations, indicating that the preparation process was effective in maintaining the intended drug content, with negligible drug losses during production (Table 19). Importantly, the entrapment efficiency which reflected the actual amount of drug encapsulated within the polymeric carrier was very high, ranging from 89.9% to 94.1% in PDLLA-based formulations when using LTZ concentrations of 5% to 30%, respectively (Table 19). Similarly, the entrapment efficiency was increased from 92.4% to 96.8% in PCL-based formulations when using LTZ concentrations of 5% to 30%, respectively (Table 19). This increase in entrapment efficiency with the increase in LTZ concentration could be related to the increase in particle size which offered smaller surface area exposed to the outer aqueous phase, hence greater drug proportions were successfully accommodated by the particles. As such, the diffusion of the drug to the aqueous medium would be much lower as compared to that of particles with smaller sizes and larger surface areas. Previous studies have shown that larger particles may have lower affinity to the aqueous medium, preserving more drug within the polymeric shell than smaller ones (89). Analysis of LTZ concentrations in the supernatants came in agreement with those measured in pellets, confirming the accurate measurement of entrapment efficiency in this study (Figure 29).

Table 19. *Summary of the Drug Loading and Entrapment Efficiency Analyses for the Different Formulations*

Formulation	**Drug loading (%)**	**Entrapment efficiency (pellet analysis) (%)**	**Entrapment efficiency (supernatant analysis) (%)**
PCL 5% LTZ	99.1 ± 0.04	92.4 ± 0.25	92.2 ± 0.08
PCL 30% LTZ	99.3 ± 0.27	96.8 ± 0.06	96.2 ± 0.06
PDLLA 5% LTZ	98.1 ± 0.26	89.9 ± 0.08	90.0 ± 0.05
PDLLA 30% LTZ	98.6 ± 0.21	94.1 ± 0.32	93.9 ± 0.13
***P*-value**	0.013	<0.001	<0.001

Reported data represents the mean ± SD, n=3.

P-values represented the differences between the 4 formulations in terms of drug loading and entrapment efficiency.

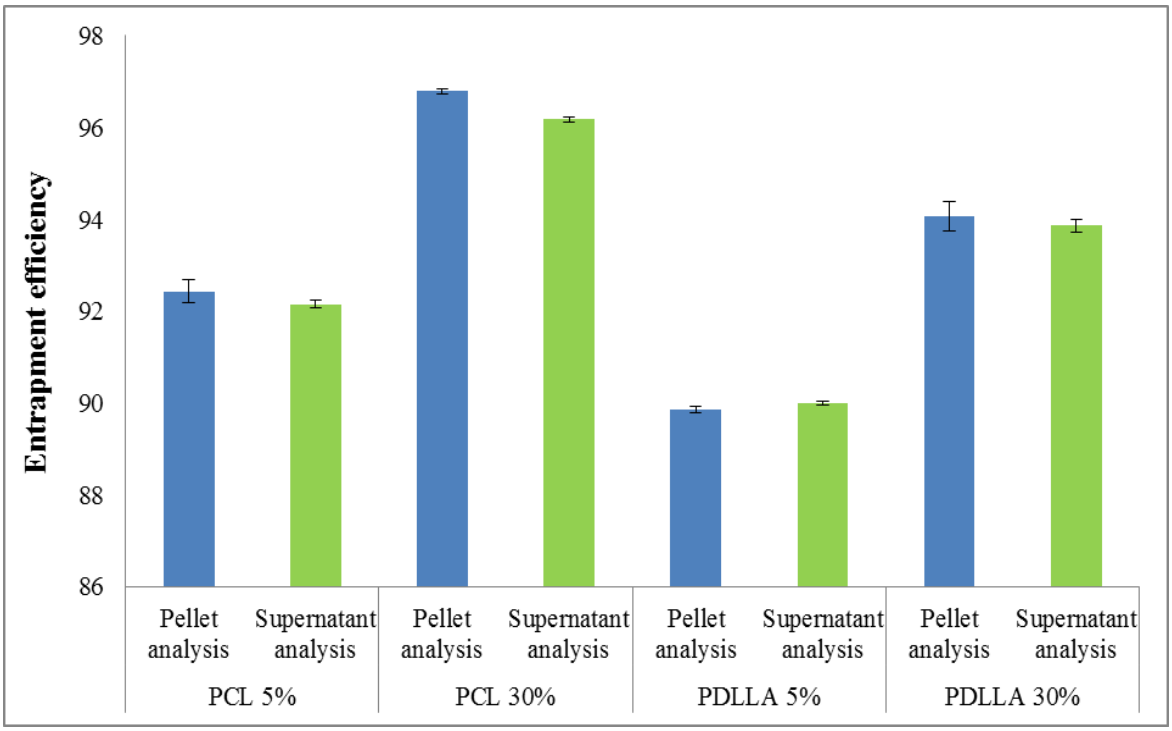

Figure 29. Difference between entrapment efficiency analysis obtained from two different methods. Bars represent the average entrapment efficiency expressed as percentage. Data reported as mean ± SD, n=3.

3.5 In Vitro Drug Release Study and Kinetic Modeling

Prior to conducting the release study, it was important to determine an appropriate diffusion medium that would provide a sink condition along with maintaining the stability of the drug over the study period. If phosphate buffer were to be used alone as a diffusion medium, large volumes of the medium would have been needed to establish the sink condition since we found that the solubility of LTZ in phosphate buffer was just 40.8

± 5.2 µg/ml. Therefore, it was important to add a co-solvent to the phosphate buffer in order to enhance the solubility of LTZ, and as such minimize the required volumes of the medium (193). In preliminary experiments, different co-solvents were tried such as Tween 20, Tween 80, and Transcutol®. It was observed that Tween 20 and Tween 80 were constantly producing air bubbles within the medium and this was a critical problem if they were to be used in the release study as they would form a barrier to the release of the drug from the diffusion membrane. Therefore, Transcutol® which only produced few air bubbles that were removed easily was the best choice. Different concentrations of Transcutol® were also tried to determine the lowest concentration possible that would establish the sink condition with the minimal volumes of the diffusion medium. We found that 20% v/v Transcutol® in phosphate buffer would satisfy our aim where the solubility of LTZ in this medium was found to be 204.24 ± 0.45 µg/ml (Table 20). This indicated that with just adding 20% v/v Transcutol® to the phosphate buffer, the solubility of LTZ was increased to 5 times that of the phosphate buffer alone. As such, the use of 210 ml of the medium would be sufficient enough to maintain the sink condition with the replacement of the withdrawn medium. The stability of LTZ was also found to be preserved where the percentage of LTZ degradation in the diffusion medium was only 1.2% which was lying within the acceptable range (Table 20) (140).

In vitro drug release study was conducted to explore the drug's behavior and the ability of the produced formulations to provide controlled release of LTZ. These studies have been used to predict the biodistribution of the drug in vivo (194). The 4 different formulations (PCL 5% LTZ, PCL 30% LTZ, PDLLA 5% LTZ, and PDLLA 30% LTZ) were tested for

drug release pattern using dialysis membranes in phosphate buffer solution (pH 6.8) containing 20% v/v Transcutol®. Sampling was done over one month period to obtain a comprehensive drug release profile since previous studies were limited to shorter periods of time (89,98,101,195), and our objective was to produce formulations that can be used for monthly administration. Figure 30 represents the cumulative percentage of drug released over time for the 4 formulations. It can be clearly seen that the release of LTZ was very slow in which 52.7%, 93%, 35.2%, and 85.4% of the drug was not released until after 30 days from PCL 5% LTZ, PCL 30% LTZ, PDLLA 5% LTZ, and PDLLA 30% LTZ, respectively. Notably, the overall release rate of LTZ increased in correspondence to the increase in its loading and entrapment efficiency within the formulation where particles with 30% LTZ content displayed the highest release rates, whereas those with 5% LTZ content exhibited the lowest release rates as evident by the release rate constant (k) values (Table 21). The increase in drug entrapment efficiency within the polymeric matrix has been reported to have an influence on drug release rate (89). The higher the entrapment efficiency, the higher the probability that more drug would accumulate either at the surface of the particle or within the particle but at close proximity to the solid/liquid interface rather than the deep core of the polymeric matrix. This is because the concentration of the drug might have exceeded its solubility in the polymer, resulting in coexistence of amorphous aggregates and crystals of the drug, with the crystals being insoluble in the matrix, protruding near the surface of the particles. Consequently, faster release rates have been observed. In contrast, the lower the entrapment efficiency, the higher the drug solubility would be in the polymeric matrix,

leading to the conversion of almost all the drug crystals into amorphous counterparts, allowing for more homogenous distribution of the drug within the matrix with the majority of the drug being expected to concentrate in the core of the particles and with no crystals likely to be near the surface. Thus, the drug release rate would be much slower. Interestingly, release rate was higher in PCL-based formulations as compared with PDLLA-based formulations that had equal drug loadings. This was mainly due to the fact that LTZ was totally amorphous in PCL-based formulations, whereas in PDLLA-based formulations, some drug crystals were present as seen previously in XRD analysis. These crystals were not seen in the SEM images of the microparticles, possibly due to their limited amount in the formulation, whilst most of the drug was efficiently dispersed in its amorphous form within the polymeric matrix. The high sensitivity of XRD enabled the detection of such trace concentrations of the drug crystals. Importantly, the extended release of LTZ for one month suggested the potential of these formulations for IM depot administration. This would constitute one dimension of our future investigations.

Data obtained from the in vitro release study had been tested against four different kinetic modeling: zero-order, first order, Higuchi model, Hixson-Crowell model, and Korsemeyer-Peppas semi-empirical model. Release rate constants (k) and correlation coefficients (R^2) of the obtained data and the corresponding kinetic models were computed for the three formulations and presented in Table 21. It can be seen that the release profiles of the three formulations were best fitted with a biphasic zero-order model where highest correlation coefficient (R^2) values were obtained (Table 21). The first phase lasted from 0-3 days, whilst the second phase started after 3 days and

continued till the end of the study period (Figure 30). Each phase had distinct release rate constants (k) and correlation coefficients (R^2). It was observed that during the first phase, there was a slight burst effect ranging from 6.0% to 7.9% which was mainly due to the rapid release of the drug particles on or near the surface of the polymeric shells. However, after 3 days, the burst effect decreased to no more than 2.4% as all drug particles near the surface were released and the remaining particles started to get released in a more controlled manner. Again, higher burst effects were noted with PCL-based formulations as compared with PDLLA-based formulations. This was due to the higher solubility of LTZ in PCL matrices as opposed to PDLLA matrices. Despite this observation, the burst effects observed with our formulations were much lower than those seen in previous studies where the burst effects in such studies were very high reaching more than 80% (98,195). Thus, our formulations presented a huge advantage over the previous formulations in which the adverse effects that might occur due to the release of high concentrations of LTZ would be avoided in our formulations. The production of formulations with biphasic zero-order release kinetics entailed that as time elapsed, constant amounts of LTZ were released (196). This is of high importance since these formulations were successful in modifying the release of LTZ from being non-linear, unpredictable, and inconsistent into linear, highly predictable, and consistent, which was the main objective of the study.

Table 20. *Solubility and Stability of LTZ in Diffusion Medium*

Day	Concentration (µg/ml)	% Degradation
Day 3	204.24 ± 0.45	1.2%
Day 31	206.18 ± 0.62	

Reported data represents the mean ± SD, n=3.

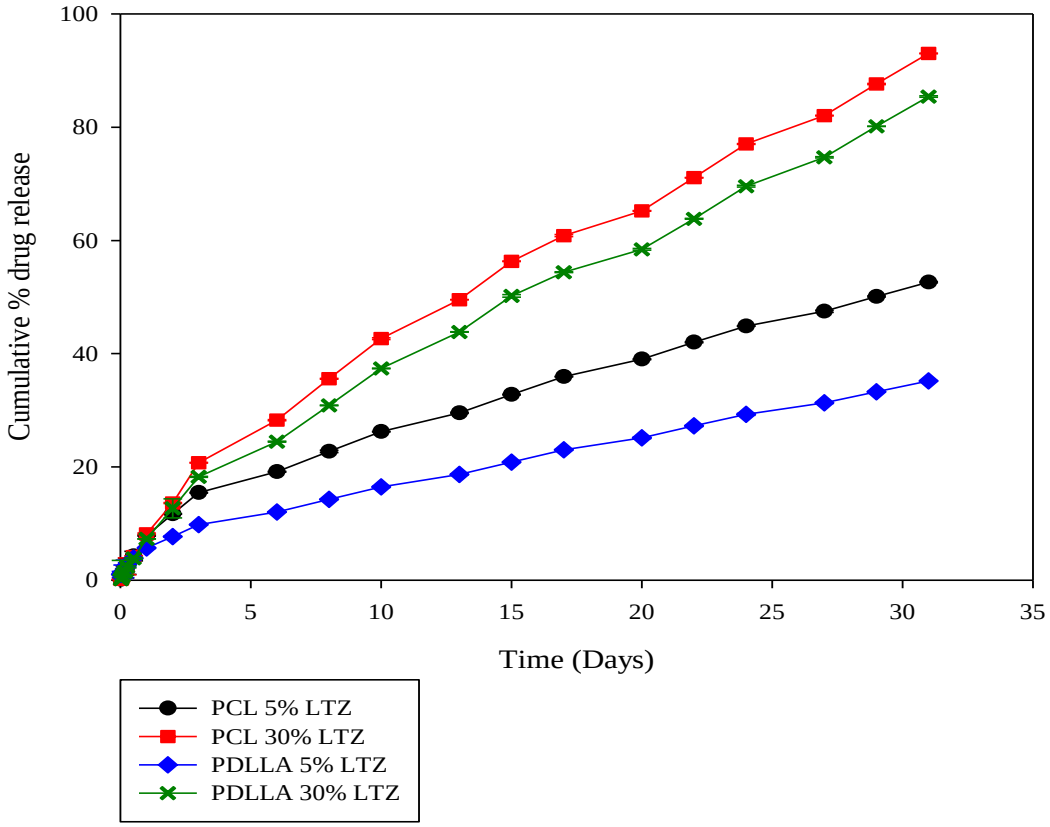

Figure 30. Drug release profile from the different formulations.

Table 21. *Drug Release Kinetic Modeling of the Different Formulations*

Formulation	**Zero order (Phase 1)**		**Zero order (Phase 2)**		**First order**		**Higuchi**		**Hixon-Crowell**		**Korsemeyer-Peppas**		
	K	**R^2**	**K**	**R^2**	**K**	**R^2**	**K**	**R^2**	**K**	**R^2**	**K**	**R^2**	**n**
PCL 5% LTZ	5927.4	0.9951	1025.7	0.9939	0.040	0.9696	2.953	0.9833	0.002	0.3457	0.576	0.8203	0.11
PCL 30% LTZ	5104.6	0.996	1803.7	0.9955	0.115	0.8531	5.224	0.9694	-0.005	0.4623	0.563	0.8521	0.13
PDLLA 5% LTZ	4551.8	0.9867	708.1	0.996	0.023	0.9695	1.876	0.9802	-0.002	0.5967	1.230	0.9246	0.08
PDLLA 30% LTZ	4533.7	0.9958	1751.1	0.9938	0.089	0.8878	4.736	0.9679	-0.005	0.5533	0.549	0.8599	0.13

The mean of the 6 replicates has been used to compute the K and R^2 values for each model.

3.6 In Vitro Cytotoxicity Studies

3.6.1 Cell Culturing

The main objective of this study was to develop new formulations of LTZ that would possess controlled drug release actions in order to prevent the fluctuations of the drug's levels in the plasma, producing its intended therapeutic effects with minimal adverse effects. LTZ was proven to be an effective agent for the treatment of ER-positive breast cancer in postmenopausal women as it works by inhibiting the aromatase enzyme responsible for the estrogen-dependent proliferation of breast cancer cells. The in vitro release profile testing showed that the optimized formulations developed in this study produced biphasic zero-order release kinetics reflecting a controlled drug release pattern. Therefore, the next step was to evaluate the ability of these formulations to inhibit the proliferation of breast cancer cells. This was achieved through in vitro testing using MCF-7 cell line which is a human breast cancer cell line that was reported to express the aromatase activity where LTZ acts on.

Cell culturing was performed in 75 cm^2 flasks with appropriate volumes of EMEM medium which was recommended by the supplier to grow the MCF-7 cells in. The cells were incubated at 37°C and 5% CO_2. The medium was changed every 2-3 days to keep the cells healthy and ensure their optimal growth. An ideal confluency of 90-95% of the MCF-7 cells was achieved in about one week. Afterwards, the cells were seeded in 96-well plates and incubated for 24 hours at 37°C and 5% CO_2 to get the chance to settle down, attach to the plate surface, and be ready to receive LTZ treatment.

3.6.2 Cytotoxicity Measurement

Optimized LTZ formulations were considered efficacious if they would produce at least an equivalent percentage of inhibition of cell proliferation to that of the pure form of LTZ. This was assessed through measuring the average number of the viable cells after 48-hours treatment of pure LTZ and the LTZ formulations at different concentrations (10 nM, 100 nM, 1 µM, 10 µM, and 100 µM). Untreated MCF-7 cells were used as a control to quantify the percentage of inhibition of cell proliferation where they were only incubated with medium for 48-hours. Another control group of untreated MCF-7 cells were only incubated with medium for just 24-hours to detect any cytotoxic effects that LTZ might have on the treated cells. Cells were treated with pure LTZ and LTZ formulations which were mixed with EMEM medium containing 1:5 v/v (acetonitrile: Transcutol®) to ensure complete solubility of LTZ within the medium after being released from the polymeric shell, while preserving the polymeric carriers intact. The ratio was selected based on preliminary experiments where different ratios of different solvents were tried till reaching this optimal solubility with these specific solvents at these specific ratios. This was an important step to ensure an appropriate cellular uptake of LTZ would be achieved. Consequently, to rule out the effects of the solvents that they might exert on cell viability, three control groups were made. The first one consisted of 1:5 v/v (acetonitrile: EMEM medium), the second one consisted of 5:1 v/v (Transcutol®: EMEM medium), and the last one consisted of EMEM medium with 1:5 v/v (acetonitrile: Transcutol®). MCF-7 cells were treated with these solvents for 48-hours to examine the individual effects of each solvent and their combination on cell viability. The percentage

of each solvent was kept similar to that used for making the treatment arms of pure LTZ and LTZ formulations. Additionally, the effects of the polymeric carriers were also assessed by treating the MCF-7 cells with each polymer at a time. Similarly, these arms consisted of either PCL or PDLLA suspended in EMEM medium with 1:5 v/v (acetonitrile: Transcutol®) to mimic the conditions of the treatment arms.

Inhibition of cell proliferation and cytotoxicity induced by LTZ was assessed using DAPI staining which is a powerful tool for evaluating cell death as the assay stains the nucleic acids of fixed cells. Complete loss of DAPI staining in the treated cells is indicative of cell death as dead cells undergo nuclear fragmentation. Therefore, the quantification of viable cells was based on the measurement of DAPI florescence signals (197). The average number of nuclei of viable cells was calculated using ArrayScan™ XTI Live High Content Platform (ThermoFisher Scientific, NY, USA) where 25 fields were selected from each well for analysis.

Results revealed that Transcutol® did not have any cytotoxic effects on MCF-7 cells where no significant change in cell count was seen after 48-hours of Transcutol® treatment. The agent was also proven to be safe as a vehicle in tissue culturing in other published studies (198,199). On the other hand, a significant reduction in cell count was observed after 48-hours of acetonitrile treatment as compared with untreated cells 48-hours post seeding ($P< 0.0001$), but it was not significant when compared with those 24-hours post seeding ($P= 0.07$). This prominent decrease in cell count might be due to the significant increase in cell count after incubating the cells with the medium for 48-hours

which allowed them to proliferate. Therefore, acetonitrile prevented the cells from proliferating, but did not cause any detectable cell death. Nonetheless, the combination of acetonitrile and Transcutol® appeared to be successful where Transcutol® masked the harmful effects of acetonitrile, providing the cells with a cytocompatible vehicle that enabled their growth and proliferation. Likewise, both PCL and PDLLA carriers were found to be cytocompatible where no difference in cell count was noted after treating the cells with these carriers for 48-hours.

Importantly, it was found that LTZ was able to induce a dose-dependent inhibition of cell proliferation where LTZ significantly resulted in 11.3%, 39.2, 48.8%, and 74.6% decrease in cell count as compared with the control (untreated cells; 48-hours post seeding) ($P< 0.0001$) at concentrations of 100 nM, 1 µM, 10 µM, and 100 µM, respectively. However, at a concentration of 10 nM, only 3.7% reduction in cell count was obtained which did not reach statistical significance ($P= 0.088$) (Figure 31). Similar findings were reported previously (200), however, in some other studies, LTZ was able to significantly inhibit cell proliferation at very low concentrations such as 1 nM (201), and even as low as 0.1 nM (202). This was mainly due to the fact that in these studies, MCF-7 cells were stably transfected with the aromatase gene which significantly intensified the aromatase activity of the cells, leading to a higher sensitivity towards LTZ treatment at very low concentrations (203). Interestingly, both PCL- and PDLLA-based formulations caused a significant reduction in cell count from baseline (48-hours post seeding) even at 10 nM concentration ($P< 0.0001$) (Figures 32-35), reflecting more potent inhibition of cell proliferation as compared with pure LTZ. This could be explained by the fact that

polymeric carriers have been shown to enhance the cellular uptake of drugs via endocytosis and decrease their efflux as compared with free drugs, hence, increasing the time available for the drug to produce its action, and eventually resulting in a greater efficacy of the drug (204). According to the release profile of these formulations, 8.78 mg, 10.22 mg, 5.76 mg, and 9.51 mg of LTZ was released after 48 hours from PCL 5% LTZ, PCL 30% LTZ, PDLLA 5% LTZ, and PDLLA 30% LTZ formulations, respectively. These amounts were even exceeding the required amount of LTZ to produce its effects (63) (due to the slight burst effect discussed earlier) which also explains the reason behind obtaining better results with the four formulations used as compared with those obtained from pure LTZ.

Statistical analysis using ANOVA revealed that both PCL- and PDLLA-based formulations displayed a dose-dependent inhibition of cell proliferation where a significant difference in the cell count between the different concentrations of the different formulations was seen. It was noted that the inhibition of cell proliferation was greater in PCL-based formulations than that of the corresponding PDLLA-based formulations. Such observation was primarily due to the higher release rates of LTZ from PCL-based formulations (Table 21), in addition to the higher solubility of LTZ within the PCL matrix as compared to that in PDLLA matrix which was evident from the XRD analyses (Figures 25-28).

Interestingly, cell death was also observed after 48-hours of treatment with LTZ, PCL- and PDLLA-based formulations baseline (24-hours post seeding). An exact similar

pattern to the inhibition of cell proliferation was encountered with cell death where pure LTZ resulted in a dose-dependent reduction in cell count ($P< 0.0001$) with 7.7%, 36.7%, 46.7% and 73.5% of cell death was achieved at concentrations of 100 nM, 1 µM, 10 µM, and 100 µM, respectively. However, at a concentration of 10 nM, cell death was not observed. Again, with PCL- and PDLLA-based formulations, cell death was significant at all concentrations even at 10 nM ($P< 0.0001$) which was mainly due to the enhanced cellular uptake and reduced drug efflux obtained with polymeric carriers (204). Now, the dose-dependent cell death achieved with PCL-based formulations was also greater than that of the corresponding PDLLA-based formulations. For example, at a concentration of 10 nM, 20.5%, 23.8%, 3.7%, and 18.8% of cells died after treatment with PCL 5% LTZ, PCL 30% LTZ, PDLLA 5% LTZ, and PDLLA 30% LTZ, respectively. Using the highest concentration (100 µM), the percentage of cell death was 81.4%, 90.4%, 76.5%, and 86.8% after treatment with PCL 5% LTZ, PCL 30% LTZ, PDLLA 5% LTZ, and PDLLA 30% LTZ, respectively. As discussed previously, the greater percentages of cell death observed in PCL-based formulations were due to the higher release rates of LTZ from PCL-based formulations along with the higher solubility of LTZ in PCL matrix as compared with that in PDLLA matrix. LTZ-induced cell death was previously reported in a study that demonstrated that these cytotoxic effects of LTZ might be due to its ability to downregulate the insulin-like growth factor I receptor (IGF-IR) which was shown to have a big role in cell growth and survival (205).

To our knowledge, the only study that examined the effects of LTZ on MCF-7 cells was the one reported by Norouzian and Azizi (101). In their study, pure form of LTZ was

compared with a PEGylated niosomal LTZ formulation that was developed in their lab. The results showed that 50% of cells died after 48-hours of treatment with 179 µM pure LTZ and 101 µM PEGylated niosomal LTZ formulation. This indicated that our formulations produced a superior performance as compared with their formulation where the lowest percentage of cell death achieved with our formulations was 76.5% at a concentration of 100 µM.

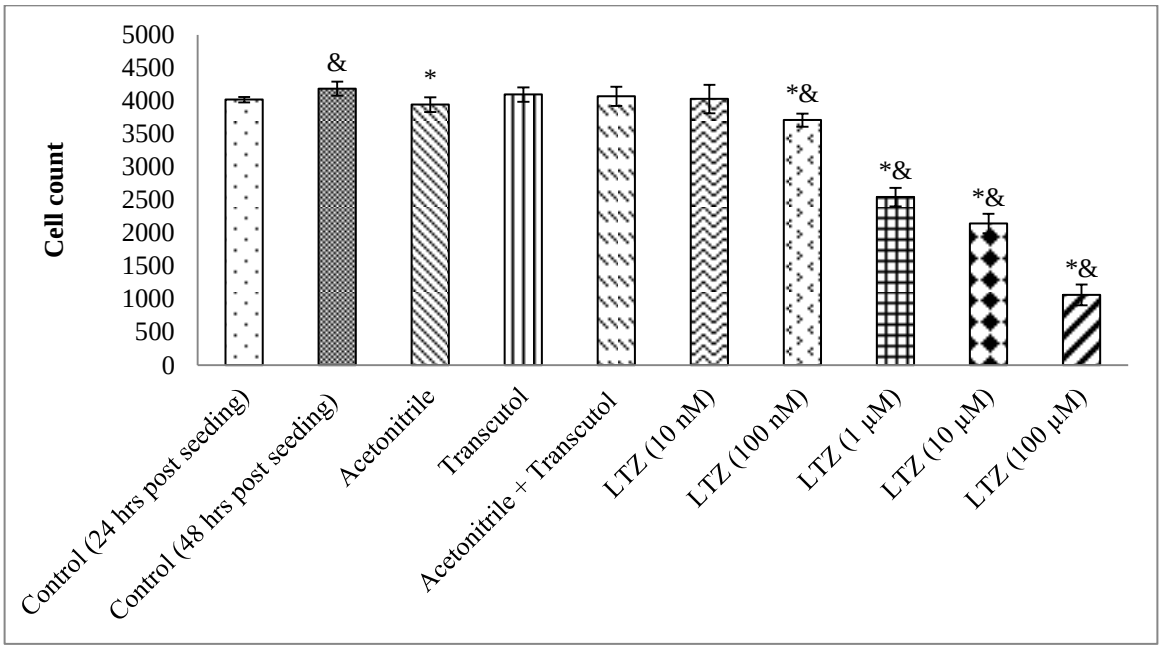

Figure 33. MCF-7 viable cells after 48-hrs treatment with LTZ at different concentrations. Bars represent the average number of nuclei of viable cells as compared with untreated controls. Cell number was assessed by automated quantitation of DAPI positive nuclei using ArrayScan XTI (Target activation module). Data presented as mean ± SD, n=3. (*): Indicates statistical significance at $P < 0.05$ compared to untreated cells (48-hrs post seeding). (&): Indicates statistical significance at $P < 0.05$ compared to untreated cells (24-hrs post seeding).

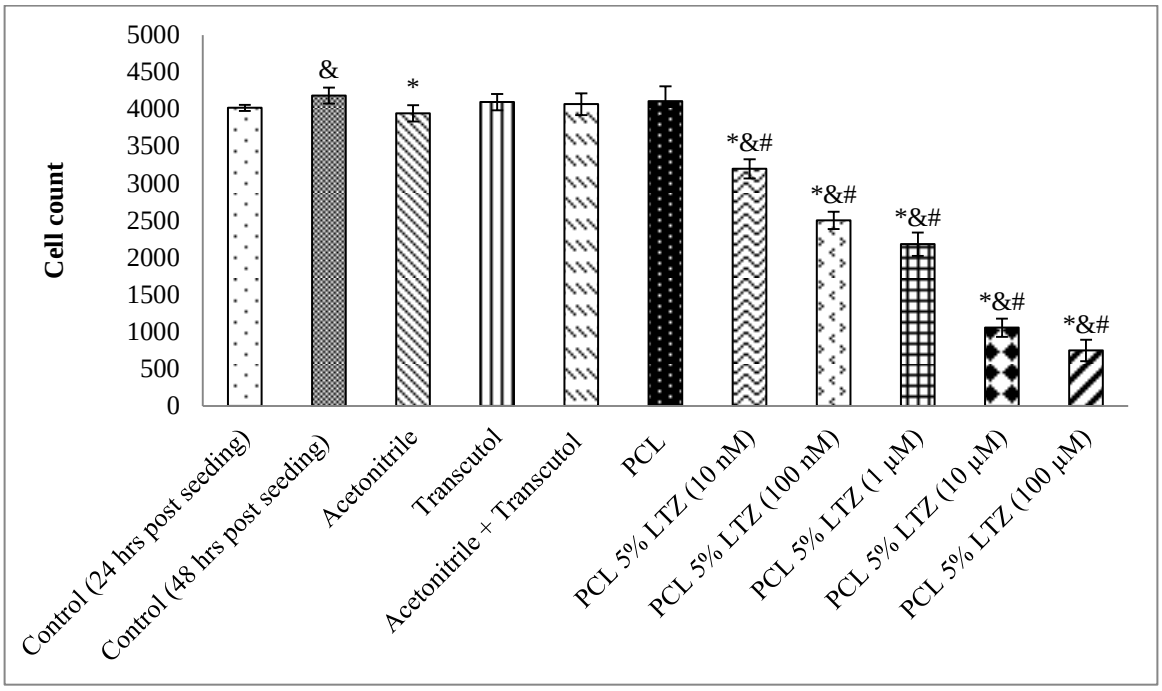

Figure 35. MCF-7 viable cells after 48-hrs treatment with PCL 5% LTZ formulation at different concentrations. Bars represent the average number of nuclei of viable cells as compared with untreated controls and PCL. Cell number was assessed by automated quantitation of DAPI positive nuclei using ArrayScan XTI (Target activation module). (*): Indicates statistical significance at P <0.05 compared to untreated cells (48-hrs post seeding). (&): Indicates statistical significance at P <0.05 compared to untreated cells (24-hrs post seeding). (#): Indicates statistical significance at P <0.05 compared to PCL.

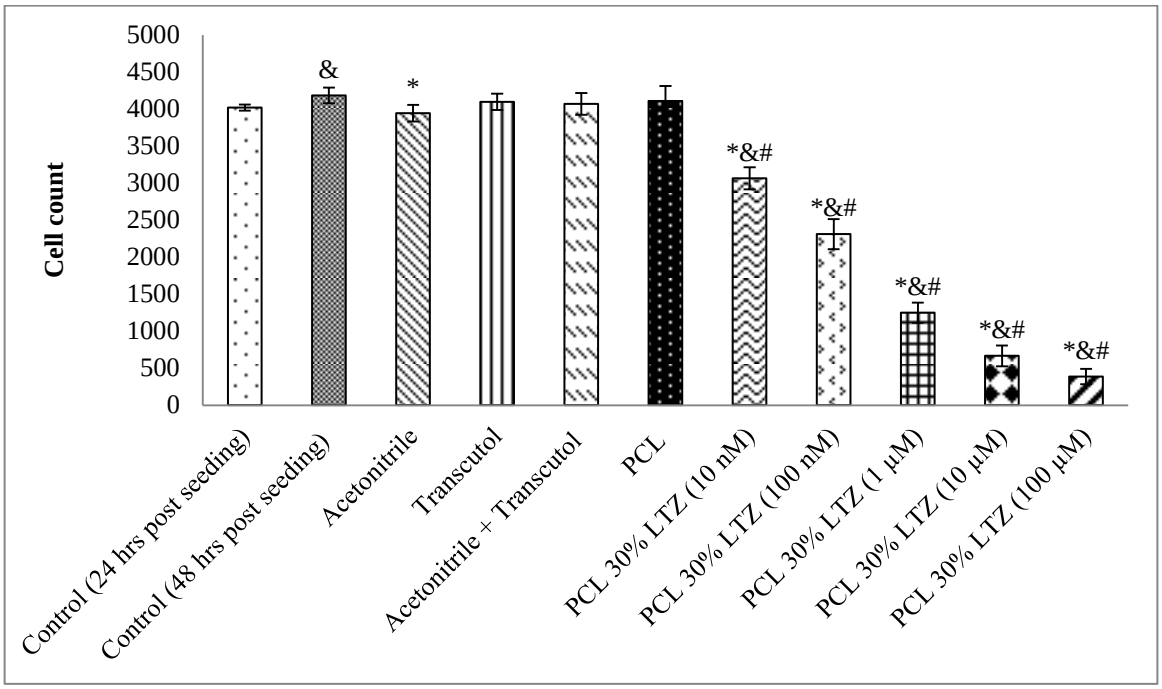

Figure 36. MCF-7 viable cells after 48-hrs treatment with PCL 30% LTZ formulation at different concentrations. Bars represent the average number of nuclei of viable cells as compared with untreated controls and PCL. Cell number was assessed by automated quantitation of DAPI positive nuclei using ArrayScan XTI (Target activation module). Data presented as mean ± SD, n=3. (*): Indicates statistical significance at P <0.05 compared to untreated cells (48-hrs post seeding). (&): Indicates statistical significance at P <0.05 compared to untreated cells (24-hrs post seeding). (#): Indicates statistical significance at P <0.05 compared to PCL.

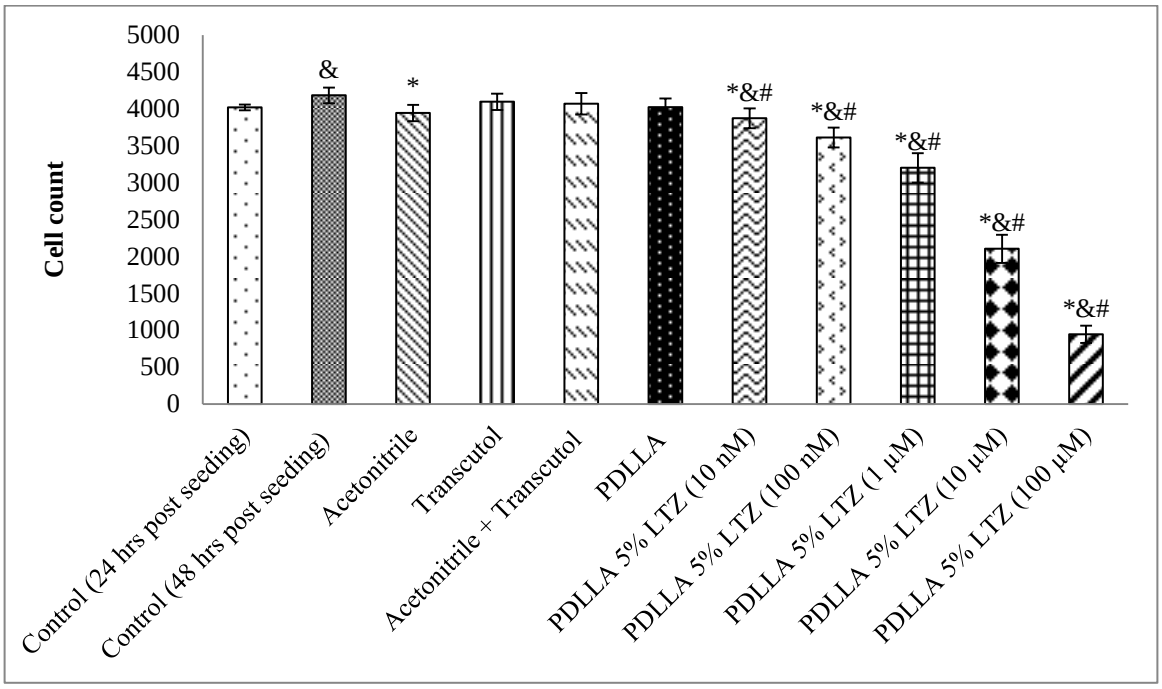

Figure 37. MCF-7 viable cells after 48-hrs treatment with PDLLA 5% LTZ formulation at different concentrations. Bars represent the average number of nuclei of viable cells as compared with untreated controls and PDLLA. Cell number was assessed by automated quantitation of DAPI positive nuclei using ArrayScan XTI (Target activation module). Data presented as mean ± SD, n=3. (*): Indicates statistical significance at P <0.05 compared to untreated cells (48-hrs post seeding). (&): Indicates statistical significance at P <0.05 compared to untreated cells (24-hrs post seeding). (#): Indicates statistical significance at P <0.05 compared to PDLLA.

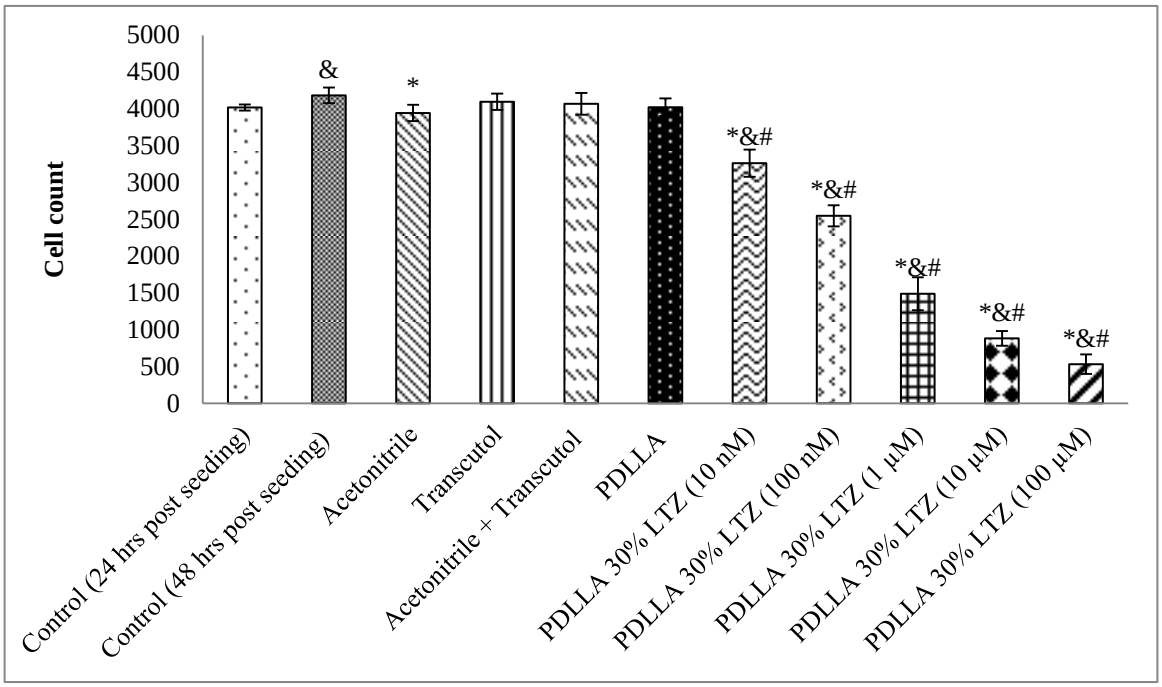

Figure 38. MCF-7 viable cells after 48-hrs treatment with PDLLA 30% LTZ formulation at different concentrations. Bars represent the average number of nuclei of viable cells as compared with untreated controls and PDLLA. Cell number was assessed by automated quantitation of DAPI positive nuclei using ArrayScan XTI (Target activation module). Data presented as mean ± SD, n=3. (*): Indicates statistical significance at P <0.05 compared to untreated cells (48-hrs post seeding). (&): Indicates statistical significance at P <0.05 compared to untreated cells (24-hrs post seeding). (#): Indicates statistical significance at P <0.05 compared to PDLLA.

CONCLUSION

This study presented a new technique that was simple, easy, and rapid for the production of monodisperse microparticles which would bring advances in the drug delivery realm. LTZ was incorporated within either PCL or PDLLA carriers in order to optimize its non-linear pharmacokinetic release profile, and hence, minimize the adverse effects associated with its use in postmenopausal women with ER-positive breast cancer. An instrument originally designed to produce monodisperse liquid jet, the VOAG, was exploited to produce the intended encapsulation of LTZ within PCL or PDLLA. Without various modifications implemented to the instrument, the production of monodisperse microparticles was enabled. Plackett-Burman design helped in further identifying the production parameters affecting the particle size distribution, which allowed the determination of the optimal values of these parameters in order to achieve the most monodisperse microparticles. Successfully produced monodisperse PCL- and PDLLA-based formulations were characterized for particle size and morphology which confirmed their narrow size distribution. LTZ loading and entrapment efficiency were very high among all formulations. Importantly, in vitro dissolution studies revealed that LTZ release from these formulations were constant, time-independent, following zero-order kinetics throughout the study. In vitro cytotoxicity showed that PCL- and PDLLA-based formulations intensified the cytotoxic effects of LTZ on MCF-7 cells at very low concentrations reaching 10 nM. The findings of this study are promising as they indicated that such monodisperse microparticles may serve as new LTZ formulations for monthly

administration that offered better release profile, which may result in minimal adverse effects. Future studies should be directed towards covering the areas that were not thoroughly investigated since they were out of the scope of this study. These include conducting a stability indicating method to validate the use of the developed UPLC method in analyzing LTZ formulations containing PCL or PDLLA. In addition, long-term stability studies should be run for the produced formulations and their release profiles should also be explored after long periods of storage. Importantly, the method of sterilizing these formulations should be considered and the impact of the chosen method on drug release profiles should also be studied. To ensure the safety of the produced formulations, their effects on normal human breast cells should be tested. Finally, in vivo studies using breast cancer animal models will be vital in providing a complete picture about the therapeutic as well as toxic effects of the produced formulations.

REFERENCES

1. Hortobagyi GN, de la Garza Salazar J, Pritchard K, Amadori D, Haidinger R, Hudis CA, et al. The global breast cancer burden: variations in epidemiology and survival. Clin Breast Cancer [Internet]. 2005 Dec [cited 2016 Sep 27];6(5):391–401. Available from: http://www.ncbi.nlm.nih.gov/pubmed/16381622.

2. Youlden DR, Cramb SM, Dunn NAM, Muller JM, Pyke CM, Baade PD. The descriptive epidemiology of female breast cancer: an international comparison of screening, incidence, survival and mortality. Cancer Epidemiol [Internet]. 2012 Jun [cited 2016 Sep 27];36(3):237–48. Available from: http://www.ncbi.nlm.nih.gov/pubmed/22459198.

3. Torre LA, Bray F, Siegel RL, Ferlay J, Lortet-Tieulent J, Jemal A. Global cancer statistics, 2012. CA Cancer J Clin [Internet]. 2015 Mar [cited 2016 Sep 27];65(2):87–108. Available from: http://www.ncbi.nlm.nih.gov/pubmed/25651787.

4. DeSantis CE, Fedewa SA, Goding Sauer A, Kramer JL, Smith RA, Jemal A. Breast cancer statistics, 2015: Convergence of incidence rates between black and white women. CA Cancer J Clin [Internet]. 2015 [cited 2016 Sep 27];66(1):31–42. Available from: http://www.ncbi.nlm.nih.gov/pubmed/26513636.

5. Pearce L. Breast cancer. Nurs Stand [Internet]. 2016 Aug 17 [cited 2016 Sep 27];30(51):15. Available from: http://www.ncbi.nlm.nih.gov/pubmed/27533387.

6. Gucalp A, Traina TA. Breast Cancer Metastasis and Drug Resistance. Breast Cancer Metastasis Drug Resist. 2013;103–5.

7. Jedy-Agba E, McCormack V, Adebamowo C, dos-Santos-Silva I. Stage at diagnosis of

breast cancer in sub-Saharan Africa: a systematic review and meta-analysis. Lancet Glob Heal [Internet]. 2016 Dec [cited 2016 Nov 28];4(12):e923–35. Available from: http://linkinghub.elsevier.com/retrieve/pii/S2214109X16302595.

8. Akinyemiju T, Ogunsina K, Sakhuja S, Ogbhodo V, Braithwaite D. Life-course socioeconomic status and breast and cervical cancer screening: analysis of the WHO's Study on Global Ageing and Adult Health (SAGE). BMJ Open [Internet]. 2016 Nov 22 [cited 2016 Nov 28];6(11):e012753. Available from: http://bmjopen.bmj.com/lookup/doi/10.1136/bmjopen-2016-012753.

9. Anton-Culver H, Chang J, Bray F, Znaor A, Stevens L, Eser S, et al. Cancer burden in four countries of the Middle East Cancer Consortium (Cyprus; Jordan; Israel; Izmir (Turkey)) with comparison to the United States surveillance; epidemiology and end results program. Cancer Epidemiol [Internet]. 2016 Oct [cited 2016 Nov 28];44:195–202. Available from: http://linkinghub.elsevier.com/retrieve/pii/S1877782116300753.

10. Karim SAM, Ghalib HHA, Mohammed SA, Rahim Fataah FH. Corrigendum to "The incidence, age at diagnosis of breast cancer in Iraqi Kurdish population and comparison to some other countries in Middle-East and West" [Int. J. Surg. 13 (2015) 71–75]. Int J Surg [Internet]. 2016 Aug [cited 2016 Nov 28];32:185. Available from: http://linkinghub.elsevier.com/retrieve/pii/S1743919116301960.

11. Bener A, Ayub H, Kakil R, Ibrahim W. Patterns of cancer incidence among the population of Qatar: a worldwide comparative study. Asian Pac J Cancer Prev [Internet]. [cited 2016 Sep 27];9(1):19–24. Available from: http://www.ncbi.nlm.nih.gov/pubmed/18439066.

12. Donnelly TT, Al-Khater A-H, Al-Kuwari M, Al-Meer N, Al-Bader SB, Malik M, et al.

Study exploring breast cancer screening practices amongst Arabic women living in the State of Qatar. Avicenna [Internet]. 2011;(2011):1. Available from: http://www.qscience.com/doi/abs/10.5339/avi.2011.1.

13. WHO. Cancer AIAfR. World cancer report 2008 & Global cancer statistics: WHO [Internet]. 2008 [cited 2016 Sep 27]. Available from: http://www.iarc.fr/en/publications/pdfs-online/wcr/2008/wcr_2008.

14. Regional Health Systems Observatory- EMRO: WHO. Qatar World Health Survey 2006 Overview Qatar [Internet]. 2006 [cited 2016 Sep 27]. Available from: http://apps.who.int/medicinedocs/documents/s17307e/s17307e.

15. Dietel M. Molecular Pathology: A Requirement for Precision Medicine in Cancer. Oncol Res Treat [Internet]. 2016 [cited 2016 Nov 28];804–10. Available from: https://www.karger.com/?doi=10.1159/000453085.

16. Kim HM, Lee YK, Koo JS. Expression of CAF-Related Proteins Is Associated with Histologic Grade of Breast Phyllodes Tumor. Dis Markers [Internet]. 2016 [cited 2016 Nov 28];2016:1–10. Available from: https://www.hindawi.com/journals/dm/2016/4218989.

17. Orlando L, Viale G, Bria E, Lutrino ES, Sperduti I, Carbognin L, et al. Discordance in pathology report after central pathology review: Implications for breast cancer adjuvant treatment. The Breast. 2016;30:151–5.

18. Tot T, Viale G, Rutgers E, Bergsten-Nordström E, Costa A. Optimal breast cancer pathology manifesto. Eur J Cancer. 2015;51(16):2285–8.

19. Aloraifi F, Boland MR, Green AJ, Geraghty JG. Gene analysis techniques and susceptibility gene discovery in non-BRCA1/BRCA2 familial breast cancer. Surg Oncol. 2015;24(2):100–9.

20. Eccles DM, Pichert G. Familial non-BRCA1/BRCA2-associated breast cancer. Lancet Oncol. 2005;6(9):705–11.

21. Li ML, Greenberg RA. Links between genome integrity and BRCA1 tumor suppression. Trends Biochem Sci. 2012;37(10):418–24.

22. Orphanos G, Kountourakis P. Targeting the HER2 Receptor in Metastatic Breast Cancer. Hematol Oncol Stem Cell Ther. 2012;5(3):127–37.

23. Palma M, Ristori E, Ricevuto E, Giannini G, Gulino A. BRCA1 and BRCA2: The genetic testing and the current management options for mutation carriers. Crit Rev Oncol Hematol. 2006;57(1):1–23.

24. Shulman LP. Hereditary Breast and Ovarian Cancer (HBOC): Clinical Features and Counseling for BRCA1 and BRCA2, Lynch Syndrome, Cowden Syndrome, and Li-Fraumeni Syndrome. Obstet Gynecol Clin North Am. 2010;37(1):109–33.

25. Alemar B, Herzog J, Brinckmann Oliveira Netto C, Artigalás O, Schwartz IVD, Matzenbacher Bittar C, et al. Prevalence of Hispanic BRCA1 and BRCA2 mutations among hereditary breast and ovarian cancer patients from Brazil reveals differences among Latin American populations. Cancer Genet. 2016;209(9):417–22.

26. Aloraifi F, Alshehhi M, McDevitt T, Cody N, Meany M, O'Doherty A, et al. Phenotypic analysis of familial breast cancer: Comparison of BRCAx tumors with BRCA1-, BRCA2-

carriers and non-familial breast cancer. Eur J Surg Oncol. 2015;41(5):641–6.

27. Hasmad HN, Lai KN, Wen WX, Park DJ, Nguyen-Dumont T, Kang PCE, et al. Evaluation of germline BRCA1 and BRCA2 mutations in a multi-ethnic Asian cohort of ovarian cancer patients. Gynecol Oncol. 2016;141(2):318–22.

28. Musolino A, Bella MA, Bortesi B, Michiara M, Naldi N, Zanelli P, et al. BRCA mutations, molecular markers, and clinical variables in early-onset breast cancer: A population-based study. The Breast. 2007;16(3):280–92.

29. Paccagnella GL, Cocco A, Ruggio F. Microinvasive fimbrial fallopian tube carcinoma in a BRCA-2 mutation carrier. Vol. 101, International Journal of Gynecology & Obstetrics. 2008.

30. Li J, Jiang Y, Liu Y, Shao Z. Identify high risk estrogen receptor-positive breast cancer patients for extended endocrine therapy. The Breast. 2017;31:173–80.

31. Rajapaksa G, Thomas C, Gustafsson J-Å. Estrogen signaling and unfolded protein response in breast cancer. J Steroid Biochem Mol Biol. 2016;163:45–50.

32. Wisinski KB, Xu W, Tevaarwerk AJ, Saha S, Kim K, Traynor A, et al. Targeting Estrogen Receptor Beta in a Phase 2 Study of High-Dose Estradiol in Metastatic Triple-Negative Breast Cancer: A Wisconsin Oncology Network Study. Clin Breast Cancer. 2016;16(4):256–61.

33. Zhou K, Sun P, Zhang Y, You X, Li P, Wang T. Estrogen stimulated migration and invasion of estrogen receptor-negative breast cancer cells involves an ezrin-dependent crosstalk between G protein-coupled receptor 30 and estrogen receptor beta signaling.

Steroids. 2016;111:113–20.

34. Lee JS, Oh M, Ahn SH, Bae JW, Bae YT, Baek JW, et al. Reproductive Factors and Subtypes of Breast Cancer Defined by Estrogen Receptor, Progesterone Receptor, and Human Epidermal Growth Factor Receptor 2: A Register-Based Study From Korea. Clin Breast Cancer. 2014;14(6):426–34.

35. Pareja F, Murray MP, Des Jean R, Konno F, Friedlander M, Lin O, et al. Cytologic assessment of estrogen receptor, progesterone receptor, and HER2 status in metastatic breast carcinoma. J Am Soc Cytopathol. 2016.

36. Shen T, Brandwein-Gensler M, Hameed O, Siegal GP, Wei S. Characterization of estrogen receptor–negative/progesterone receptor–positive breast cancer. Hum Pathol. 2015;46(11):1776–84.

37. Lesurf R, Aure MR, Mørk HH, Vitelli V, Sauer T, Geisler J, et al. Molecular Features of Subtype-Specific Progression from Ductal Carcinoma In Situ to Invasive Breast Cancer. Cell Rep. 2016;16(4):1166–79.

38. Naito M, Aokage K, Saruwatari K, Hisakane K, Miyoshi T, Hishida T, et al. Microenvironmental changes in the progression from adenocarcinoma in situ to minimally invasive adenocarcinoma and invasive lepidic predominant adenocarcinoma of the lung. Lung Cancer. 2016;100:53–62.

39. Salem H, Attiya G, El-Fishawy N. Classification of Human Cancer Diseases by Gene Expression Profiles. Appl Soft Comput. 2016.

40. Si M-J, Tao X-F, Du G-Y, Cai L-L, Han H-X, Liang X-Z, et al. Thin-section computed

tomography–histopathologic comparisons of pulmonary focal interstitial fibrosis, atypical adenomatous hyperplasia, adenocarcinoma in situ, and minimally invasive adenocarcinoma with pure ground-glass opacity. Eur J Radiol. 2016;85(10):1708–15.

41. Leonardi MC, Ricotti R, Dicuonzo S, Cattani F, Morra A, Dell'Acqua V, et al. From technological advances to biological understanding: The main steps toward high-precision RT in breast cancer. The Breast. 2016;29:213–22.

42. Zagouri F, Liakou P, Bartsch R, Peccatori FA, Tsigginou A, Dimitrakakis C, et al. Discrepancies between ESMO and NCCN breast cancer guidelines: An appraisal. Vol. 24, The Breast. 2015.

43. Balduzzi A, Bagnardi V, Sandri MT, Dellapasqua S, Cardillo A, Montagna E, et al. Intermittent Letrozole Administration as Adjuvant Endocrine Therapy for Postmenopausal Women With Hormone Receptor–Positive Early Breast Cancer: A Biologic Study. Clin Breast Cancer. 2015;15(5):e257–62.

44. Xuan Q, Gao K, Song Y, Zhao S, Dong L, Zhang Z, et al. Adherence to Needed Adjuvant Therapy Could Decrease Recurrence Rates for Rural Patients With Early Breast Cancer. Clin Breast Cancer. 2016;16(6):e165–73.

45. McDonald ES, Clark AS, Tchou J, Zhang P, Freedman GM. Clinical Diagnosis and Management of Breast Cancer. J Nucl Med [Internet]. 2016 Feb [cited 2016 Sep 27];57 Suppl 1:9S–16S. Available from: http://www.ncbi.nlm.nih.gov/pubmed/26834110.

46. Phillips C, Jeffree R, Khasraw M. Management of breast cancer brain metastases: A practical review. The Breast. 2017;31:90–8.

47. De Camargo Cancela M, Comber H, Sharp L. HR+/Her2- breast cancer in pre-menopausal women: The impact of younger age on clinical characteristics at diagnosis, disease management and survival. Cancer Epidemiol. 2016;45:162–8.

48. Spooner D, Stocken DD, Jordan S, Bathers S, Dunn JA, Jevons C, et al. A Randomised Controlled Trial to Evaluate both the Role and the Optimal Fractionation of Radiotherapy in the Conservative Management of Early Breast Cancer. Clin Oncol. 2012;24(10):697–706.

49. Criscitiello C, Curigliano G, Burstein HJ, Wong S, Esposito A, Viale G, et al. Breast conservation following neoadjuvant therapy for breast cancer in the modern era: Are we losing the opportunity? Eur J Surg Oncol. 2016.

50. Sutherland S, Miles D, Makris A. Use of maintenance endocrine therapy after chemotherapy in metastatic breast cancer. Eur J Cancer. 2016;69:216–22.

51. Santorelli ML, Hirshfield KM, Steinberg MB, Rhoads GG, Lin Y, Demissie K. Hormonal therapy for breast cancer and diabetes incidence among postmenopausal women. Ann Epidemiol. 2016;26(6):436–40.

52. Abraham J. Hormonal therapy for cancer. Medicine (Baltimore). 2016;44(1):30–3.

53. Charehbili A, Fontein DBY, Kroep JR, Liefers GJ, Mieog JSD, Nortier JWR, et al. Neoadjuvant hormonal therapy for endocrine sensitive breast cancer: A systematic review. Cancer Treat Rev. 2014;40(1):86–92.

54. Thürlimann B, Keshaviah A, Coates AS, Mouridsen H, Mauriac L, Forbes JF, et al. A comparison of letrozole and tamoxifen in postmenopausal women with early breast

cancer. N Engl J Med [Internet]. 2005 Dec 29 [cited 2016 Sep 27];353(26):2747–57. Available from: http://www.ncbi.nlm.nih.gov/pubmed/16382061.

55. Tan WW, Allred JB, Moreno-Aspitia A, Northfelt DW, Ingle JN, Goetz MP, et al. Phase I Study of Panobinostat (LBH589) and Letrozole in Postmenopausal Metastatic Breast Cancer Patients. Clin Breast Cancer. 2016;16(2):82–6.

56. Scott LJ, Keam SJ. Letrozole : in postmenopausal hormone-responsive early-stage breast cancer. Drugs [Internet]. 2006 [cited 2016 Sep 27];66(3):353–62. Available from: http://www.ncbi.nlm.nih.gov/pubmed/16526826.

57. Scholar E. Letrozole. In: xPharm: The Comprehensive Pharmacology Reference. 2007. p. 1–4.

58. Carolina N, Reserve CW. O ncologist. 2011;1138–43.

59. Cohen MH, Johnson JR, Li N, Chen G, Pazdur R. Approval Summary : Letrozole in the Treatment of Postmenopausal Women with Advanced Breast Cancer. 2002;8(March):665–9.

60. Higgins MJ, Liedke PER, Goss PE. Extended adjuvant endocrine therapy in hormone dependent breast cancer: The paradigm of the NCIC-CTG MA.17/BIG 1–97 trial. Crit Rev Oncol Hematol. 2013;86(1):23–32.

61. Chia YH, Ma CX, Ellis MJ. Letrozole Therapy Alone or in Sequence with Tamoxifen in Women with Breast Cancer: The BIG 1-98 Collaborative Group (International Breast Cancer Study Group [IBCSG] Coordinating Center, Bern, Switzerland) N Engl J Med 361:766-776, 2009§. Vol. 21, Breast Diseases: A Year Book Quarterly. 2010. p. 168–9.

62. Regan MM, Neven P, Giobbie-Hurder A, Goldhirsch A, Ejlertsen B, Mauriac L, et al. Assessment of letrozole and tamoxifen alone and in sequence for postmenopausal women with steroid hormone receptor-positive breast cancer: the BIG 1-98 randomised clinical trial at 8·1 years median follow-up. Lancet Oncol. 2011;12(12):1101–8.

63. Haynes B., Dowsett M, Miller W., Dixon J., Bhatnagar A. The pharmacology of letrozole. J Steroid Biochem Mol Biol. 2003;87(1):35–45.

64. Chan HJ, Petrossian K, Chen S. Structural and functional characterization of aromatase, estrogen receptor, and their genes in endocrine-responsive and –resistant breast cancer cells. J Steroid Biochem Mol Biol. 2016;161:73–83.

65. Ghomian N, Khosravi A, Mousavifar N. A randomized clinical trial on comparing the cycle characteristics of two different initiation days of letrozole treatment in clomiphene citrate resistant PCOS patients in IUI cycles. Int J Fertil Steril. 2015;9(1):17–26.

66. Martin GDA, Narvaez J, Bulmer R, Durrant MC. Biotransformation and molecular docking studies of aromatase inhibitors. Steroids. 2016;113:95–102.

67. Ahmad I, Shagufta. Recent developments in steroidal and nonsteroidal aromatase inhibitors for the chemoprevention of estrogen-dependent breast cancer. Eur J Med Chem. 2015;102:375–86.

68. Di Leo A, Curigliano G, Diéras V, Malorni L, Sotiriou C, Swanton C, et al. New approaches for improving outcomes in breast cancer in Europe. The Breast. 2015;24(4):321–30.

69. Benet LZ. The role of BCS (biopharmaceutics classification system) and BDDCS

(biopharmaceutics drug disposition classification system) in drug development. J Pharm Sci [Internet]. 2013 Jan [cited 2017 Jan 8];102(1):34–42. Available from: http://www.ncbi.nlm.nih.gov/pubmed/23147500.

70. Awada A, Cardoso F, Fontaine C, Dirix L, De Grève J, Sotiriou C, et al. The oral mTOR inhibitor RAD001 (everolimus) in combination with letrozole in patients with advanced breast cancer: Results of a phase I study with pharmacokinetics. Eur J Cancer. 2008;44(1):84–91.

71. Bennett PN, Brown MJ, Sharma P. Clinical pharmacology. 2012.

72. Jin S-J, Jung JA, Cho S-H, Kim U-J, Choe S, Ghim J-L, et al. The pharmacokinetics of letrozole – its association with key body mass metrics. Int J Clin Pharmacol Ther [Internet]. 2012 Aug 1 [cited 2016 Nov 28];50(8):557–65. Available from: http://www.dustri.com/article_response_page.html?artId=9831&doi=10.5414/CP201709&L=0.

73. Zamagni C, Martoni A, Lelli G, de Braud F, Cacciari N, Morritti MG, et al. Single and multiple dose pharmacokinetics of letrozole (® Femara) in elderly and younger postmenopausal patients (pts) with advanced breast cancer. Eur J Cancer. 1999;35:S292–3.

74. Mora-Huertas CE, Fessi H, Elaissari A. Influence of process and formulation parameters on the formation of submicron particles by solvent displacement and emulsification–diffusion methods: Critical comparison. Adv Colloid Interface Sci. 2011;163(2):90–122.

75. Quintanar-Guerrero D, Tamayo-Esquivel D, Ganem-Quintanar A, Allémann E, Doelker E. Adaptation and optimization of the emulsification-diffusion technique to prepare lipidic

nanospheres. Eur J Pharm Sci [Internet]. 2005 Oct [cited 2016 Nov 28];26(2):211–8. Available from: http://www.ncbi.nlm.nih.gov/pubmed/16046105.

76. Mondal N, Pal TK, Ghosal SK. Development, physical characterization, micromeritics and in vitro release kinetics of letrozole loaded biodegradable nanoparticles. Pharmazie. 2008;63(5):361–5.

77. Pawar VK, Singh Y, Meher JG, Gupta S, Chourasia MK. Engineered nanocrystal technology: In-vivo fate, targeting and applications in drug delivery. J Control Release. 2014;183:51–66.

78. Song X, Zhao Y, Hou S, Xu F, Zhao R, He J, et al. Dual agents loaded PLGA nanoparticles: Systematic study of particle size and drug entrapment efficiency. Eur J Pharm Biopharm. 2008;69(2):445–53.

79. Kouchakzadeh H, Shojaosadati SA, Shokri F. Efficient loading and entrapment of tamoxifen in human serum albumin based nanoparticulate delivery system by a modified desolvation technique. Chem Eng Res Des [Internet]. 2014;92(9):1681–92. Available from: http://dx.doi.org/10.1016/j.cherd.2013.11.024.

80. Ghadiri M, Fatemi S, Vatanara A, Doroud D, Najafabadi AR, Darabi M, et al. Loading hydrophilic drug in solid lipid media as nanoparticles: Statistical modeling of entrapment efficiency and particle size. Int J Pharm. 2012;424(1):128–37.

81. Hattrem MN, Kristiansen KA, Aachmann FL, Dille MJ, Draget KI. Ibuprofen-in-cyclodextrin-in-W/O/W emulsion – Improving the initial and long-term encapsulation efficiency of a model active ingredient. Int J Pharm [Internet]. 2015 Jun [cited 2016 Nov 28];487(1–2):1–7. Available from:

http://linkinghub.elsevier.com/retrieve/pii/S0378517315002756.

82. Grund J, Koerber M, Walther M, Bodmeier R. The effect of polymer properties on direct compression and drug release from water-insoluble controlled release matrix tablets. Int J Pharm [Internet]. 2014 Jul [cited 2016 Nov 28];469(1):94–101. Available from: http://linkinghub.elsevier.com/retrieve/pii/S0378517314002610.

83. Nabi-Meibodi M, Vatanara A, Najafabadi AR, Rouini MR, Ramezani V, Gilani K, et al. The effective encapsulation of a hydrophobic lipid-insoluble drug in solid lipid nanoparticles using a modified double emulsion solvent evaporation method. Colloids Surfaces B Biointerfaces [Internet]. 2013 Dec [cited 2016 Nov 28];112:408–14. Available from: http://linkinghub.elsevier.com/retrieve/pii/S0927776513003895.

84. Li C, Wang W, Wang X, Jiang H, Zhu J, Lin S. Fabrication of porous polymer microspheres by tuning amphiphilicity of the polymer and emulsion–solvent evaporation processing. Eur Polym J. 2015;68:409–18.

85. Zhang R, Yang L, Tu R, Huo J, Wang J, Zhou J, et al. Emulsion phase inversion from oil-in-water (1) to water-in-oil to oil-in-water (2) induced by in situ surface activation of CaCO3 nanoparticles via adsorption of sodium stearate. Colloids Surfaces A Physicochem Eng Asp. 2015;477:55–62.

86. Tsabet È, Fradette L. Effect of the properties of oil, particles, and water on the production of Pickering emulsions. Chem Eng Res Des. 2015;97:9–17.

87. Kaci M, Meziani S, Arab-Tehrany E, Gillet G, Desjardins-Lavisse I, Desobry S. Emulsification by high frequency ultrasound using piezoelectric transducer: Formation and stability of emulsifier free emulsion. Ultrason Sonochem [Internet]. 2014 May [cited

2016 Nov 28];21(3):1010–7. Available from: http://linkinghub.elsevier.com/retrieve/pii/S1350417713002903.

88. Schlender M, Spengler A, Schuchmann HP. High-pressure emulsion formation in cylindrical coaxial orifices: Influence of cavitation induced pattern on oil drop size. Int J Multiph Flow. 2015;74:84–95.

89. Mandal B, Dey SK, Bhowmik M, Ghosh LK. Development and in vitro evaluation of Letrozole loaded biodegradable nanoparticles for breast cancer therapy. Brazilian J Pharm Sci. 2009;45:585–91.

90. Gal N, Massalha S, Samuelly-Nafta O, Weihs D. Effects of particle uptake, encapsulation, and localization in cancer cells on intracellular applications. Med Eng Phys [Internet]. 2015 May [cited 2016 Nov 28];37(5):478–83. Available from: http://linkinghub.elsevier.com/retrieve/pii/S1350453315000697.

91. England CG, Miller MC, Kuttan A, Trent JO, Frieboes HB. Release kinetics of paclitaxel and cisplatin from two and three layered gold nanoparticles. Eur J Pharm Biopharm. 2015;92:120–9.

92. Siepmann J, Siepmann F. Mathematical modeling of drug delivery. Int J Pharm. 2008;364(2):328–43.

93. Helgason T, Salminen H, Kristbergsson K, McClements DJ, Weiss J. Formation of transparent solid lipid nanoparticles by microfluidization: Influence of lipid physical state on appearance. J Colloid Interface Sci [Internet]. 2015 Jun [cited 2016 Nov 28];448:114–22. Available from: http://linkinghub.elsevier.com/retrieve/pii/S0021979715001654.

94. Mérian J, De Souza R, Dou Y, Ekdawi SN, Ravenelle F, Allen C. Development of a liposome formulation for improved biodistribution and tumor accumulation of pentamidine for oncology applications. Int J Pharm [Internet]. 2015 Jul [cited 2016 Nov 28];488(1–2):154–64. Available from: http://linkinghub.elsevier.com/retrieve/pii/S0378517315003683.

95. Uchechi O, Ogbonna JDN, Attama AA. Nanoparticles for Dermal and Transdermal Drug Delivery. [cited 2016 Nov 28]; Available from: http://dx.doi.org/10.5772/58672.

96. Chun BJ, Choi J Il, Jang SS. Molecular dynamics simulation study of sodium dodecyl sulfate micelle: Water penetration and sodium dodecyl sulfate dissociation. Colloids Surfaces A Physicochem Eng Asp. 2015;474:36–43.

97. Weber S, Zimmer A, Pardeike J. Solid Lipid Nanoparticles (SLN) and Nanostructured Lipid Carriers (NLC) for pulmonary application: A review of the state of the art. Eur J Pharm Biopharm [Internet]. 2014 Jan [cited 2016 Nov 28];86(1):7–22. Available from: http://linkinghub.elsevier.com/retrieve/pii/S0939641113002920.

98. Nerella A, Basava R, Devi A. Formulation, optimisation and in vitro characterisation of letrozole loaded solid lipid nanoparticles. Int J Pharm Sci Drug Res. 2014;6(3):183–8.

99. Moghassemi S, Hadjizadeh A. Nano-niosomes as nanoscale drug delivery systems: An illustrated review. J Control Release. 2014;185:22–36.

100. Uchegbu IF, Vyas SP. Non-ionic surfactant based vesicles (niosomes) in drug delivery. Int J Pharm. 1998;172(1):33–70.

101. Azizi S, Norouzian D. Characteristics of pegylated niosomal letrozole. 2015;7(2):423–7.

102. Bentley PH. High Performance Biomaterials. A Comprehensive Guide to Medical and Pharmaceutical Applications. J R Soc Med. 1992;85(12):775.

103. Lüönd F, Schlatter J. Improved monodispersity of size selected aerosol particles with a new charging and selection scheme for tandem DMA setup. J Aerosol Sci. 2013;62:40–55.

104. Mariutti RB, Caruso IP, Ullah A, De Morais FR, Rehders D, Arni RK. Functional expression, monodispersity and conformational changes in the SBMV virus viral VPg on binding TFE. Int J Biol Macromol. 2016;83:178–84.

105. Gan SW, Vararattanavech A, Nordin N, Eshaghi S, Torres J. A cost-effective method for simultaneous homo-oligomeric size determination and monodispersity conditions for membrane proteins. Anal Biochem. 2011;416(1):100–6.

106. Wu X-F, Hu G-S, Wang B-B, Yang Y-F. Synthesis and characterization of superfine magnesium hydroxide with monodispersity. J Cryst Growth. 2008;310(2):457–61.

107. Enomoto N, Takata M, Kamada K, Hojo J, Fudouzi H. Novel processing for improving monodispersity of ceramic spheres and colloidal crystallinity. Sci Technol Adv Mater. 2006;7(7):662–6.

108. Dickinson E, Parker R, Lal M. Polydispersity and the colloidal order-disorder transition. Chem Phys Lett. 1981;79(3):578–82.

109. Salgi P, Rajagopalan R. Polydispersity in colloids: implications to static structure and scattering. Adv Colloid Interface Sci. 1993;43(2–3):169–288.

110. Naeem M, Choi M, Cao J, Lee Y, Ikram M, Yoon S, et al. Effect of Particle Size on the Dissolution of Glibenclamide. Am Hear Assoc J. 2015;26(1):869–79.

111. Selomulya C, Liu W, Wu WD, Chen XD. Uniform chitosan microparticles prepared by a novel spray-drying technique. Int J Chem Eng. 2011;2011.

112. Sugimoto T. Underlying mechanisms in size control of uniform nanoparticles. J Colloid Interface Sci. 2007;309(1):106–18.

113. Zweers MLT, Grijpma DW, Engbers GHM, Feijen J. The Preparation of Monodisperse Biodegradable Polyester Nanoparticles with a Controlled Size. J Biomed Mater Res - Part B Appl Biomater. 2003;66(2):559–66.

114. Lee YC, Jeng FT, Chen CC. Technique for aerosol generation with controllable micrometer size distribution. Chemosphere. 2008;73(5):760–7.

115. Itoh H, Sugimoto T. Systematic control of size, shape, structure, and magnetic properties of uniform magnetite and maghemite particles. J Colloid Interface Sci. 2003;265(2):283–95.

116. Bindhu MR, Umadevi M. Synthesis of monodispersed silver nanoparticles using Hibiscus cannabinus leaf extract and its antimicrobial activity. Spectrochim Acta - Part A Mol Biomol Spectrosc [Internet]. 2013;101:184–90. Available from: http://dx.doi.org/10.1016/j.saa.2012.09.031.

117. Liu G, Liu P. Synthesis of monodispersed crosslinked nanoparticles decorated with surface carboxyl groups via soapless emulsion polymerization. Colloids Surfaces A Physicochem Eng Asp. 2010;354(1–3):377–81.

118. Kamat V, Marathe I, Ghormade V, Bodas D, Paknikar K. Synthesis of Monodisperse Chitosan Nanoparticles and in Situ Drug Loading Using Active Microreactor. ACS Appl

Mater Interfaces [Internet]. 2015;151008120710000. Available from: http://pubsdc3.acs.org/doi/10.1021/acsami.5b05100.

119. Partouche E, Waysbort D, Margel S. Surface modification of crosslinked poly(styrene-divinyl benzene) micrometer-sized particles of narrow size distribution by ozonolysis. J Colloid Interface Sci. 2006;294(1):69–78.

120. Venkatesan A, Krishna Chandar N, Arjunan S, Marimuthu KN, Mohan Kumar R, Jayavel R. Structural, morphological and optical properties of highly monodispersed PEG capped V2O5 nanoparticles synthesized through a non-aqueous route. Mater Lett [Internet]. 2013;91:228–31. Available from: http://dx.doi.org/10.1016/j.matlet.2012.09.117.

121. Cho SH, Park SY, Kim C, Choi PP, Park JK. Stabilization of monodispersed spherical silica particles and their alignment with reduced crack density. Colloids Surfaces A Physicochem Eng Asp [Internet]. 2014;441:354–9. Available from: http://dx.doi.org/10.1016/j.colsurfa.2013.09.025.

122. Camli ST, Buyukserin F, Balci O, Budak GG. Size controlled synthesis of sub-100 nm monodisperse poly(methylmethacrylate) nanoparticles using surfactant-free emulsion polymerization. J Colloid Interface Sci [Internet]. 2010;344(2):528–32. Available from: http://dx.doi.org/10.1016/j.jcis.2010.01.041.

123. Yamada Y, Sakamoto T, Gu S, Konno M. Soap-free synthesis for producing highly monodisperse, micrometer-sized polystyrene particles up to 6 ??m. J Colloid Interface Sci. 2005;281(1):249–52.

124. Li Q, Liu CG, Yu Y. Separation of monodisperse alginate nanoparticles and effect of particle size on transport of vitamin e. Carbohydr Polym. 2015;124:274–9.

125. Wu HT, Ding CC, Chen KJ. Preparation of monodispersed PMMA particles and composite particles containing pigment green 36 by dispersion polymerization. J Taiwan Inst Chem Eng [Internet]. 2013;44(4):691–9. Available from: http://dx.doi.org/10.1016/j.jtice.2012.12.026.

126. Chen CW, Chen CY, Lin CL. Preparation of monodisperse poly(methyl methacrylate) microspheres: Effect of reaction parameters on particle formation, and optical performances of its diffusive agent application. J Polym Res. 2011;18(4):587–94.

127. Park JH, Allen MG, Prausnitz MR. Polymer microneedles for controlled-release drug delivery. Pharm Res. 2006;23(5):1008–19.

128. Li H, Yu Y, Faraji Dana S, Li B, Lee C-Y, Kang L. Novel engineered systems for oral, mucosal and transdermal drug delivery. J Drug Target [Internet]. 2013;21(7):611–29. Available from: http://www.ncbi.nlm.nih.gov/pubmed/23869879.

129. Yang T, Wan Z, Liu Z, Li H, Wang H, Lu N, et al. In situ mineralization of anticancer drug into calcium carbonate monodisperse nanospheres and their pH-responsive release property. Mater Sci Eng C. 2016;63:384–92.

130. Otto T, Zones SI, Iglesia E. Challenges and strategies in the encapsulation and stabilization of monodisperse Au clusters within zeolites. J Catal. 2016;339:195–208.

131. Udey RN, Jones a D, Farquar GR. Aerosol and Microparticle Generation Using a Commercial Inkjet Printer. Aerosol Sci Technol [Internet]. 2013;47(4):361–72. Available from: http://www.tandfonline.com/doi/abs/10.1080/02786826.2012.752790.

132. Lin YS, Yang CH, Wang CY, Chang FR, Huang KS, Hsieh WC. An aluminum

microfluidic chip fabrication using a convenient micromilling process for fluorescent poly(DL-lactide-co-glycolide) microparticle generation. Sensors. 2012;12(2):1455–67.

133. Berglund RN, Liu BYH. Generation of monodisperse aerosol standards. Environ Sci Technol [Internet]. 1973 Feb [cited 2016 Nov 28];7(2):147–53. Available from: http://pubs.acs.org/doi/abs/10.1021/es60074a001.

134. Booker DR, Horton KD, Marshall IA. The suitability of the vibrating orifice aerosol generator (VOAG) as a number and mass aerosol concentration standard. J Aerosol Sci. 1995;26(8):1325–6.

135. TSI Incorporated. Model 3450 Vibrating Orifice Aerosol Generator. 2002.

136. Awotwe-Otoo D, Zidan AS, Rahman Z, Habib MJ. Evaluation of anticancer drug-loaded nanoparticle characteristics by nondestructive methodologies. AAPS PharmSciTech [Internet]. 2012;13(2):611–22. Available from: http://www.pubmedcentral.nih.gov/articlerender.fcgi?artid=3364390&tool=pmcentrez&rendertype=abstract.

137. Mainardes RM, Evangelista RC. PLGA nanoparticles containing praziquantel: Effect of formulation variables on size distribution. Int J Pharm. 2005;290(1–2):137–44.

138. Vatanara A, Rouholamini Najafabadi A, Gilani K, Asgharian R, Darabi M, Rafiee-Tehrani M. A Plackett-Burman design for screening of the operation variables in the formation of salbutamol sulphate particles by supercritical antisolvent. J Supercrit Fluids. 2007;40(1):111–6.

139. Chauhan K, Trivedi U, Patel KC. Statistical screening of medium components by Plackett-

Burman design for lactic acid production by Lactobacillus sp. KCP01 using date juice. Bioresour Technol. 2007;98(1):98–103.

140. International Conference on Harmonization. Requirements for Registration of Pharmaceuticals for Human Use. ICH Harmon Tripart Guidel. 2009;8(August):1–28.

141. Mitchell JP, Waters S. Improvements to the Vibrating Orifice Aerosol Generator (VOAG) for the Production of Methylene Blue Particles. J Aerosol Sci. 1986;17(3).

142. Westenberger S, Heibel T, Gebhart J, Roth C. Continuous monitoring of droplet production of a vibrating orifice generator by laser light extinction. J Aerosol Sci. 1990;21(SUPPL. 1):547–50.

143. Leong KH. On the continuous operation of the vibrating orifice aerosol generator. J Aerosol Sci. 1986;17(5):855–8.

144. Berkland C, Kim K, Pack DW. Fabrication of PLG microspheres with precisely controlled and monodisperse size distributions. J Control Release [Internet]. 2001 May 18 [cited 2016 Nov 12];73(1):59–74. Available from: http://www.ncbi.nlm.nih.gov/pubmed/11337060.

145. Vanderpool R, Rubow K. Generation of large, solid, monodisperse calibration aerosols. Aerosol Sci Technol [Internet]. 1988;6826(June):37–41. Available from: http://www.tandfonline.com/doi/abs/10.1080/02786828808959195.

146. Rama Rao G V., López GP, Bravo J, Pham H, Datye AK, Xu HF, et al. Monodisperse mesoporous silica microspheres formed by evaporation-induced self assembly of surfactant templates in aerosols. Adv Mater. 2002;14(18):1301–4.

147. Rajagopalan V, Grulke E, Ray A. Generation of multicomponent polymer particles using microdroplet evaporation technique. Chem Eng Trans. 2011;24:607–12.

148. Kreyling W., Erbe F. Continuous dispersion of aqueous solutions by a modified vibrating orifice aerosol generator. J Aerosol Sci. 1985;16(3):261–3.

149. Mitchell JP, Snelling KW, Stone RL. Improvements to the vibrating orifice aerosol generator. J Aerosol Sci. 1987;100(4):801–2.

150. Rahman Z, Zidan AS, Habib MJ, Khan MA. Understanding the quality of protein loaded PLGA nanoparticles variability by Plackett-Burman design. Int J Pharm [Internet]. 2010;389(1–2):186–94. Available from: http://dx.doi.org/10.1016/j.ijpharm.2009.12.040.

151. Sastry S V., Reddy IK, Khan MA. Atenolol gastrointestinal therapeutic system: Optimization of formulation variables using response surface methodology. J Control Release. 1997;45(2):121–30.

152. Palamakula a, Nutan MTH, Khan M a. Response surface methodology for optimization and characterization of limonene-based coenzyme Q10 self-nanoemulsified capsule dosage form. AAPS PharmSciTech. 2004;5(4):e66.

153. Sastry S V., Khan MA. Aqueous based polymeric dispersion: Plackett-Burman design for screening of formulation variables of atenolol gastrointestinal therapeutic system. Pharm Acta Helv. 1998;73(2):105–12.

154. Nazzal S, Nutan M, Palamakula A, Shah R, Zaghloul AA, Khan MA. Optimization of a self-nanoemulsified tablet dosage form of Ubiquinone using response surface methodology: Effect of formulation ingredients. Int J Pharm. 2002;240(1–2):103–14.

155. Oita I, Halewyck H, Pieters S, Dejaegher B, Thys B, Rombaut B, et al. Improving the capillary electrophoretic analysis of poliovirus using a Plackett-Burman design. J Pharm Biomed Anal. 2009;50(4):655–63.

156. Bose A, Wong TW, Singh N. Formulation development and optimization of sustained release matrix tablet of Itopride HCl by response surface methodology and its evaluation of release kinetics. Saudi Pharm J [Internet]. 2013;21(2):201–13. Available from: http://dx.doi.org/10.1016/j.jsps.2012.03.006.

157. Hamed E, Sakr A. Application of multiple response optimization technique to extended release formulations design. J Control Release. 2001;73(2–3):329–38.

158. Wang X, Su MX, Cai XS. Effects of Material Viscosity on Particle Sizing by Ultrasonic Attenuation Spectroscopy. Procedia Eng. 2015;102:256–64.

159. Shewan HM, Stokes JR. Analytically predicting the viscosity of hard sphere suspensions from the particle size distribution. J Nonnewton Fluid Mech. 2015;222:72–81.

160. Bi X, Hemar Y, Balaban MO, Liao X. The effect of ultrasound on particle size, color, viscosity and polyphenol oxidase activity of diluted avocado puree. Ultrason Sonochem. 2015;27:567–75.

161. Deepak Selvakumar R, Dhinakaran S. Effective viscosity of nanofluids — A modified Krieger–Dougherty model based on particle size distribution (PSD) analysis. J Mol Liq. 2017;225:20–7.

162. Nakashima Y, Takai C, Wanghui C, Razavi-Khosroshahi H, Shirai T, Fuji M. Control size distribution of hollow silica nanoparticles by viscosity of emulsion template. Colloids

Surfaces A Physicochem Eng Asp. 2016;507:164–9.

163. Fava LW, Serpa PBS, Külkamp-Guerreiro IC, Pinto AT. Evaluation of viscosity and particle size distribution of fresh, chilled and frozen milk of Lacaune ewes. Small Rumin Res. 2013;113(1):247–50.

164. Rezaee M, Basri M, Raja Abdul Rahman RNZ, Salleh AB, Chaibakhsh N, Fard Masoumi HR. A multivariate modeling for analysis of factors controlling the particle size and viscosity in palm kernel oil esters-based nanoemulsions. Ind Crops Prod. 2014;52:506–11.

165. Zeng H, Yang J, Katagiri D, Rang Y, Xue S, Nakajima H, et al. Investigation of monodisperse droplet generation in liquids by inkjet. Sensors Actuators, B Chem [Internet]. 2015;220:958–61. Available from: http://dx.doi.org/10.1016/j.snb.2015.06.027.

166. Xu Q, Hashimoto M, Dang TT, Hoare T, Kohane DS, Whitesides GM, et al. Preparation of monodisperse biodegradable polymer microparticles using a microfluidic flow-focusing device for controlled drug delivery. Small. 2009;5(13):1575–81.

167. Mondal N, Pal TK, Ghosal SK. Development and validation of RP-HPLC method to determine letrozole in different pharmaceutical formulations and its application to studies of drug release from nanoparticles. Acta Pol Pharm [Internet]. [cited 2016 Nov 24];66(1):11–7. Available from: http://www.ncbi.nlm.nih.gov/pubmed/19226963.

168. Zarghi A, Foroutan SM, Shafaati A, Khoddam A. HPLC Determination of Letrozole in Plasma Using Fluorescence Detection: Application to Pharmacokinetic Studies. Chromatographia [Internet]. 2007 Nov 2 [cited 2016 Nov 5];66(9–10):747–50. Available from: http://www.springerlink.com/index/10.1365/s10337-007-0381-9.

169. Mondal N, Pal TK, Ghosal SK. Development and validation of a spectrophotometric method for estimation of letrozole in bulk and pharmaceutical formulation. Pharmazie [Internet]. 2007 Aug [cited 2016 Nov 24];62(8):597–8. Available from: http://www.ncbi.nlm.nih.gov/pubmed/17867554.

170. M.Ganesh, K.Kamalakannan RP, Upadhyay S, Srivatsava A, Sivakumar T, Ganguly S. a Validated UV Spectrophotometric Method for the Determination of Letrozole in Bulk and Solid Dosage Form. Small. 2008;1(1):55–8.

171. Marfil F, Pineau V, Sioufi A, Godbillon SJ. High-performance liquid chromatography of the aromatase inhibitor, letrozole, and its metabolite in biological fluids with automated liquid-solid extraction and fluorescence detection. J Chromatogr B Biomed Appl [Internet]. 1996 Aug 30 [cited 2016 Nov 24];683(2):251–8. Available from: http://www.ncbi.nlm.nih.gov/pubmed/8891923.

172. Sen S, Laha T, Patnaik R. Reverse phase high performance liquid chromatographic method for the analysis of letrozole in pharmaceutical dosage forms. Indian J Pharm Sci [Internet]. 2008 [cited 2016 Nov 5];70(3):401. Available from: http://www.ijpsonline.com/text.asp?2008/70/3/401/43019.

173. Dhole SM, Khedekar PB, Amnerkar ND. Comparison of UV spectrophotometry and high performance liquid chromatography methods for the determination of repaglinide in tablets. Pharm Methods [Internet]. 2012 Jul [cited 2016 Nov 24];3(2):68–72. Available from: http://www.ncbi.nlm.nih.gov/pubmed/23781481.

174. Gumustas M, Kurbanoglu S, Uslu B, Ozkan SA. UPLC versus HPLC on Drug Analysis: Advantageous, Applications and Their Validation Parameters. Chromatographia [Internet].

2013 Nov 27 [cited 2016 Nov 24];76(21–22):1365–427. Available from: http://link.springer.com/10.1007/s10337-013-2477-8.

175. Annapurna MM, Mohapatro C, Narendra A. Stability-indicating liquid chromatographic method for the determination of Letrozole in pharmaceutical formulations. J Pharm Anal. 2012;2(4):298–305.

176. International Conference on Harmonization. Validation of Analytical Procedures : Text and Methodology. Int Conf Harmon. 2005;1994(November 1996):17.

177. Volckens J, Peters TM. Counting and particle transmission efficiency of the aerodynamic particle sizer. J Aerosol Sci. 2005;36(12):1400–8.

178. Roth C, Westenberger S, Kreyling WG. Production of 111In-labelled monodisperse aerosol particles. J Aerosol Sci. 1989;20(8):1289–92.

179. Orihara S, Konno M. A Simple Method for Producing Micrometer-Sized Monodisperse Polystyrene Particles in Aqueous Media. J Colloid Interface Sci [Internet]. 2000;230(1):210–2. Available from: http://www.ncbi.nlm.nih.gov/pubmed/10998308.

180. Ouyang Y, Shi H, Fu R, Wu D, Asgharian B, Fang CP, et al. Highly monodisperse microporous polymeric and carbonaceous nanospheres with multifunctional properties. Aerosol Sci Technol [Internet]. 2013;3(2):1430. Available from: http://www.tandfonline.com/doi/abs/10.1080/02786829208959540.

181. Gilroy JB, Gädt T, Whittell GR, Chabanne L, Mitchels JM, Richardson RM, et al. Monodisperse cylindrical micelles by crystallization-driven living self-assembly. Nat Chem [Internet]. 2010;2(7):566–70. Available from:

http://www.ncbi.nlm.nih.gov/pubmed/20571575.

182. Rosca ID, Watari F, Uo M, Uo M. Microparticle formation and its mechanism in single and double emulsion solvent evaporation. J Control Release. 2004;99(2):271–80.

183. Astete CE, Kumar CSSR, Sabliov CM. Size control of poly(d,l-lactide-co-glycolide) and poly(d,l-lactide-co-glycolide)-magnetite nanoparticles synthesized by emulsion evaporation technique. Colloids Surfaces A Physicochem Eng Asp. 2007;299(1):209–16.

184. Palamoor M, Jablonski MM. Comparative study on diffusion and evaporation emulsion methods used to load hydrophilic drugs in poly(ortho ester) nanoparticle emulsions. Powder Technol. 2014;253:53–62.

185. Overbeek JTG. Monodisperse colloidal systems, fascinating and useful. Adv Colloid Interface Sci. 1982;15(3–4):251–77.

186. Dey SK, Mandal B, Bhowmik M, Ghosh LK. Development and in vitro evaluation of Letrozole loaded biodegradable nanoparticles for breast cancer therapy. Brazilian J Pharm Sci [Internet]. 2009 Sep [cited 2016 Nov 28];45(3):585–91. Available from: http://www.scielo.br/scielo.php?script=sci_arttext&pid=S1984-82502009000300025&lng=en&nrm=iso&tlng=en.

187. Jin F, Li J, Ye X, Wu C. Effects of pH and Ionic Strength on the Stability of Nanobubbles in Aqueous Solutions of r-Cyclodextrin.

188. Carneiro-Da-Cunha MG, Cerqueira MA, Souza BWS, Teixeira JA, Vicente AA. Influence of concentration, ionic strength and pH on zeta potential and mean hydrodynamic diameter of edible polysaccharide solutions envisaged for multinanolayered films

production. Carbohydr Polym. 2011;85:522–8.

189. Egorova EM, Dukhin AS, Svetlova IE, Svetlova IE. Some problems of zeta potential determination in electrophoretic measurements on lipid membranes. Biochim Biophys Acta - Biomembr. 1992;1104(1):102–10.

190. Rask MB, Knopp MM, Olesen NE, Holm R, Rades T. Influence of PVP/VA copolymer composition on drug–polymer solubility. Eur J Pharm Sci. 2016;85:10–7.

191. Azevedo MC, Reis RL, Claase MB, Grijpma DW, Feijen J. Development and properties of polycaprolactone/ hydroxyapatite composite biomaterials. 1(1):0–3.

192. Tang Y-Z, Zhou M, Huang J, Cao Z, Qi T-T, Huang G-H, et al. Synthesis, Crystal Structure, and Characterization of three New Letrozole Complexes. Zeitschrift für Anorg und Allg Chemie [Internet]. 2012;638(2):372–6. Available from: http://doi.wiley.com/10.1002/zaac.201100426.

193. Damitz R, Chauhan A. Rapid dissolution of propofol emulsions under sink conditions. Int J Pharm. 2015;481(1):47–55.

194. Balzus B, Colombo M, Sahle FF, Zoubari G, Staufenbiel S, Bodmeier R. Comparison of different in vitro release methods used to investigate nanocarriers intended for dermal application. Int J Pharm. 2016;513(1):247–54.

195. Kumar Jana S. Letrozole and Curcumin Loaded-PLGA Nanoparticles: A Therapeutic Strategy for Endometriosis. J Nanomedine Biotherapeutic Discov [Internet]. 2014;4(1):1–10. Available from: http://www.omicsonline.org/open-access/letrozole-and-curcumin-loadedplga-nanoparticles-a-therapeutic-strategy-for-endometriosis-2155-

983X.1000123.php?aid=23470.

196. Dekyndt B, Verin J, Neut C, Siepmann F, Siepmann J. How to easily provide zero order release of freely soluble drugs from coated pellets. Int J Pharm. 2015;478(1):31–8.

197. Gichner T, Mukherjee A, Velemínský J. DNA staining with the fluorochromes EtBr, DAPI and YOYO-1 in the comet assay with tobacco plants after treatment with ethyl methanesulphonate, hyperthermia and DNase-I. Mutat Res Toxicol Environ Mutagen. 2006;605(1):17–21.

198. Sullivan DW, Gad SC, Julien M. A review of the nonclinical safety of Transcutol®, a highly purified form of diethylene glycol monoethyl ether (DEGEE) used as a pharmaceutical excipient. Food Chem Toxicol [Internet]. 2014 Oct [cited 2017 Jan 7];72:40–50. Available from: http://linkinghub.elsevier.com/retrieve/pii/S0278691514003251.

199. Osborne DW. Diethylene glycol monoethyl ether: an emerging solvent in topical dermatology products. J Cosmet Dermatol [Internet]. 2011 Dec [cited 2017 Jan 7];10(4):324–9. Available from: http://doi.wiley.com/10.1111/j.1473-2165.2011.00590.x.

200. Azria D, Larbouret C, Cunat S, Ozsahin M, Gourgou S, Martineau P, et al. Letrozole sensitizes breast cancer cells to ionizing radiation. Breast Cancer Res [Internet]. 2005;7(1):R156–63. Available from: http://www.pubmedcentral.nih.gov/articlerender.fcgi?artid=1064115&tool=pmcentrez&rendertype=abstract.

201. Macedo LF, Guo Z, Tilghman SL, Sabnis GJ, Qiu Y, Brodie A. Role of androgens on MCF-7 breast cancer cell growth and on the inhibitory effect of letrozole. Cancer Res.

2006;66(15):7775–82.

202. Mitropoulou TN, Tzanakakis GN, Kletsas D, Kalofonos HP, Karamanos NK. Letrozole as a potent inhibitor of cell proliferation and expression of metalloproteinases (MMP-2 and MMP-9) by human epithelial breast cancer cells. Int J Cancer. 2003;104(2):155–60.

203. Santner SJ, Chen S, Zhou D, Korsunsky Z, Martel J, Santen RJ. Effect of androstenedione on growth of untransfected and aromatase-transfected MCF-7 cells in culture. J Steroid Biochem Mol Biol. 1993;44(4–6):611–6.

204. Liechty WB, Kryscio DR, Slaughter B V, Peppas NA. Polymers for drug delivery systems. Annu Rev Chem Biomol Eng [Internet]. 2010 [cited 2017 Jan 5];1:149–73. Available from: http://www.ncbi.nlm.nih.gov/pubmed/22432577.

205. Lisztwan J, Pornon A, Chen B, Chen S, Evans DB. The aromatase inhibitor letrozole and inhibitors of insulin-like growth factor I receptor synergistically induce apoptosis in in vitro models of estrogen-dependent breast cancer. Breast Cancer Res. 2008;10(4):R56.